THE PENNSYLVANIA STATE UNIVERSITY
SCHREYER HONORS COLLEGE

DEPARTMENT OF MATERIALS SCIENCE AND ENGINEERING

FINITE ELEMENT MODELING OF LEADING EDGE CURL PHENOMENON

GEORGE M. SLOTA

FALL 2009

A thesis
submitted in partial fulfillment
of the requirements
for a baccalaureate degree
in Computer Engineering
with honors in Materials Science and Engineering

Reviewed and approved by the following:

Douglas E. Wolfe
Assistant Professor of Materials Science and Engineering
Thesis Supervisor

Lee D. Coraor
Associate Professor of Computer Science and Engineering
Honors Advisor

R. Allen Kimel
Assistant Professor of Materials Science and Engineering
Honors Advisor

Abstract

Leading edge curl is a deformation phenomenon that has been observed to occur on the first 0.01-0.03 inches of the leading edge of compressor blades in jet turbine aircraft operating in sandy or dusty environments. This deformation affects the aerodynamic properties of the blade, causing decreases in engine performance and time between required maintenance. This thesis focused on re-creating the leading edge curl phenomenon using finite element modeling (FEM) to design dynamic two and three dimensional models of particles impacting a compressor blade leading edge. Once a modeling methodology was determined in which curl could be re-created with consistency, a range of conditions was finally identified in which curling could be expected to occur, including particle velocities, particle sizes, and angles of impingement. In total, approximately five thousand different blade, particle, impact, and modeling configurations were simulated.

Additional modeling efforts were performed in an attempt to explore possible methods of reducing or mitigating the deformation and curling caused under these identified conditions. Thicker leading edge blade geometry was modeled and compared against the original blade geometry. It was found that thickening the leading edge of the blade prohibited significant deformation and could prevent all curling in the absence of erosion. New materials were explored for the blade model, including a more elastic titanium alloy and a less elastic nickel chromium superalloy. These materials were found to perform slightly less than the original material in terms of deformation protection,

likely due to both materials' lower yield stresses in comparison to the original material. Finally, thin titanium nitride (TiN) coatings were modeled on a blade model to determine how effective ceramic coatings were against impacting particles. Coatings were modeled with a range of Young’s moduli in order to determine its effect on erosion resistance. Thin TiN-based coatings were found to decrease deformation under all conditions, but were susceptible to damage under high velocity and large particle impacts. The difference in erosion protection offered with differing Young’s moduli was minimal based on the obtained simulation results.

Table of Contents

List of Figures

List of Tables

Acknowledgements

I would like to extend a large degree of gratitude to my thesis advisor, Dr. Douglas E. Wolfe, for giving me the opportunity to work in his lab and complete the research for this thesis. His guidance and continuous help and effort has made this thesis a possibility. I would also like to thank my honors advisors, Dr. Lee D. Coraor and Dr. R Allen Kimel, for their assistance and guidance in my academic pursuits. Thanks are also extended to Tom Medill and John Pitterle for their work, assistance, and support in the early stages of these modeling efforts. Finally, I would like to thank Penn State's High Performance Computer Group for allowing my use of their computers to process most of the simulations created for this research.

Chapter 1

Introduction

This thesis explores the usage of finite element modeling (FEM) to examine turbojet aircraft compressor blade leading edge curl and possible solutions for the prevention of its occurrence. Leading edge curl is a type of deformation that has been observed to take place on turbojet engine first stage compressor blades of aircraft operating in sandy or dusty environments. Small granular particles are ingested into the engines' intakes, where they erode and deform the first 0.01-0.03 inches of the blades' leading edges into a curled shape. This deformation affects the aerodynamic properties of the blade, decreasing engine performance and increasing maintenance costs.

Solutions for the prevention of curl and erosion to compressor blades include filtering incoming air to remove most large particles from the airstream, the application of a thin ceramic coating to the compressor blades, changing the material composition of the blades, and altering the blades' leading edge geometry to be more resistant to deformation and erosion. Most turbojet aircraft already have air filtration systems incorporated into their design. However, the effectiveness of filtration systems suffers in two main ways. They tend to decrease the overall air intake into the engine, which can reduce engine performance, and they still allow a number of large particles to bypass the filtration system and impact compressor components, causing deformation and erosion. Therefore, the alternative approaches of a thin erosion resistant coating, different blade materials, and a change of blade geometry were all explored through FEM simulation.

A variety of particle impact conditions were simulated on a finite element model created based on the geometry of an existing aircraft compressor blade. Differing particle sizes, particle velocities, and particle impact angles were examined in an effort to determine under which conditions curling was most probable to occur. After observing curl, the blade model's geometry was changed to a new geometry expected to be more resistant to deformation. The original blade model was also examined with a new material composition. A thin ceramic coating was then applied to the new blade model in order to determine its ability to resist erosion and prevent deformation of the blade. These new configurations were all simulated under the same particle impact conditions that curling was initially observed with the differences in the blade models' deformation responses being observed. This allowed a quantitative judgment about the efficacy of these solutions with regard to the prevention of compressor blade leading edge curl.

Objectives

The primary objective of this work was to determine the particle impact conditions under which leading edge blade curl is most probable to occur. This included modeling the blade material, blade leading edge geometry, particle diameter, angle and velocity of particle impacts, as well as different numbers of particle impacts. Upon modeling these conditions, it was then necessary to validate the model through comparing results to compressor blades deformed in situ and those deformed in the lab through in-house testing. By gaining a thorough understanding of the component working environment that results in leading edge deformation, solutions to mitigate or suppress the leading edge curl could be proposed.

A secondary set of objectives was developed in order to identify effective ways to accomplish the goal of minimized leading edge deformation. These objectives included:

- Observe the efficacy of thicker leading edge geometry with respect to curl prevention
- Observe the efficacy of a new blade material with respect to curl prevention
- Observe the efficacy of a thin ceramic coating with respect to curl prevention
- Determine the most effective way to prevent or minimize leading edge erosion and curl deformation based on all observations

Chapter 2

Literature Review and Modeling Characteristics

Turbojet engines operating in sandy or dusty environments are likely to intake a large number of small granular particles up to ~0.04 inches or larger in diameter. A majority of this intake occurs as the aircraft creates a dust plume while landing and taking off. The intake of these particles results in significant erosion and deformation to engine components, especially to first stage compressor blades/blisks. Although there has been little research specifically studying leading edge curl, compressor blade erosion has been studied in more detail.

2.1 Compressor Blade Erosion

As turbojet aircraft intake particles, these particles will possibly impact the leading and trailing edges of the engines' compressor blades. Typical trajectories of particles were calculated through numerical methods by Hamed and Tabakoff [1] and are shown in Figure 2.1. It is apparent from Figure 2.1 that the expected trajectories of ingested particles are heavily dependent on particle size, with smaller particle following the airstream and larger particle following a more ballistic trajectory.

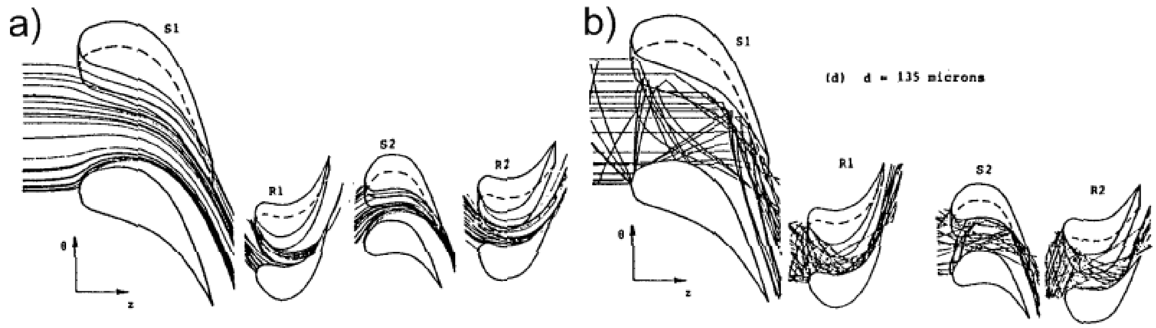

Figure 2.1 - Typical trajectories of (a) 2.5 micron diameters and (b) 135 micron diameters particles in a turbojet engine compressor section.

A large number of impacts will often erode and deform the blades to the point where engine performance can be significantly impaired. It is observed by Nagy et al. [2] that the thinner trailing edge of the compressor blade will suffer greater erosion compared to the thicker leading edge as demonstrated in Figure 2.2, although this effect can be heavily dependent on the geometry of the component. Eroded compressor blades increase engine vibration, fuel consumption, and combustion temperatures [3]. This leads to higher maintenance costs and a shorter engine life expectancy. Erosion and other types of foreign object damage are estimated to cost in excess of 4 billion dollars annually [4].

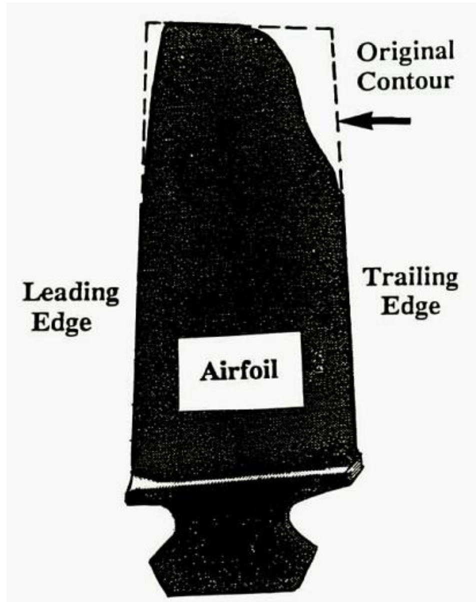

Figure 2.2 - Erosion of a first stage compressor blade. It can be observed that the trailing edge of the blade has suffered considerably more erosion damage than the leading edge. [2]

2.2 Leading Edge Curl

As the compressor blades continue to erode, the leading edge decreases in thickness, and can eventually deform into a curled shape as shown in Figure 2.3. The horizontal and vertical magnitudes of the deformation, measured using the method shown in the figure, are expected to each be between 0.01-0.03 inches. This final curling magnitude is heavily dependent on the geometry of the leading edge.

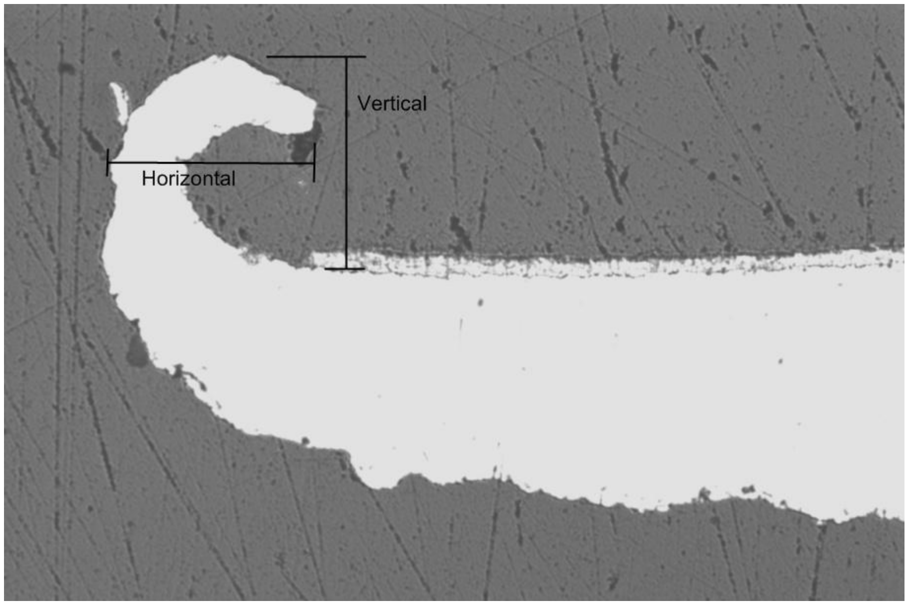

Figure 2.3 – Leading edge of a first stage compressor blade demonstrating the geometry of curling. This figure also gives the method used for measuring the magnitude of both vertical and horizontal deformation with regard to curling.

Currently, no systematic studies exist in the literature examining the exact conditions under which curling is likely to occur. It has been observed that, depending on leading edge thickness, larger diameter particles can deform the leading edge without smaller particles first thinning the leading edge through erosion. Smaller particles are unable to plastically deform the blade without significant erosion. The velocity and trajectories (angle and location of impact) of impacting particles have been studied, but purely in the context of erosion. The investigation and substantiation of the possibility of curl without preliminary erosion and the particle impact conditions under which curl occurs was one of the primary aims of this thesis.

One thing is certain, however, the combined effects of erosion and curling deformation severely limit engine performance. Several solutions have been proposed to counter this damage, including filters to remove particles from the air stream, altering the material properties or geometry of the compressor blade, and adding an erosion resistant coating to the compressor blades.

2.3 Engine Air Particle Separators (EAPS)

Filtration systems, commonly known as engine air particle separators (EAPS), are designed to filter out particles from the airflow of the engine intake. EAPS have been used for decades with a high degree of success. Separation efficiencies of 93 to 98.5 percent can be achieved. However, large particles of sufficient mass will follow a ballistic trajectory as was demonstrated by Figure 2.1, bypassing an EAPS's centrifugal air flow to impact and damage the first stage compressor [1, 5]. Because filtration systems work by filtering incoming air, they decrease the overall air intake into the engine and can affect engine performance. Filtration systems can also fail or become clogged, at which point bypass ducts open up to allow all particles to flow into the engine's compressor section. Although filtration systems are presently the primary means to prevent compressor damage from small particles, they do not meet current system performance.

2.4 Erosion Resistant Systems

Due to the prevalence of damaging impacts even with a filtration system, a secondary means of protection is necessary to prevent damage to the compressor blades. A thin coating on the order of 20 to 50 microns in thickness can be applied to a compressor blade without affecting the aerodynamic properties. Currently, many coatings are approved for use to protect turbojet compressor blades, including monolithic and multilayer titanium nitride and ternary nitrides coating systems.

Along with the addition of protective coating systems, properties of the compressor blade, such as its material makeup and leading edge geometry, are being investigated and studied for possible improvements. Possible first stage compressor blade materials include titanium alloys such as Ti-6Al-4V, precipitation-hardening stainless steels such A-286 and AM-355, and nickel-chromium based superalloys such as Inconel-718. Thicker leading edge geometry for the blade has also been considered to suppress leading edge curl by increasing the energy necessary to damage the blade. A combination of these new properties in addition to a coating will possibly offer the greatest protection.

2.4.1 Ductile Erosion Mechanisms

Increases in observed compressor blade life with the addition of a thin erosion resistant ceramic coating can be explained through the differing mechanisms at which erosion occurs for the ductile blade material versus the brittle coating. The ductile erosion mechanism occurs primarily through plastic deformation of the blade surface. As particles harder than the ductile blade material strike the blade surface, they plough the material in the direction of impact to create an impact crater with a buildup of material around the edge as shown in Figure 2.4a. This buildup of material is called a platelet in the literature by Levy and others [6-8]. Once enough material has been displaced to the edge of the impact zone, a subsequent impact breaks the built-up material free from the surface. This process repeats for each particle striking the blade surface. After enough impacts, significant material loss will occur. The highest degree of ductile erosion has been observed in experimentation to result from impacts occurring at ~30 degrees as shown graphically in Figure 2.5, but is heavily dependent on the material system [8-10].

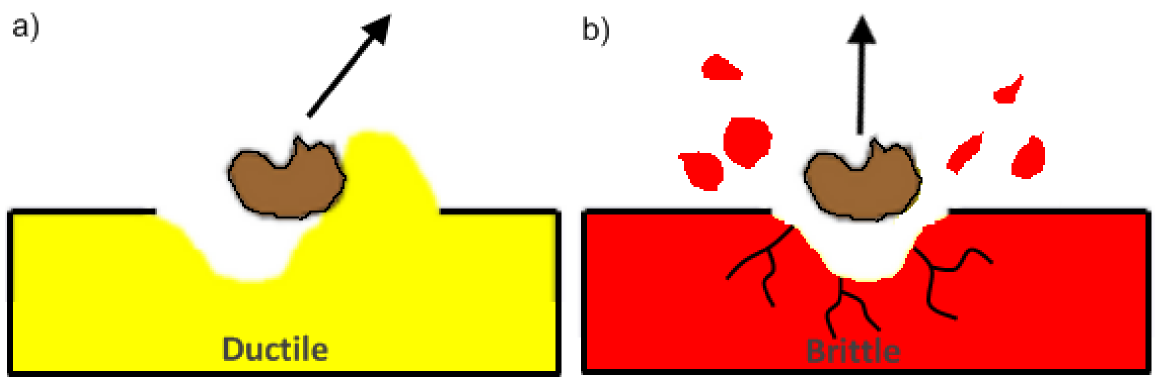

Figure 2.4 – Examples of the effects of high energy particle impacts upon (a) ductile and (b) brittle materials. The ductile material shows plastic deformation and abrasion after impact, while the brittle material shows subsurface cracking, cratering, fracturing and spallation of material.

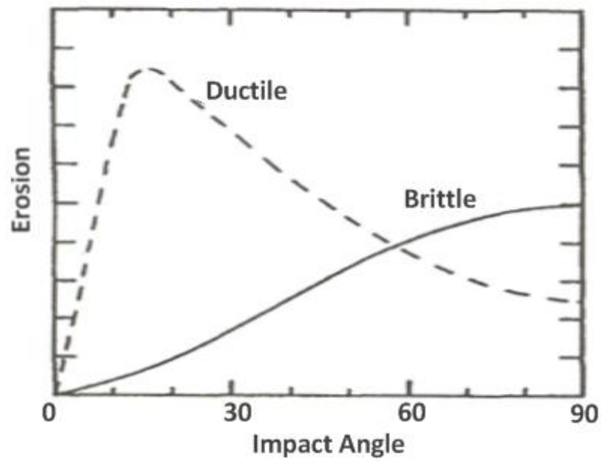

Figure 2.5 - General erosion trends for ductile and brittle materials as a function of impact angle. This graph shows the erosion peak for ductile materials at low angles, while the erosion peak for brittle materials is at 90 degrees. (adapted from [9]).

2.4.2 Brittle Erosion Mechanism

Ceramic materials with a high hardness and Young's modulus, such as titanium nitride or ternary nitride systems, undergo a different erosion mechanism than ductile materials. Erosion primarily occurs in these materials through crack coalescence generated by multiple particles impacting the surface as was shown in Figure 2.4b. Each impact needs to have high enough energy to initiate or propagate a crack within the material [11, 12]; otherwise the particles simply deflect off without damaging the material. Since this erosion mechanism is primarily dependent on how much energy the particle directly transfers to the coating upon impact, higher angle impacts are the greatest source of damage, with angles of 90 degrees, shown in Figure 2.5, being the most damaging. This has been verified through experimentation on multiple ceramic materials and coating systems [2, 9, 10, 13, 14].

2.4.3 Baseline and New Contour Blades

An initial compressor blade was modeled based off of an existing component. This blade specifically came from the first stage compressor of a turboshaft engine that is currently widely used in helicopters operating in relatively extreme environments. This blade model is referred to as the Baseline. A newer blade model for the same engine was developed in an effort to suppress leading edge curl deformation by thickening the leading edge geometry. This updated model is referred to as the New Contour Model. Verification through simulation was performed to determine the magnitude of possible deformation as well as the erosion protection the thicker leading edge provided. The two blade geometries investigated are shown in Figure 2.6.

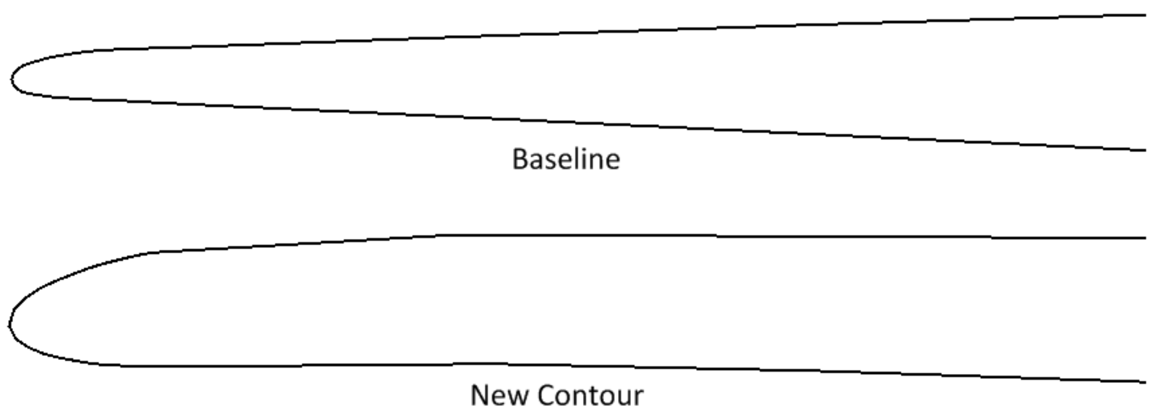

Figure 2.6 - Outlines of the Baseline and New Contour blades' leading edges.

The outlines shown in the figure are of the first ~0.16 inches of each blade's leading edge. The leading edge of each blade is on the left, the suction side is on the top, and the pressure side is on the bottom. These outlines were produced from measurements taken on physical blades by a coordinate-measuring machine (CMM). Although measurements were taken on almost the entire blade length, the entire length of each blade model was rarely used. Since only the leading edge response was being observed, it was much more computationally efficient to simulate only the first ~0.02-0.16 inches of the blade. The material properties of the blades used in the finite element model are discussed in the following paragraphs.

2.4.4 Blade Material Properties

One of the most important aspects of this finite elements modeling work was choosing and determining the correct material parameters to represent the blades. The Baseline and New Contour blades are composed of AM355 SCCRT stainless steel. AM355 is a precipitation hardening stainless steel. Its high tensile strength after heat treatment and very good corrosion resistance make it well suited for the environments a first stage compressor blade is expected to encounter.

In addition to AM355, the Baseline blade was further modeled using both a titanium and nickel-chromium based alloy. The alloys chosen were Ti-6Al-4V and Inconel 718. Ti-6Al-4V is considerably more elastic and lighter than AM355, having a lesser Young's modulus, hardness and density. Inconel 718 has a higher Young's modulus, a lesser hardness, but a similar density. The response of these materials with respect to leading edge curl deformation was compared to that of the Baseline's AM355.

Plastic and elastic data for all compressor blade materials were found in The Atlas of Stress-Strain Curves 2nd Ed [15] and the ASM Handbook Volume 19: Fatigue and Fracture [16]. The ASM Handbook was used to determine yield stresses and Young's

Moduli for Ti-6Al-4V [16 pp. 833, 967, 978] and Inconel 718 [16 pp. 35, 377]. AM355's yield stress and modulus were calculated from its elevated temperature curve in The Atlas of Stress-Strain Curves [15 pp. 259]. Other material data for AM355 was found in the ASM Handbook [16 pp. 713, 715]. A comparison of each material's Young's modulus, Poisson's ratio, hardness, density, and yield stress is s in Table 2.1.

Table 2.1 - Elastic and physical properties of the blade materials

Property/Material	**AM355**	**Ti-6Al-4V**	**Inconel 718**
Young's Modulus (kpsi)	23,500	17,000	29,000
Poisson's Ratio	0.3	0.33	0.3
Hardness (HRC)	52	40	42
Density lb/cu	0.2857	0.1600	0.2930
Yield Stress - 0.2% (kpsi)	260	145	170

AM355: Test Direction: longitudinal. Sheet thickness = 0.457 mm (0.018 inches). SCCRT: subcooled, cold rolled, tempered. RT, room temperature. Composition: Fe-15.5Cr-4.5Ni-3Mo. UNS S35500.
Ti-6Al-4V: Mill annealed - $\alpha + \beta$ hot work, anneal at 705°C for 30 min to several hours, air cool.
Inconel 718: Heat treatment: 980°C (1800°F) 3/4h, air cool; double age 720°C (1325°F) 8 h, furnace cool to 620°C (1150°F), hold for 10h, air cool.

2.4.5 Protective Coatings

The use of ceramic coating systems to prevent erosion can be partially based on the observed angle at which particles impact the blade. Tabakoff [17] used numerical simulation to find the trajectories of sand particles as they flowed through a turbojet engine. An example of different particle trajectories is shown in Figure 2.7. As is shown, a large number of impacts occur along the entire length of the pressure surface. Particles are also observed to impact off the leading edge and strike the suction side of the blade after rebound.

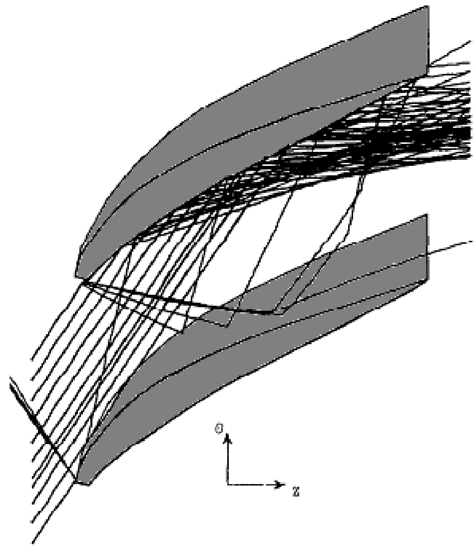

Figure 2.7 - 165 micron particle trajectories through a compressor. Two compressor blades are visible. (adapted from [17])

It was found that the impacts from large particles could occur anywhere along the entire turbine blade and at any angle. However, the highest velocity and most damaging impacts occurred nearest the leading edge. These impacts tended to occur at angles closest to 30-45 degrees. Due to the relatively small angle of these impacts, ductile erosion was prevalent on uncoated blades [17]. As previously mentioned, studies have shown that ductile erosion occurs mostly due to low angle impacts from small high energy particles. Also, these findings would suggest that a thin ceramic coating would offer significantly more protection from these small angle impacts than a ductile coating or just the substrate itself.

2.4.5.1 Titanium Nitride

An ideal coating material would need to be highly resistant to low angle and high energy hard particles. A promising material for coating application is titanium nitride

(TiN). TiN is a widely used surface coating that has found applications ranging from cutting tool edges to jewelry to prosthetic limbs. Because of its present widespread usage, the properties of and application methods for TiN have been extensively studied [2, 6, 10, 18, 20, 21]. Titanium nitride has been previously explored as a first stage compressor blade coating with positive results. This is due to its high hardness and Young's modulus as well as its relative inertness. Titanium nitride also has strong adhesion characteristics and a similar coefficient of thermal expansion to compressor materials. Preliminary studies have demonstrated that coatings as thin as 20 microns show a threefold increase in erosion life over just the base substrate [2]. Although TiN does not have as high erosion protection at large angles due to its highly brittle nature, it is still highly resistant to erosion at lower angles [17]. Since it has been demonstrated that a majority of impacts that occur on jet engine compressor blade leading edges are low angle, a thin TiN coating would potentially offer protection against erosion and curling of the blade.

The coating thickness has been shown to be directly proportional to how effective it is at protecting the underlying substrate, but depends on the working environment and erodent material, velocity, size, and morphology. The previously mentioned study by Nagy et al. [2] showed that increasing coating thickness prevents erosive wear up to a plateau at about 400 micron thickness (0.016 inches), as demonstrated in Figure 2.8.

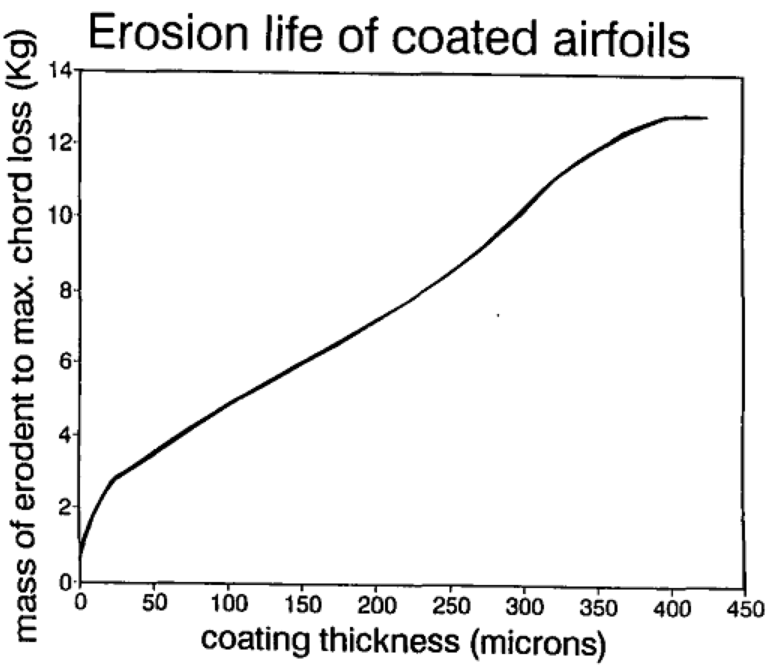

Figure 2.8 - As is demonstrated in this graph, the effectiveness of a coating system on a compressor blade is proportional to the thickness of the coating. However, in order to preserve the aerodynamic properties of the blade, coating thicknesses greater than 50 microns are rarely considered for practical use. [2]

A very thin coating has minimal to no impact on the aerodynamic properties of the blade, while increasing the coating thickness beyond 50 microns will begin to cause a less than negligible degree of impairment to engine performance. The ideal coating system should offer the best combination of erosion resistance and cost effectiveness, with a minimal impact on airflow or engine performance.

2.4.5.2 Material Properties of Titanium Nitride

Relative to the underlying substrate (AM355) used for this modeling work, TiN has a much higher modulus of elasticity and hardness but a much lower density. Material data for a TiN coating, including the Young's modulus and hardness, was taken from Latella et al. [18]. Other material properties for TiN were found in [19-21].

Table 2.2 - Elastic and physical properties of titanium nitride

Property	**Value**
Young's Modulus (ksi)	57,300
Poisson's Ratio	0.25
Hardness (HV)	2060
Density (lb/cu)	0.1951

[18] TiN: Deposition method: dual source pulsed cathodic arc system. Pulse length of 0.5ms with a frequency of 4.5 Hz. Arc current of 220 A and system base pressure of $1x10^{-5}$ Torr ($1x10^{-3}$ Pa) with N_2 gas flow rate at 50 sccm and chamber pressure at $6x10^{-4}$ Torr (0.08 Pa) during deposition.

2.4.5.3 Ternary Nitrides

Other coating materials considered for applications on turbojet compressor blades are titanium aluminum nitride (TiAlN) and titanium chromium nitride (TiCrN). Both of these materials belong to a class of compounds known as ternary nitrides. Ternary nitrides are compounds that consist of three elements, one of which is nitrogen, and can show a highly variable range of properties, depending on composition.

2.4.5.3.1 Titanium Aluminum Nitride

Titanium aluminum nitride (TiAlN), the most studied tertiary wear resistant compound, is a defect structure having a wide range of compositions and properties including hardness. TiAlN provides added oxidation and corrosion protection as aluminum can migrate to the surface forming a protective Al_2O_3 layer. TiAlN coatings have exhibited both high hardness as well as high erosion resistance. A peak in TiAlN hardness occurs where the lattice parameter is a minimum and the material is close to transitioning from a NaCl crystal structure to a ZnS crystal structure. The hardness increase of TiAlN (3500 VHN as compared to TiN) is most likely due to complexities of the crystal structure. Physical properties of TiAlN system which varies as a function of composition are: E = 434.7 GPa, G = 178.4 GPa, melting temperature of 2930^{o}C, thermal expansion coefficient = 7.5 µm/m-^{o}C, and specific gravity = 4.6 g/cc.

Interestingly, composite materials or composite features already exist in the ternary systems. For example, TiAlN, based on the composition of the bulk coating can be considered a composite material of TiN and AlN comprised of the Rocksalt and Wurtzite structures, respectively. It is believed that the proper ratio of the Rocksalt/Wurtzite phases is what gives TiAlN its unique properties of increased hardness and increased toughness under certain deposition parameters. Typically, increased hardness results in lower toughness. Current research efforts are expected to clarify this complex relationship of composition, Rocksalt/Wurtzsite ratio, hardness, and fracture toughness. The nanocomposite behavior of TiAlN is also seen with $Ti_{(1-x)}S_xN$. [22-25]

2.4.5.3.2 Titanium Chromium Nitride

Titanium chromium nitride (TiCrN) coatings are a class of coatings which typically incorporate Cr into a TiN based coating system in order to enhance specific characteristics of TiN including high temperature hardness and corrosion resistance. The increased resistance to corrosion and degradation of mechanical properties at higher temperatures is typically contributed to formation of protective chromium oxide compounds. The coating composition and microstructure is very dependent on the deposition technique. A wide variety of coating compositions can be produced including single phase TiCrN, or a mixture of phases such as TiN, CrN, Cr_2N, and the microstructure of these coatings can range from nanoscale columnar grains to an amorphous like microstructure. For many PVD techniques, a single phase of TiCrN with the NaCl structure is typically produced or a mixture of NaCl structured stoichiometric TiN and CrN compounds. The hardness values of the coatings can be tailored from similar to CrN (1200-2000 Hv) to greater than that of TiN (>3000 Hv). Other mechanical properties such as wear resistance can also be tailored with deposition parameters, so TiCrN is readily adaptable for a wide range of applications. [25-29]

2.5 Previous Finite Element Modeling Work

All modeling work for this thesis was performed using the finite element analysis (FEA) software Simulia Abaqus/Explicit v.6.7-1. Simulations were solved using an explicit time integration method. This method solves only for the displacements, velocities, and accelerations of the model for every time increment, which are on the order of fractions of nanoseconds [$0.1x10^{-9}$ seconds] in duration. The explicit solution method is relatively efficient at calculating solutions for very dynamic and non-linear responses. Since the non-linear plastic response of the blade upon particle impact occurs in less than a microsecond [10^{-6} seconds], this makes Abaqus/Explicit an excellent choice for particle impact modeling. The use of Abaqus for the finite element modeling of erosion and deformation to compressor blade substrate and coating materials has been successfully demonstrated in a number of studies.

2.5.1 Deformation to Metallic Substrates under Impact from Small Particles

Xi Chen used Abaqus/Explicit to examine the stresses resulting from particle impacts simulating foreign object damage. In two separate studies [4, 30], Chen analyzed the residual stresses and geometric stress concentrations resulting from simulated small particle impacts on the leading edge and main body of Ti-6Al-4V turbine blades. The resulting implication these stresses had on fatigue cracking was also explored.

In each study, a single rigid particle was modeled to impact and rebound from the substrate at a normal angle. The substrate model for the leading edge was simplified to be a thin metallic sheet and the model for the blade body was a semi-infinite axisymmetric block. For impacts along the blade body, Chen found that the impact crater's normalized depth and width, δ/D and w/D (where D is particle diameter, δ is indent depth, w is indent width) is primarily dependent on a dimensionless kinetic energy parameter Ω, and can be determined analytically as shown in equation 2.1.

$$\Omega = KE/(\sigma_Y D^3) = \pi/12(\rho_P/\sigma_Y)v_0^2 \qquad (2.1)$$

Where:

Ω = dimensionless kinetic energy parameters

σ_Y = substrate yield stress

D = the impacting particle diameter

ρ_P = particle density

v_0 = initial particle velocity

Chen also found that stress concentrations and deformation size along a leading edge were primarily dependent on the normalized residual penetration depth, δ/D, and therefore also highly dependent on the kinetic energy parameter. Stress concentrations were highest along the impact crater base, and increased with increasing penetration. Residual stresses also increased the stresses acting on small fatigue cracks, especially at the bulge tips and outside the indent [4]. These findings show the weakened plastically deformed areas around the particle indent characteristic of the beginnings of ductile erosion.

2.5.2 Erosion of Metallic Substrates

Eltobgy and Elbestawi [31] also used Abaqus/Explicit to model erosive wear on a block of Ti-6Al-4V under impact from small rigid steel particles. Erosion rates and volume for the substrate was studied based on number of particle impacts, particle speed, impact angle, and particle size. Their results closely matched those previously reported in literature [32-35] through experimentation and numerical methods. Erosion rates of the metallic block were found to be an exponential function of particle velocity and a parabolic trend with angle of impact.

2.5.3 Erosion and Deformation of Titanium Nitride Coating Systems

Sun and Bell [36] used Abaqus to model the plastic deformation of multiple titanium nitride coated substrates contacted by a rigid sphere. The substrate materials of high speed steel, a titanium alloy, and an aluminum alloy with TiN coatings of various thicknesses between 0 to 9 microns were modeled. They found that yielding almost always initiated in the coating/substrate interface and would grow in the substrate along the interface and away from the coating. Yielding of the coating at the interface would not occur until significant plastic deformation has taken place in the substrate. The strains in these two distinct plastic zones can lead to interfacial microcracking and eventually decohesion of the coating. Decohesion can also occur when shear stresses at the interface surpasses the bond strength; however, coating deposition methods allow for optimization of bond strength which results in plastic strains in the substrate causing a majority of coating decohesion. Sun and Bell also determined that the overall load bearing capacity of the TiN/substrate interface increases with increasing substrate strength (yield strength and Young's modulus) and increasing coating thickness. They also found that there is a greater relative increase in coating-substrate system strength for softer substrates. This implies that titanium nitride is more effective at increasing the load bearing ability of softer substrate materials.

BieLawski and Beres [37] used Abaqus/Explicit to model the tensile surface stresses in multi-layered TiN coatings on 17-4 PH steel under single particle impacts. Because the primary mechanism for coating erosion is brittle fracture due to tensile surface stresses, coating layer thicknesses, Young's moduli, and bond layer effects were parametrically studied in an attempt to minimize the surface tensile stresses. They found for monolayer coatings, a higher thickness and lower Young's modulus resulted in the best stress reduction. A titanium bond layer was found to decrease surface stresses, although only marginally. For multilayer coatings, the best coating architecture from a surface stress reduction standpoint was a low surface layer Young's modulus with a relatively higher subsurface layer Young's modulus. These results were achieved through modeling only the first stages of coating erosion before crack propagation.

Hassani et al. [38] used Abaqus/Explicit to model various titanium nitride coating systems on titanium alloy and stainless steel substrates to estimate their erosion resistance based on maximum tensile surface stresses. They parametrically studied coating thicknesses between 1 and 10 microns, TiN Young's moduli between 200 and 600 GPa, and particle impact velocities between 50 and 300 m/s with 10-200 micron diameter particles. Their results correspond to BieLawski and Beres, in that a lower Young's modulus and higher thickness corresponded to better stress reduction. They also determined that stronger substrates outperform weaker ones since penetration depth of the impacting particle has a large impact on coating surface stresses. Hassani et al. also calculated a critical stress threshold, σ_{crit}, based on equation 2.2.

$$\sigma_{crit} = K_c/(\pi * l) \qquad (2.2)$$

Where:

σ_{crit} = the critical stress for cracking

$K_{c,}$ = the fracture toughness

π = 3.141…

l = the initial defect size

From this calculated critical stress (3.95 GPa) they determined cracking was likely to occur under a majority of the tested conditions. They also found that most of their tested multilayer coating combinations resulted in at least a half stress reduction compared to a monolayer TiN.

2.6 Abaqus FEM Calculations

There were several different methods within Abaqus to evaluate the different material responses (elastic, plastic, and brittle) being examined. From these methods, it had to be determined which were the best suited for the modeling efforts. This section will explain the materials and solutions methods chosen.

2.6.1 Abaqus/Explicit

The Abaqus software package has two main solution methods for FEM analysis, Standard and Explicit. For simulations that are highly dynamic and contain large deformations, it is more efficient to use the Explicit solver. Explicit solves for the displacements, velocities and accelerations of each node using explicit integration, meaning the solution is dependent only on the inputs from the immediate preceding state. Standard solves for each time increment by using an iterative method to solve a set of nonlinear dynamic equations. The efficiency that is produced from using Explicit comes mainly from the lack of iteration and simpler matrix inversions.

2.6.2 Material Models

There are a number of different ways available within Abaqus to model the elastic, plastic, and failure responses of materials. A primary goal of finite element modeling is to use the proper models that will accurately reproduce the materials' response. This becomes difficult when material data is lacking, or the material definition within Abaqus asks for esoteric data that would only result from a highly specific set of experiments.

2.6.2.1 Elasticity Model

The elastic response of the blade, coating, and particles were all modeled using Abaqus's linear elastic behavior model [39 s. 17.2]. This model is valid and stable for strains less than 5 percent. Modeling particles using only an elastic model introduced some initially difficult to diagnose instability that resulted in simulation abortion. It was found that, under some conditions, particles were undergoing strains much higher than 5 percent. This required minor reconfigurations to the simulation parameters. All materials were also assumed to be viscoelastic. Viscoelasticity implies the materials behave purely as solids, in that their straining was not a function of time but only of applied stresses.

An isotropic material definition was assumed. All materials were considered to be non-directionally dependent. The shear modulus (G) used for stress and strain calculation was determined by Equation 2.3.

$$G = E/2(1+\nu) \qquad (2.3)$$

Where:

E = the material's Young's modulus

ν = the material's Poisson's ratio

Using this calculated shear modulus along with the material's Young's modulus and Poisson's ratio, the normal (ε) and shear (γ) strains for two dimensions can be determined. The matrix used to determine the relationship between stresses and strains is given in Equation 2.4

$$\begin{Bmatrix} \varepsilon_{11} \\ \varepsilon_{22} \\ \gamma_{12} \end{Bmatrix} = \begin{bmatrix} 1/E & -\nu/E & 0 \\ -\nu/E & 1/E & 0 \\ 0 & 0 & 1/G \end{bmatrix} \begin{Bmatrix} \sigma_{11} \\ \sigma_{22} \\ \sigma_{12} \end{Bmatrix} \qquad (2.4)$$

Further expanding these calculations into the third dimension yields a total of six stress and strain variables, with the relationships between them given in Equation 2.5.

$$\begin{Bmatrix} \varepsilon_{11} \\ \varepsilon_{22} \\ \varepsilon_{33} \\ \gamma_{12} \\ \gamma_{13} \\ \gamma_{23} \end{Bmatrix} = \begin{bmatrix} 1/E & -\nu/E & -\nu/E & 0 & 0 & 0 \\ -\nu/E & 1/E & -\nu/E & 0 & 0 & 0 \\ -\nu/E & -\nu/E & 1/E & 0 & 0 & 0 \\ 0 & 0 & 0 & 1/G & 0 & 0 \\ 0 & 0 & 0 & 0 & 1/G & 0 \\ 0 & 0 & 0 & 0 & 0 & 1/G \end{bmatrix} \begin{Bmatrix} \sigma_{11} \\ \sigma_{22} \\ \sigma_{33} \\ \sigma_{12} \\ \sigma_{13} \\ \sigma_{23} \end{Bmatrix} \qquad (2.5)$$

(Equations adapted from [39 s. 17.2.1])

2.6.2.2 Plasticity Model

Abaqus's classical metal plasticity model with isotropic hardening was used for all modeled ductile materials [39 s. 18.2]. A Mises yield surface was used with this model. Mises yield surfaces assume yielding is independent of equivalent pressure stress. This is an assumption that has been confirmed experimentally for most metals, except under certain specific conditions that are not expected to be encountered during particle impact and deformation. With the Mises yield surface, an isotropic hardening model was used for plastic straining.

Isotropic hardening assumes that there are uniform changes to yield surface size and yield stresses in all directions as plastic deformation occurs. This was used for current leading edge modeling since Abaqus recommends the use of it for gross plastic straining. Using this model, the yield stress is defined as a tabular function of plastic strain, with Yield stresses for states between given data points being interpolated and yield stresses for states past the last strain value are constant at the last value given.

The yield stress for most materials has a large degree of dependence on the strain rate the material is undergoing. Larger strain rates usually result in a larger yield stress. Since the impacts occurring in this simulation work were highly dynamic, strain rates are expected to be very large. This required the inclusion of rate-dependent yield stress, or work hardening.

To define work hardening within Abaqus yield stress ratios were used. This assumed that the strain rate behavior is separable, and stress-strain dependence is similar at all strain rates. Equation 2.6 shows how the dynamic stress-strain behavior is calculated.

$$\bar{\sigma}(\bar{\varepsilon}^{pl}, \dot{\bar{\varepsilon}}^{pl}) = \sigma^0(\bar{\varepsilon}^{pl}) R(\dot{\bar{\varepsilon}}^{pl}) \qquad (2.6)$$

Where:

$\bar{\sigma}(\bar{\varepsilon}^{pl}, \dot{\bar{\varepsilon}}^{pl})$ = the dynamic stress-strain behavior

σ^0 = the static yield stress

$\bar{\varepsilon}^{pl}$ = the equivalent plastic strain

$\dot{\bar{\varepsilon}}^{pl}$ = the equivalent plastic strain rate

R = the ratio of the yield stress at nonzero strain rates to the static yield stress.

R is defined to be equal to 1.0 when $\dot{\bar{\varepsilon}}^{pl}$ = 0.0. Specifying R within Abaqus consisted of supplying a table of R values for certain strain rates.

2.6.2.3 Brittle Model

The brittle model within Abaqus contains three main parts: a brittle cracking model to simulate tensile weakening of the material upon damage, a shear retention model to simulate weakening shear retention of the material, and a failure model that removes elements upon tensile failure. The brittle model within Abaqus is useful for modeling concrete and other brittle materials [39 s. 18.5.2].

2.6.2.3.1 Cracking

To define the brittle fracture and failure properties for the brittle material (TiN) used in the coating models, Abaqus's concrete cracking model was used. This model provided a capability for modeling the progressive damage and failure of brittle materials. The model's main assumption is that cracking is the primary response of the material behavior upon loading. The model also assumes that the behavior of the response of the material is dominated by tensile stresses and that compression is a purely linear elastic response. These assumptions are valid in that the response of titanium nitride is nearly that of a purely brittle material.

The concrete model further assumes that the material follows an elastic response based on the material's Young's Modulus until a certain critical tensile cracking stress is reached. Upon reaching that stress, the material is damaged and progressively weakens until complete failure at a certain strain. The cracking model does not track individual micro-cracks, but only macro-cracks. This correlates to numerous microcracks existing at a certain point within the model, the presence of which affects the stress and material stiffness associated with the point during calculation.

The post failure behavior of the material is defined by tension stiffening. A stress-strain curve associated with the cyclic behavior of this is given in Figure 2.10. Once the material passes the critical stress/strain value, it follows a curve of stress strain values until complete failure. If the stresses on the material relax then the material follows an elastic curve given as the slope between the origin and the stress for the highest strain value the material reached.

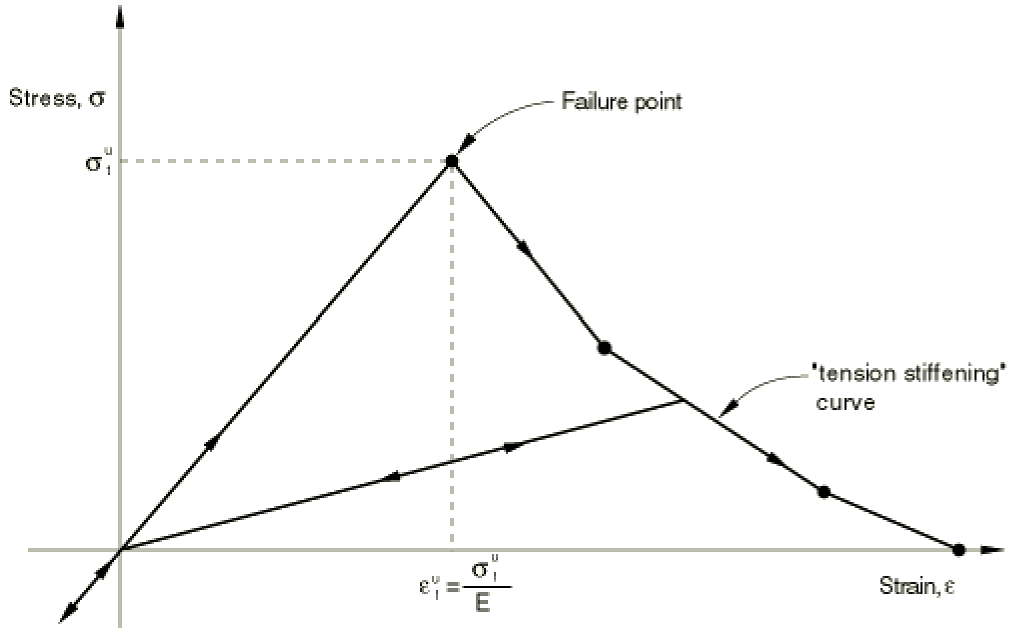

Figure 2.10 - Curve describing the assumed stress strain response of brittle materials. The material reacts elastically based on its Young's modulus until the failure stress is reached. The material then follows a 'tension stiffening curve' which is specified in a table. (adapted from [39 s. 18.5.2])

2.6.2.3.2 Shear Retention

Using this cracking model, it is also necessary to define the shear retention of the material as it undergoes progressive cracking and damage. This is due to how the shear stiffness of a brittle material diminishes as it cracks. The definition for shear retention is a function of the opening strain across the crack, with shear retention given as a ratio of the damaged shear modulus to the undamaged shear modulus. These values are defined in a table, with a minimum of two points needed. One point denotes 100 percent shear retention with zero strain, and a second point is used to denote zero percent shear retention at a given failure strain. A curve of shear retentions and associated strains between those two points can also be defined for additional accuracy. As will be discussed in the next chapter, the material definition for only used two points, assuming a linear relationship between crack initiation and eventual failure.

2.6.2.3.3 Failure

In order to simulate erosion of the coating, it was necessary to include a brittle failure criterion into the simulation. This criterion removes completely failed elements from the simulation when a certain strain value is reached for one, two, or three coordinate directions. The main disadvantage to using this model was the fact that it relied purely on tensile stresses for calculation. This can bring inaccuracies into the simulation through the fact that most brittle materials can still withstand compressive stresses even after experiencing tensile failure. However, as will be discussed in the next chapter, preliminary modeling of the brittle fracture of TiN-based coatings replicated the progression of erosive failure observed in the field.

Chapter 3

Experimental Procedure for Finite Element Modeling with Abaqus

There are many advantages to using finite element analysis to model dynamic events such as particles impacting a compressor blade. Modeling aids in the design process of complex aerospace components in which complex phenomenon can be modeled without the high cost and long lead times in constructing prototype systems. In addition, modeling allows faster and cheaper ways of investigating different material systems and designs while also allowing for a closer examination of the transient stresses and strains that occur during high velocity impacts. The methodology used to create and setup simulations using Abaqus will be discussed in this chapter, as well as the different material models used within Abaqus to define the material properties for the blades, coatings, and particles.

3.1 Model Creation and Simulation Setup

Every individual component of the simulation required a separate model to be created. In general, these models included both the components' and particles' geometries and property definitions. Separate models were developed for each particle size, each blade design, and the various coating thicknesses for each blade design. As mentioned previously, the blades were modeled at both their full length and only the leading edge to reduce simulation processing time. The leading edge was most commonly modeled as the first 0.16 inches of the blade. Model parameters were often selected to decrease the overall simulation time and size in an attempt to balance computational efficiency with simulation accuracy.

3.1.1 Part Geometry

Coordinate data used for the blade geometry model was obtained from coordinate measuring machine (CMM) measurements of the Baseline and New Contour blades. To create the blade models for use within Abaqus, a program was created to process the coordinate data and output an appropriate blade model. The program used data for all of the (x, y) coordinate pairs taken from the blade measurements. The component blade model was constructed by iterating over and drawing lines between the ordered (x, y) pairs to obtain a two dimensional outline of the component, which was then used to create the final two or three dimensional model.

The geometry for the ceramic coating was created by first taking the boundary coordinates for the metallic blade model as the inner layer of the coating, which was to be in direct contact with the blade. For every coordinate on this layer, another coordinate point was created with an offset of the desired coating thickness. The offsetting angle for this point was derived from the slope between the two neighboring coordinate points. For coordinates on the far edges of the full length Baseline and New Contour and all 0.16 inch leading edge models where there is only one neighboring point, the offset was just taken +/- vertically.

The creation of a three dimensional model involved taking the base two dimensional model and extruding it some width into the third dimension. Extrusions were initially performed to the blade's full width of ~1.8 inches, but were shortened to 1.0

inches and then eventually to 0.5 inches. This was done to limit computation time and improve efficiency. The shortened width of the blade was not believed to greatly effects its overall response since observations of the three dimensional blade model during and after particle impacts have shown its elastic and plastic responses to be relatively localized.

The particles were modeled to be circular for two dimensional work, and spheres for three dimensional work. The geometry of the impacting particle can have a significant impact on the resulting deformation. However, modeling different geometries was well beyond the scope of this effort. Different particle geometries and types were used for in-house analysis, including irregularly shaped alumina and modified c-spec particles, as well as spherically shaped glass beads. A comparison of the different particle shapes in shown in Figure 3.1. The irregularly shaped particles, (a) alumina and (c) modified c-spec, are more likely representative of particles impacting in-field blades. The (b) glass beads are more representative of the (d-e) particle models impacting the blade in this modeling work.

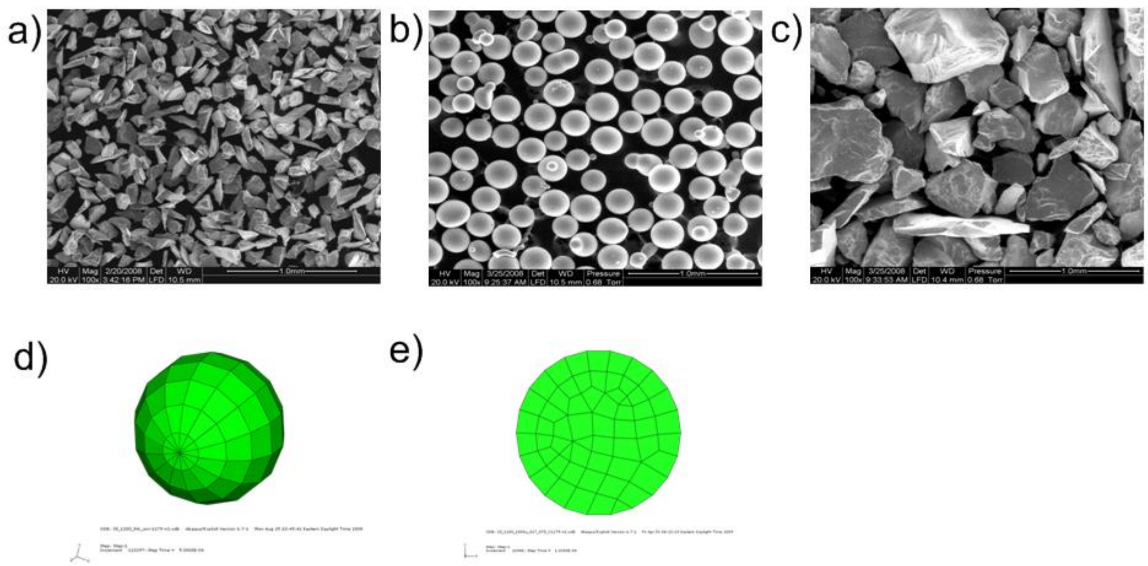

Figure 3.1 - A comparison of the different particle geometries used for in-house testing and finite element analysis: (a) irregular alumina, (b) spherical glass beads, (c) modified c-spec (silica), (d) three dimensional particle model, (e) two dimensional particle model.

The particles were also modeled under the assumption that they elastically respond upon impact, but do not deform plastically or fracture. This has been observed to not always be the case, especially for high velocity impacts. Post analysis of impinging media has confirmed that some particles do fracture after impact.

3.1.2 Property Assignment

After a component's geometry was created, a set of property definitions were assigned to it. The property definitions were assigned through what Abaqus terms a section assignment. A section assignment takes a geometric section of a component part (for current modeling work it was only necessary to create a single section for every component) and assigns certain properties to it. These properties include an in-plane thickness for two dimensional models, which will be explained in the next section, and a material property definition. A material property definition contains all of the material data necessary for modeling the component as an actual material.

3.1.2.1 Section Assignment and In-plane Thickness

As was previously stated, a section is used to assign material properties to a given part. For two dimensional models, the section may also contain a value for the part's in-plane thickness. The in-plane thickness can be thought of as the distance the part extends into the plane; the hypothetical width of the part's third dimension. A larger value would result in less deformation for a given particle impact, while a smaller value would result in greater deformation. An appropriate value would be close to the amount of blade width affected by a single particle impact. Based on observations made during the three dimensional modeling work, this value had been demonstrated to be between about 0.005 and 0.08 inches. However, it was heavily dependent upon particle size and velocity. The value used for a majority of the simulations was 0.027 inches, since it had provided accurate results while keeping consistency with all previous work. Parametric evaluation of different in-plane thicknesses at varying velocities, angles, and particle sizes had also shown this value of 0.027 inches to be appropriate. Appropriate, in this sense, meaning that accurate magnitudes of deformation were obtained using the tested thicknesses, velocities, angles, and particles sizes as compared to field evaluated components.

3.1.2.2 Material Properties

When creating a section on a given component part, a material property had to be assigned to it. A material property includes definitions for the physical, elastic, plastic, brittle, and failure properties of the material. It is also possible to specify more specific properties such as electrical, thermal, and fluidic characteristics. Not all properties need to be specified for a simulation to run. For modeling contact between impacting bodies, only the density of each material needs to be defined. Each additional material definition adds more accuracy to the model.

3.1.2.2.1 Elastic Properties

For current modeling work, all material properties were given the physical property of density, and the elastic property definitions of Young's modulus and Poisson's ratio. The impacting hard particles were specified using only this definition. The material for the particles was assumed to be that of sedimentary rock, with a Young's modulus value provided by Mark's Standard Handbook for Mechanical Engineers [40]. The Poisson's ratio and density for the particle were assumed. The properties for all of the other materials were discussed in the previous chapter. Table 3.1 lists the Young's moduli, Poisson's ratios, and densities used to define the materials used in this modeling effort.

Table 3.1 – Elastic property definition for all materials

	AM355	**Ti-6Al-4V**	**Inconel 718**	**TiN**	**Particle**
Young's Modulus (ksi)	23,500	17,000	29,000	60,000	15,000
Poisson's Ratio	0.3	0.33	0.3	0.27	0.3
Density (lbf s^2/in^4)	0.00074	0.0004144	0.0007589	0.000505	0.000258

3.1.2.2.2 Plastic Properties

The three ductile metals modeled (AM355, Ti-6Al-4V, Inconel 718) all required the use of a plastic material definition. These definitions were used to specify both the plastic and work hardening behaviors of all of the materials. As was mentioned in the previous chapter, the plastic behavior for a given material is defined by a table of yield stresses versus plastic strains. The values used to define the three materials modeled are listed in Table 3.2.

Table 3.2 – Plastic behavior of AM355, Ti-6Al-4V, and Inconel 718

AM355		**Inconel 718**		**Ti-6Al-4V**	
Yield Stress (psi)	**Plastic Strain**	**Yield Stress (psi)**	**Plastic Strain**	**Yield Stress (psi)**	**Plastic Strain**
240,000	0.0	161,500	0.0	151,013	0.0
259,100	0.000773	170,000	0.002	158,961	0.002
1,792,000	1.719	853,526	2.0	792,266	2.0

As listed in Table 3.2, the table of yield stresses and strains has three rows of values. The first row defines a point at the highest applied stress immediately prior to yielding. The second row gives a point defining the initiation of yielding of the material. The values for AM355 were calculated and determined from a stress-strain curve [14], while Ti-6Al-4V and Inconel 718 used given 0.2 percent yield stress values [15]. The third value was created for additional model stability, and was calculated based on the slope between the materials' yield stresses and the materials' ultimate tensile stresses. This extra data point was calculated for a point far beyond the strain limits the material would experience during simulation. For modeling without a material definition including material failure, if a part of the model would strain beyond the final data point, model instability would occur and the simulation processing would possibly cease or produce poor results. An example of the results of a simulation with and without the extra point is presented in Figure 3.2. As can be observed, the additional data point greatly increased model stability without have a large effect on the overall deformation shape or magnitude.

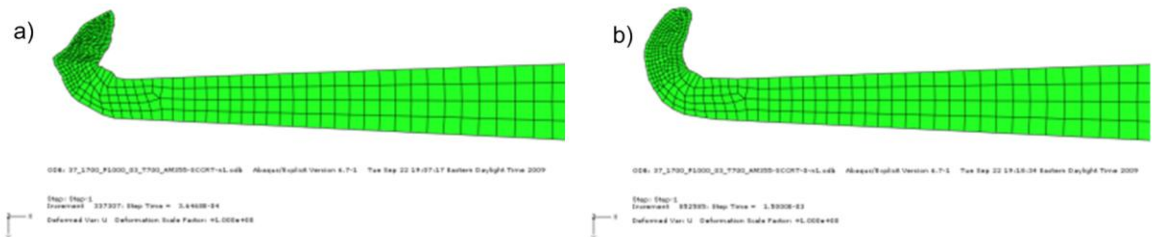

Figure 3.2 - Curled Baseline blade (a) without and (b) with the extra data point.

In addition to the plastic behavior of the material, a definition for work hardening was included. As was mentioned in the previous chapter yield stress ratios were used to define work hardening within Abaqus. Table 3.3 lists the values used to define the work hardening behavior for all of the material by the relationship given in Equation 2.6. These values were calculated by Pitterle [41] to define work hardening of 10 percent.

Table 3.3 – Work hardening behavior given defined as the plastic strain rate for different yield stress ratios

Yield Stress Ratio (σ)	**Equivalent Plastic Strain Rate (R)**
1.00	0
1.05	0.001
1.10	0.01
1.15	0.1
1.40	10
1.60	100
2.00	900

3.1.2.2.3 Brittle Properties

Titanium nitride required a brittle definition within Abaqus to specify its post-cracking damage and failure behaviors. Table 3.4 lists the values used to define the post-cracking behavior for TiN modeling.

Table 3.4 – Table used to specify post-cracking-initiation behavior for TiN

Direct Stress After Cracking (psi)	Direct Cracking Strain
122,000	0
55,000	0.0186
0	0.0481

Table 3.4 lists three rows of data. The first row is a given stress value immediately before cracking initiates. The third row is the strain value at which there is crack saturation within the material. The middle row is an intermediate value for addition accuracy in the model. The values in Table 3.4 were determined from given values in Latella et al. [18].

The brittle material model for TiN also needed a definition for shear retention. The definition used for simulation was a curve of two points, which are listed in Table 3.5.

Table 3.5 – Values used to specify shear retention for TiN

Shear Retention Factor	Crack Opening Strain
1	0
0	0.0481

The first point given specifies that there is one hundred percent shear retention for zero damage, or a strain beneath the damage initiation value. The other point specifies that there is zero percent shear retention, or complete shear failure, for the strain at which the coating fails. There is a linear relationship interpolated for strain values between the two points. This simplified definition was used due to a lack of data on the shear retention behavior for titanium nitride.

The brittle model for titanium nitride also included a value used to define failure removal of failed elements. This value was the same strain value specified previously for shear retention and post-cracking behavior failure: 0.0481. It was also observed that models without this failure option tended to produce unrealistic results as shown in Figure 3.3. It should be obvious from the figure why the choice was made to include this option in most simulation work.

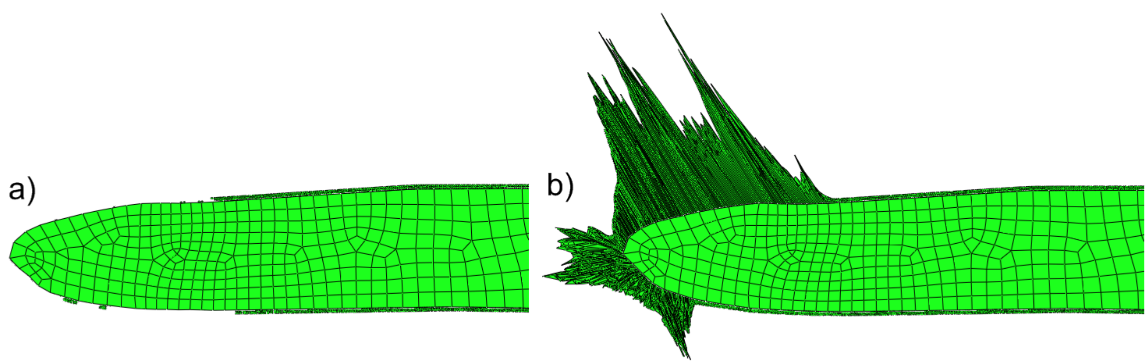

Figure 3.3 - The result of a simulation with (left) and without (right) a specified failure point for element deletion.

3.2 Meshing

A mesh is the FEM representation of a geometric model defined through nodes and elements. The meshing process takes the basic geometric shape of the model and converts it into the nodes and elements necessary for processing the FEM calculations. A node can be considered a discrete point, while elements are a finite shape made of connected nodes. Most of the element shapes used for this modeling were quadrilateral, and were composed of four connected nodes for two dimensional modeling and eight connected nodes for three dimensional modeling. Figure 3.4 gives an example of both two and three dimensional elements.

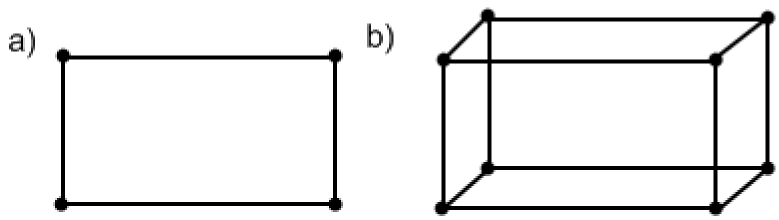

Figure 3.4 – A single (a) two dimensional element and (b) three dimensional element.

3.2.1 FEM Mesh Considerations

Considerations for meshing include how fine (size of elements) the mesh is throughout the different regions of the part, the shape of elements, and the type elements that are used. Generally, it is ideal to have small element sizes near the area of greatest deformation. This improves accuracy of the model, and helps to prevent failure and instability of the mesh during simulation. In compressor blade modeling, smaller elements were used on the leading edge, with a gradual increase in element sizes as distance from the leading edge increased. Tapering element sizes allowed more elements to be placed where accuracy was important while still keeping the number of total nodes and elements down to limit the amount of processing. A well-configured mesh will strike the ideal balance between simulation accuracy and computation time.

3.2.2 Seeding

The creation of a mesh within Abaqus was done by first selecting a meshing method and applying seeds. Seeds are the basis for mesh creation by being the initial nodes from which the mesh is developed. They are only applied to the edges of the model geometry. Internal nodes are created based on the particular meshing algorithm selected. Creating a higher density of seeds along a certain edge will result in a finer mesh throughout that region of the model. Although it is possible to manually create a mesh without using Abaqus's internal meshing algorithms, this was not done because of the minimal benefits and increases to turnaround time between mesh creation for different models.

3.2.3 Element Types

Along with defining the mesh for the model, the type of elements for the model also needed to be specified. The element types determine which specific calculations Abaqus uses for the given simulation. Abaqus provides a large number of different element types [39 s. 21-26], with each element type being useful for specific applications. For two dimensional modeling of curl or erosion, the most appropriate element type was that of ‘Plane Strain.’ This element type uses zero normal and shear strains for the third dimension under the assumption that the modeled part has a large in-plane thickness relative to the planar (x, y) dimensions. This correlates to an aircraft compressor blade as part of a blisk, which has a much longer radial length than thickness or width. For three dimensional modeling, the element type ‘3D Stress’ was used. This element type was the most appropriate three dimensional element, in that it does not make any assumptions about the stresses and strains the model will undergo during simulation.

3.2.4 Preventing Mesh Instability and Simulation Failure

In simulations with particles of a large enough size and velocity to result in high energy impacts with large deformation, distortion of a mesh to the point where the simulation is unstable and resultantly fails had a high possibility. This failure occurred due to instability in the calculations, where the solution for a certain increment is unable to be produced. High energy impacts that cause a large deformation wave tend to have a high probability of distorting meshes. There are a number of options within Abaqus to control these distortions to prevent or delay the failure of the simulation. The two used for current modeling work were Distortion Control and ALE (Arbitrary Lagrangian-Eulerian) Adaptive Meshing.

3.2.4.1 Distortion Control

Distortion Control [39 s. 21.1.4] attempts to prevent the elements comprising the model from distorting beyond a certain limit. This limit is defined in a way to ideally prevent failure of the simulation caused by excessive compression of the mesh. When a mesh is not fine enough relative to the strain gradient or amount of compression, an element might invert in on itself resulting in a negative or undefined area. This is demonstrated in Figure 3.5.

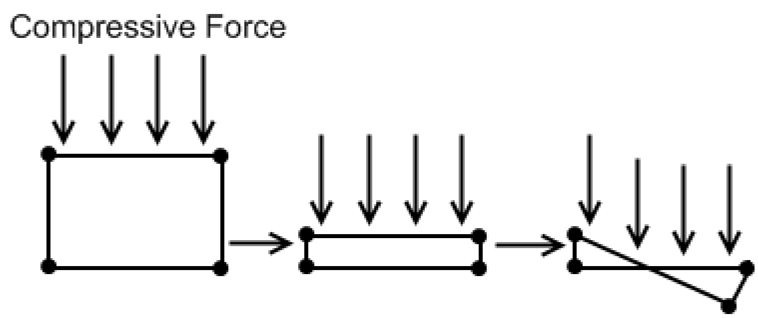

Figure 3.5 - The progression of a quadrilateral element to failure under a high compressive load. The final state is an example of an element with a negative or undefined area.

Distortion control attempts to prevent this type of mesh failure by not allowing an element to deform beyond a certain length ratio. This value is the ratio of element characteristic lengths between the distorted and undistorted elements. A characteristic length (L_c) can be considered the average distance between connected nodes on an element and is determined by Equation 3.1 for two dimensional elements.

$$L_c = \alpha * \mathrm{sqrt}(\ A_e\ ) \qquad (3.1)$$

Where:

α = a constant (1.0 for two dimensional elements)

A_e = the area of the element

The default value for the ratio of distorted to undistorted characteristic lengths for a given element, 0.1, was used in most simulations.

3.2.4.2 ALE Adaptive Meshing

ALE Adaptive Meshing [39 s. 12.2] is a tool that remeshes the model as the simulation runs. This remeshing allows the mesh to move independently of the material. Every given number of increments, Abaqus will analyze what portions of the mesh have undergone deformation and remesh the region appropriately to prevent mesh distortions from occurring. An example of how ALE Adaptive Remeshing might alter a mesh within a simulation is demonstrated in Figure 3.6. It is observed that the structure of the mesh is changed independently from the geometry of the deformed model.

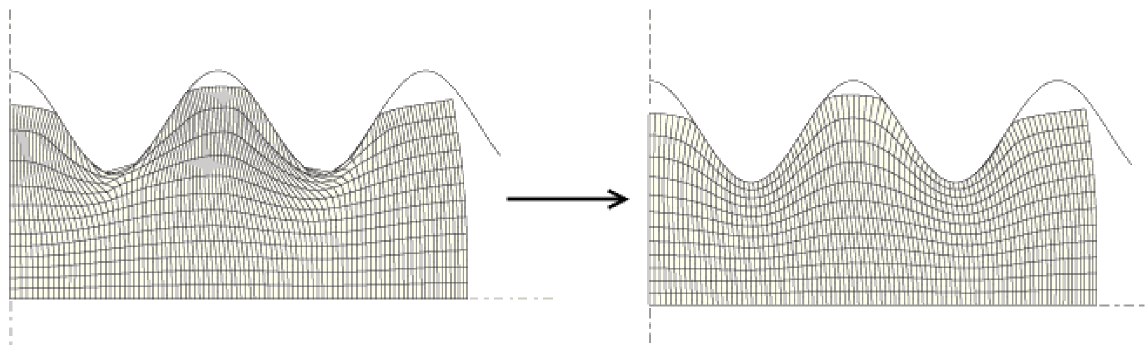

Figure 3.6 - A demonstration of how ALE Adaptive Meshing might remesh a deformed model. (adapted from [39 s. 12.2.1])

Adaptive remeshing will slightly increase the processing time for a simulation. This time increase is dependent on how often remeshing is set to occur. ALE Adaptive Meshing is especially useful in simulations where drastic plastic deformation is expected to occur, such as to a blade undergoing leading edge curl.

Distortion Control and ALE Adaptive Meshing could only be used exclusively from one another. They were also not able to work with a brittle material model, so they were only applied to the blade meshes. It was also observed that these methods were not absolutely effective. Distortion and failure of meshes still regularly occurred on many models, even with the highest possible degree of distortion control set. It is worth mentioning that the initial mesh configuration for a model was far more effective in preventing failure than any settings for distortion control.

3.3 Assembly and Simulation Parameters

Once the individual parts for a simulation were created and defined, they were imported into an assembly. The assembly held the parts' final configurations and relative positioning for the simulation. The assembly also contained the definitions for the parameters of the simulation, including boundary conditions, velocities, interactions, and constraints.

3.3.1 Boundary Conditions

Boundary conditions are the part of the model that is held fixed relative to one or all global or rotational coordinates. Boundary conditions can be defined as part nodes, element edges, or certain geometric features. The main purpose of the added boundary condition for this simulation work was to stabilize the blade and remove the possibility of large deflections. Large deflections were caused by particles impacting the blade at such a high rate or with such high energy that the blade continues to deflect without being able to oscillate around its level position. After enough impacts, the blade would eventually deform into the highly deflected state as shown in Figure 3.7. The high frequency of particle impacts deflected and eventually deformed the blade model to an unrealistic degree. This geometry of deformation has never been observed and is likely impossible to occur in reality, so the additional boundary condition was necessary.

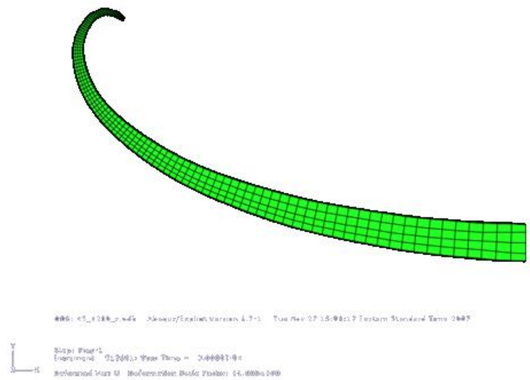

Figure 3.7 - The result of an early simulation attempt.

The boundary condition was reasonable to assume for a number of reasons. One reason is that the impact of large particles was occurring at a much greater frequency in the simulations than would likely occur in situ. Also, most compressor blades/blisks have design features that limit oscillations, which the simplified models used in the simulations were lacking. Rather than allow time for the blade deflections and oscillations to dampen out, it was much more computationally efficient to help force the damping through an expanded boundary condition.

Most of the simulations were run with a boundary condition set at 0.02 to 0.16 inches back from the leading edge. This allowed only a small percentage of the blade to deform during the simulation. A range of boundary condition sizes was evaluated in order to determine the most appropriate size for reproducing leading edge curling. A boundary condition too small would be too restrictive and not allow the blade to curl or be unrealistic and only allow the blade to deform into a given geometry and magnitude. A boundary condition too large would result in higher than observed deformation sizes with distorted geometries.

3.3.2 Velocity Fields

The velocity field is what is termed in Abaqus as a predefined field. This means the field is specified by the user. The velocity field was applied only to the particle nodes. All velocities are non-time-dependent and are defined only at the initial start of the simulation. For simulations with multiple impacts, this meant that the particles had to be offset from the blade and each other by enough distance to allow most blade oscillations to dampen.

3.3.3 Interactions

In order for impacts to be defined, it was necessary to define interactions between the separate parts. For all simulations, the interactions existed between the blade and particles or the blade and coating and coating and particles if applicable. Particles were not defined to interact with each other. Rebounding particles interacting with each other and new impacting particles would have increased the complexity and added too many additional variables into the simulation. This was considered beyond the scope of this effort.

When defining an interaction, it was necessary to specify a contact friction coefficient. The frictional coefficient allows for a definition of the maximum shear stress along the contact boundary. This is according to the relationship given in Equation 3.2.

$$\tau = \mu p \qquad (3.2)$$

Where:

τ = the maximum allowed shear stress

μ = the friction coefficient

p = the pressure stress between the contacting surfaces

When the maximum allowed shear stress is reached, slipping begins to occur with the frictional coefficient switching between the static and kinetic modes according to the Coulomb frictional model [39 s. 30.1.5].

For all simulations, a coefficient of friction was set at 0.3. This was chosen as it has been observed with other simulation work that crater depth for impacting particles has a strong dependence on the frictional coefficient between 0.0 and 0.1. For values between 0.1 and 0.5 the differences in dependencies are negligible [42]. A value of 0.3 is both physically realistic and more than suitable for the current simulation work.

3.3.4 Constraints

A constraint is similar to a boundary condition in that it adds a restriction to the movement of parts within the assembly. However, while a boundary condition restricts absolute movement relative to the global coordinate system, a constraint restricts the movement of one part relative to that of another. This made constraints useful in defining the surface boundary between the blade and coating models.

The type of constraint used in the blade/coating interfacial surface boundary was a Tie. A Tie is termed as such because it 'ties' both surfaces together and does not allow any relative motion or sliding between the surfaces. This forced the assumption that there existed an infinite bond strength between the surfaces, so erosion and delamination will occur through fracture of the coating at the interface. This interface could be defined between the coating and substrate or within the coating itself, depending on the mesh size. This assumption is not wholly inaccurate and corresponds to previous observations [36-38].

It was initially attempted to define the bonding interaction of the blade/coating interface in terms of bond and shear strengths. To do this required the creation of a layer of cohesive elements. Cohesive elements are used in Abaqus to model the bond strength of interfaces. Numerous attempts at modeling with cohesive elements failed, including modifying the cohesive layer properties far outside the realm of physical possibility, differing cohesive layer thicknesses, modifying interaction properties, and changing mesh distortion controls. Based on repeated failure through model instability, it was decided that the use of cohesive elements in Abaqus is not particularly well-suited for modeling the highly dynamic response of an interfacial boundary layer between a ductile metal and a brittle material that is anticipated to fail and erode. Figure 3.8 shows the results typically obtained with cohesive layer attempts.

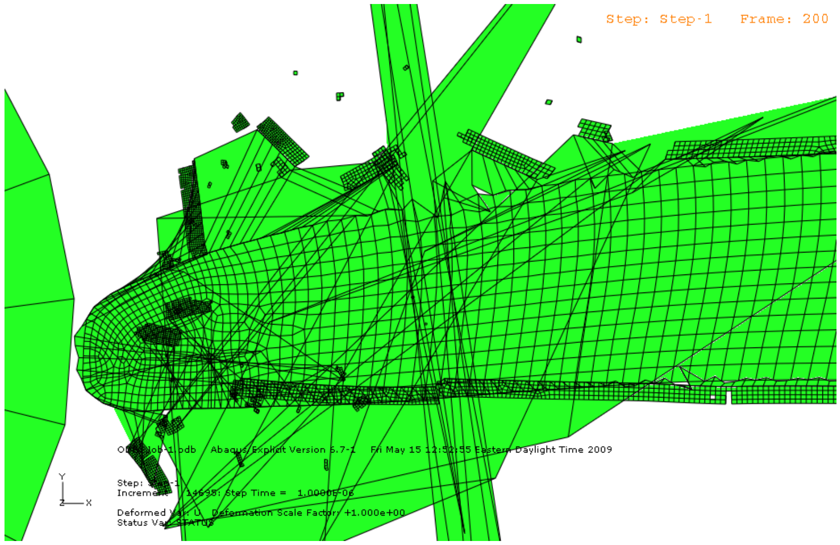

Figure 3.8 – Example of model instability seen for all attempts to model a cohesive layer

3.4 Processing Simulations – Running Jobs

Jobs are referred to within Abaqus as being the way in which the processing of a single simulation is handled. They can be run either locally on the machine used to create the simulation, or the jobs can be processed on a dedicated server. The choice to process locally or not depended on the size of the model. Particularly, the number of total elements and the time duration of the simulation give a good correlation to the duration of time the simulation needs to be processed. Other factors, including model instability due to certain parameters and definitions can influence time duration as well.

For larger models, or large sets of models, it was more efficient to use the Penn State High Performance Computing Group's (HPC) supercomputing clusters for processing. There are two files needed to run a job on these servers: The Abaqus input file containing all of the model data and a Portable Batch System (PBS) file which tells the server how to process the simulation. For large sets, a third file was needed as a script to submit multiple PBS files. Using the Penn State HPC's supercomputers allowed for parametric studies evaluating multiple variables with hundreds of simulations to be completed in a fraction of the time that would otherwise be required.

Chapter 4

Results and Discussion

The first section of Chapter 4 discusses the methodology for simulating the geometry, vertical, and horizontal displacements of leading edge curl of the Baseline blade. Once a methodology was created that successfully produced curl on the two dimensional Baseline blade model, modeling efforts were expanded onto three dimensional models. Modeling in the third dimension introduced a number of new problems, but, once these problems were resolved, curling of the Baseline leading edge was also produced on the three dimensional model.

After determining the particle impact parameters and model setup parameters that consistently achieved curling on the Baseline blade, a new goal of modeling different deformation suppression techniques was approached. The first attempts at curl suppression involved modeling the thicker leading edge geometry of the New Contour blade model under the same conditions that previously produced curl on the Baseline. Subsequent simulations tested different materials using the Baseline model. The last section of Chapter 4 discusses the final simulations that were run using coating models of various thicknesses on the New Contour model to determine if further curl suppression was possible.

4.1 Preliminary Attempts at Modeling Curl on Baseline Blade

Initial attempts at modeling curl on the Baseline blade produced a variety of unsuccessful results. The majority of simulations produced blade deformation of a magnitude that far exceeded anything observed on blades retrieved from the field or produced through in-house testing. However, the main goal of these initial efforts was to determine the model parameters that were necessary for future modeling work.

4.1.1 Initial Two Dimensional Modeling

A preliminary parametric study was performed using the two dimensional Baseline blade model. The parameters examined included angles between 0 and 90 degrees, velocities between 900 and 1785 feet per second (274 to 544 meters per second), and particle diameters of 6, 12 and 40 mils (150, 300, 1000 microns, respectively). These parameters were chosen to encompass the spectrum of conditions possibly encountered in an aircraft engine compressor. Based on previous testing, it was believed that curl would be produced with an angle close to 37 degrees. Figure 4.1 illustrates a particle impingement angle of 37 degrees to the Baseline leading edge with respect to the rotation of the blisk and engine geometry. Due to the relatively high velocity of the compressor blisk relative to the airstream velocity, impacts on the leading edge should be close to but slightly less than this 37 degree value. Velocity values were chosen based on the corresponding linear velocity of the Baseline blisk's known angular velocity.

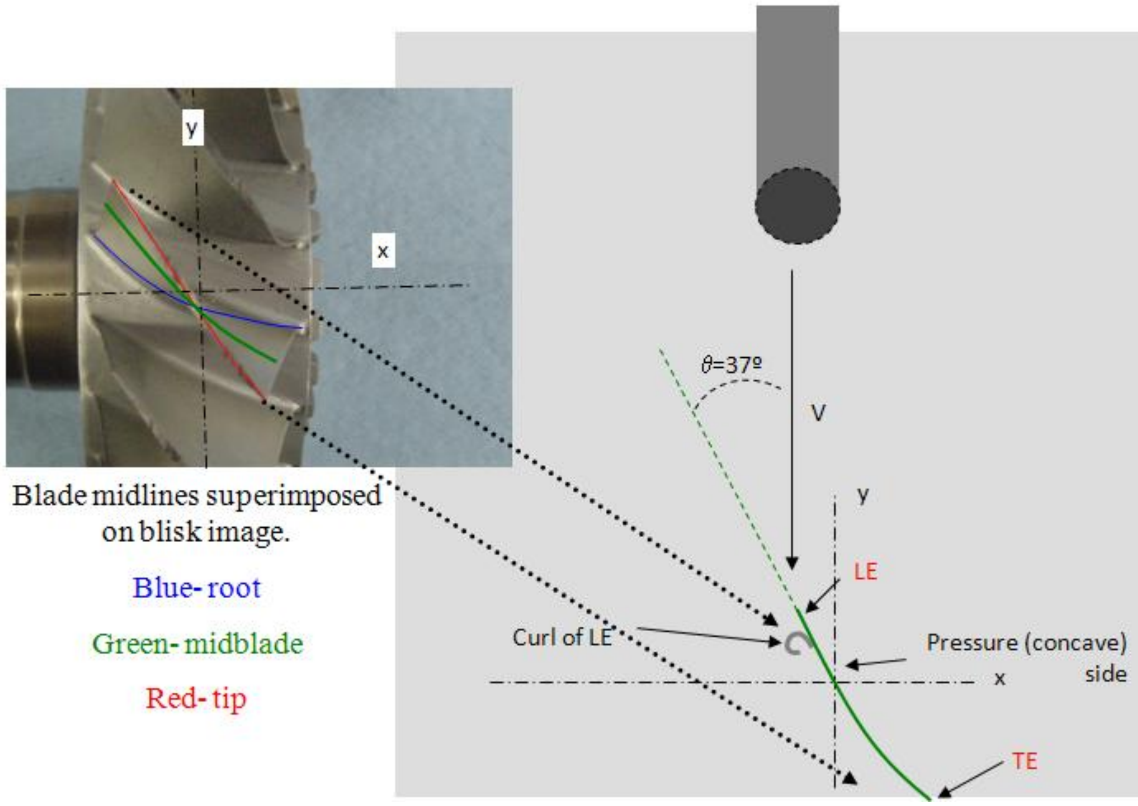

Figure 4.1 – Schematic illustration showing an impact angle of 37 degrees based upon the blade coordinate tangent to the pressure surface at the leading edge midway between the root and the tip.

Ten and twenty particle impacts were initially modeled. It was believed that significant deformation of the blade should result from these numbers of impacts. For early testing, a boundary condition was only applied to the edge opposite the leading edge. As a result, the entire model was unconstrained to move in both (x, y) directions, except for the nodes located on the far edge, which were held fixed. Table 4.1 gives a complete listing of the parameters tested using the two dimensional Baseline model. The initial model and mesh used for these preliminary simulations is shown in Figure 4.2. As previously discussed, the mesh element size was reduced at the leading edge to more accurately depict the degree of deformation for a given set of conditions.

Table 4.1 – Parameters and variables used for initial two dimensional modeling

Parameter	Values
Blade Model	2D Baseline
Particle Diameter	6, 12, 40 mil
Particle Velocity	900, 1200, 1490, 1700, 1785 fps
Impact Angle	10°, 20°, 30°, 37°, 45°, 60°, 90°
Boundary Condition	Full length unconstrained
Number of Impacts	10, 20

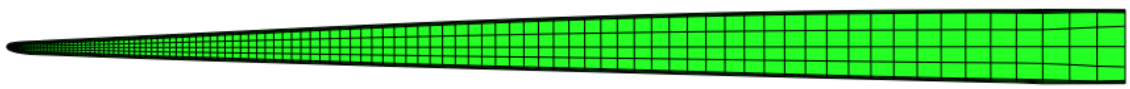

Figure 4.2 - Two dimensional Baseline mesh used for initial study.

An example of the initial setup for the simulations is given by Figure 4.3. The particles were aligned at an angle termed to be the impact angle. At the start of the simulation, all modeled particles were given the same initial velocity and followed the same trajectory to strike the leading edge of the blade. Specifically, a line drawn through the farthest horizontal (-x) point of the leading edge and offset from the horizontal by the impact angle would pass through the center of every particle. The particles were initially offset from each other by 0.1 inches. It was anticipated that this spacing would allow enough time for a single impact to deform the blade and rebound off. This assumption was later found to be, although technically correct, faulted for a different reason. The particles did have enough time to plastically deform and rebound off of the blade, but the elastic response of the blade did not have enough time to dampen.

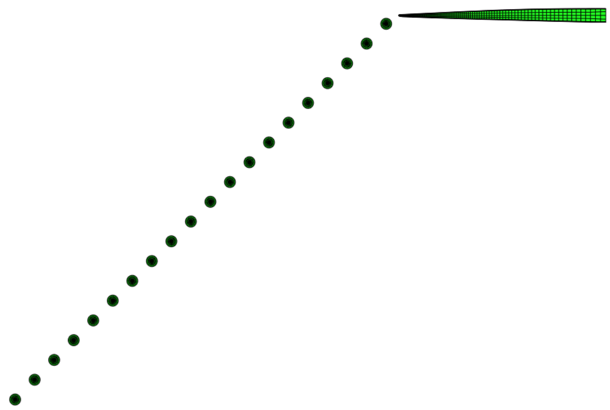

Figure 4.3 - Initial simulation setup for twenty 40 mil diameter particle impacts at 45° on the Baseline model

One of the most significant problems encountered during initial modeling work was the elastic deflection of the blade upon particle impact. These deflections did not quickly dampen and would cause the blade to be oscillating in a non-negligible way for subsequent impacts. The impacting particles would cause progressively greater deflections and oscillations that resulted in the location of particle impacts moving back along the pressure side of the blade and away from the leading edge. This change in the impact location of the particles also resulted in the impact no longer being at an angle to strike and glance off of the leading edge. This caused increased blade deflection at a much higher magnitude than could ever occur under realistic conditions, resulting in deformations of unrealistic geometry and magnitude. This problem was most apparent with the 40 mil particles and compounded at higher velocities.

Figure 4.4 shows a two dimensional model result for ten impacts with 40 mil particles, at a 30 degree angle, and with a 1700 feet per second particle velocity, in which the vertical and horizontal displacements were found to be about 0.24 and 0.16 inches, respectively. These values were determined to be unrealistic during fielded applications, suggesting refinement of the model was required.

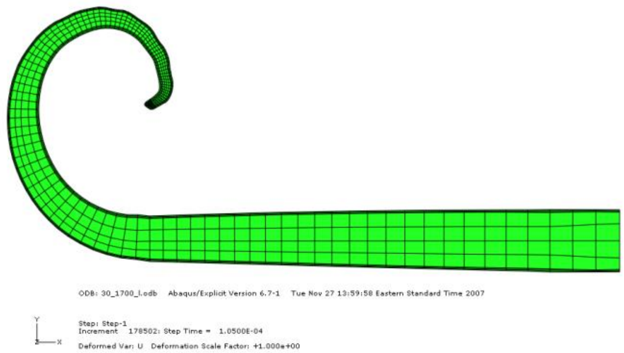

Figure 4.4 – The result of twenty 40 mil particle impacts at 30 degrees and 1700 feet per second on the Baseline blade model.

Under the tested conditions, most simulations resulted in deformation across the entire 0.75” length of the modeled blade cross section. This value was much greater than those values typically observed to occur in the field, in which only the first 0.01-0.03 inches of the blade’s leading edge was observed to deform. Irregardless of parameters, no simulation resulted in accurate curling magnitude for the horizontal or vertical displacements under these modeling parameters, and was thought to be primarily caused by the larger-than-normal impact frequency being simulated. Due to computational limitations, the option of simply decreasing impact frequency was unavailable; a single impact would result in blade oscillations that would not dampen to negligible amounts for about 0.2 milliseconds. This duration is comparable to the time length of an entire simulation. Therefore, it was decidedly necessary to adjust the simulations in a way to remove the possibility of large deflections.

4.1.2 Attempts to Reduce Blade Deflections

In order to control the large deflections that resulted from simulating multiple particle impacts on a blade, four methods were attempted. These methods included adjusting the size of the boundary condition, using multiple particle impact angles within the same simulation, increasing the blade's in-plane thickness, and thinning the leading edge of the blade to simulate the occurrence of erosion.

4.1.2.1 Boundary Condition

The primary purpose of a boundary condition was to hold certain nodes within the simulation constant relative to the global coordinate system. Initial testing with a boundary condition applied only to the nodes on the edge opposite the leading edge resulted in large deflections occurring throughout the entire blade length. Therefore, it was thought that expanding the boundary condition towards the leading edge of the blade would help add a degree of stability to the blade without sacrificing accuracy of the simulation, since the blade model was not expected to deflect or deform as far from the tip as was being observed.

The effects of the boundary condition at locations of 0.1, 0.25, and 0.375 inches back from the leading edge were tested. The boundary condition values define the amount of blade length being unconstrained within a simulation. The complete set of parameters tested is listed in Table 4.2. Models were tested using various particle sizes, particle velocities, impact angles, and boundary conditions for twenty impacting particles.

Table 4.2 – Boundary condition study parameters and values selected for minimizing the amount of deflection within the model

Parameter	Values
Blade Model	2D Baseline
Particle Diameter	6, 12, 40 mil
Particle Velocity	900, 1200, 1490, 1700, 1785 fps
Impact Angle	10°, 20°, 30°, 37°, 45°, 60°
Boundary Condition	0.1”, 0.25”, 0.375” from LE
Number of Impacts	20

As shown in Figure 4.5, the simulations produced the intended and expected results: larger boundary conditions resulted in smaller deformation. However, the entire length of the non-fixed blade was still observed to deflect and deform. Even with the most restrictive boundary condition tested, the deflections were still far too large for what was observed in the field. Larger particle diameters and higher velocities tended to produce larger curl as in Figure 4.5. Lower velocities and particle diameters did not tend to fully curl the whole blade, and only resulted in small to negligible deformations. The use of a boundary condition larger than just the nodes on the far edge appeared to be necessary to improve the accuracy of the simulation. However, it still appeared that attempting other methods along with a boundary condition was necessary for reproducing curling on the Baseline blade model.

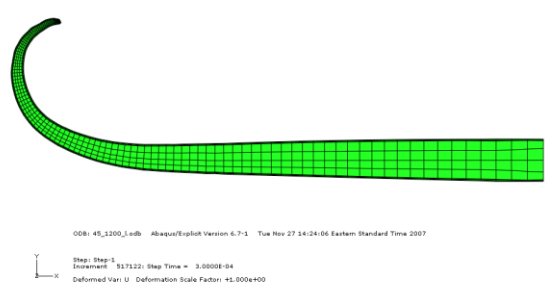

Figure 4.5 - Model resulting from twenty 40 mil particle at 45 degrees with a velocity of 1200 feet per second impact, showing a large degree of curling even with a 0.25 inch boundary condition.

4.1.2.2 Varying and Multiple Impact Angles

Further attempts to reduce and control deflections on the two dimensional Baseline blade model were made by altering the initial particle angles at which the particles were set and by using multiple impact angles within a single situation. Altering the initial particle angles included setting up the initial particles and spacing so that, as the simulation progressed, the particles would ‘follow’ the leading edge as it deformed. This was accomplished by either offsetting the impact angle setup of the particles while keeping their velocity vector constant or by keeping the impact angle setup constant while altering the particles’ velocity vectors. Both of these allowed for a linearly increasing horizontal offset as the simulation progressed. Due to the complicated nature of setup, this method was only tested at 37 degrees. The use of multiple impact angles within a simulation was done by having two impacts each from a range of angles between 0 and 37 degrees as illustrated in Figure 4.6. The impacts progressed from higher to lower angles during the simulation. It was believed that by initially deforming the blade vertically with high angle impacts combined with subsequent low angle impacts would create deformation horizontally into a curled geometry.

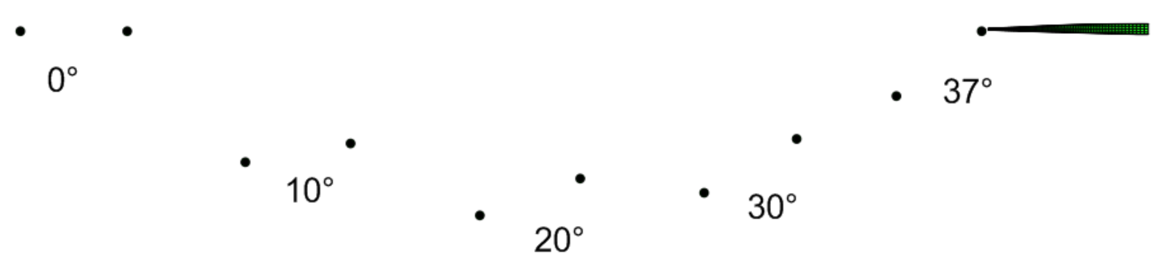

Figure 4.6 - The setup of a multiple impact angle simulation where impacts progress from 37 to 0 degrees.

4.1.2.2.1 Initial Particle Angles

As previously mentioned, altering initial particle impingement angles was attempted by two approaches. The first approach was through slightly offsetting the particles' initial impact angle as shown in Figure 4.7a, and the second was through slightly offsetting the particles' initial velocity vector as shown in Figure 4.7b. The set of parameters tested for this configuration is given in Table 4.3.

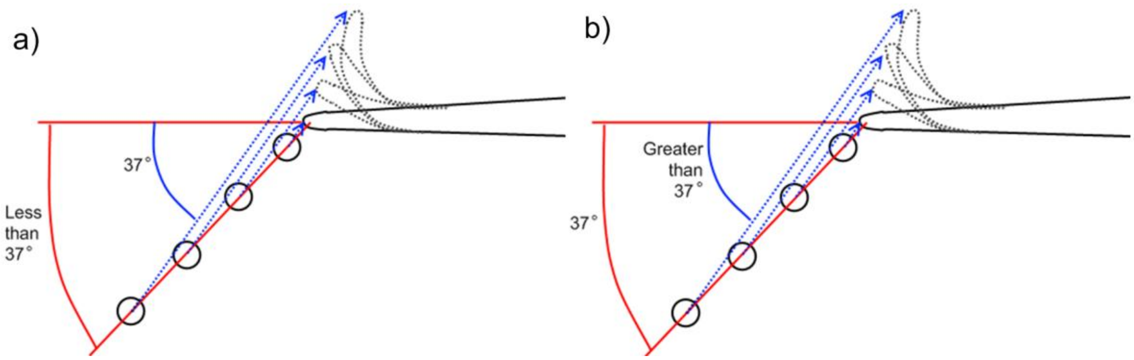

Figure 4.7 - Altering the initial (a) impact angle and (b) velocity vector in an attempt to ensure consistent particle impacts on the leading edge tip as the blade deformed throughout a simulation.

Table 4.3 – Particle angles study parameters and values

Parameter	**Values**
Blade Model	2D Baseline
Particle Diameter	40 mil
Particle Velocity	1490, 1700 fps
Impact Angle	37° [~35°-39°]
Boundary Condition	0.375" from LE
Number of Impacts	10

Altering the initial particle impact and velocity angles in order to get the particles to follow the leading edge of the blade proved to be, in practice, quite challenging to realize. As particles impacted the leading edge and rebounded off, they caused the blade to deform locally while also causing a small amount of deflection. This deflection caused minute oscillations to occur along the entire blade width. These oscillations did not fully dampen when the next impact occurred so the impact location for the particles was slightly 'off' by an almost unpredictable amount. The end result was usually a large degree of unpredictability in how the blade deformed. Because of this, the necessary spacing and offset between impacts within any particular simulation was nearly impossible to determine. Even worse, a slight change to simulation parameters, such as velocity or impact angle, would require a complete reworking of the spacing and offset. Attempts to produce curl by iteratively modifying values for each individual particle also proved to be impractical. The complexity and statistical variation combined with these undesirable factors eliminated the possibility of this method as being useful for modeling curl on the Baseline blade model. However, more advanced computation programs may be capable of utilizing this approach.

4.1.2.2.2 Multiple Impact Angles

The next method attempted for controlling deflections and reproducing curl involved using multiple impact angles within a single simulation. Up until this method was attempted, curl had not been achieved through a single simulation at a single impact angle with any combination of reasonable parameters. Therefore, it was determined to incorporate multiple impact angles within a single simulation. A setup of 10 impacts (2 at 37°, 2 at 30°, 2 at 20°, 2 at 10°, and 2 at 0°) was created with the test parameters listed in Table 4.4. As was demonstrated in Figure 4.6, the particles progressed from larger to smaller impact angles in order to deform the blade vertically first and then horizontally.

Table 4.4 – Multiple impact parameters and values

Parameter	Values
Blade Model	2D Baseline
Particle Diameter	40 mil
Particle Velocity	1490, 1700 fps
Impact Angle	[0°, 10°, 20°, 30°, 37°]
Boundary Condition	0.375” from LE
Number of Impacts	10 – (2 from each angle)

Figure 4.8 shows the result of a 1700 fps simulation with a boundary condition of 0.375” for the leading edge. Using this method produced reasonable success, in that curling of a relatively appropriate shape and magnitude was produced. The initial assumption and basis for attempting this method was proven successful, in that the first few impacts deform the leading edge vertically while the subsequent impacts contributed more towards giving the deformation a curled shape.

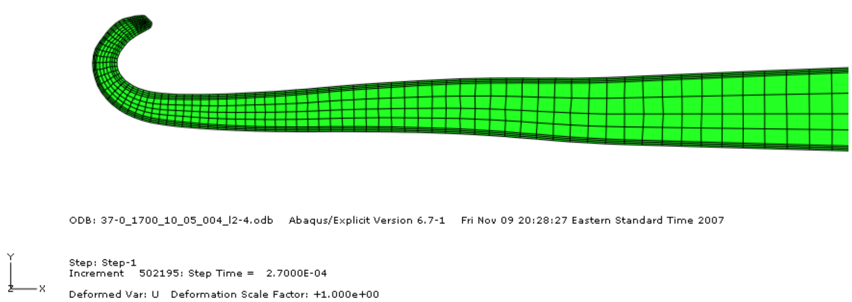

Figure 4.8 - Appropriate curling geometry and magnitude (about 0.034 inches vertical and 0.02 inches horizontal) produced on the Baseline blade using multiple impact angles.

However, it is unlikely a blade would experience such consistent impacts spread over such a large angular difference. Using multiple impact angles also suffered from some of the same problems as varying initial angles, in that the initial setup of the simulation required assumptions or knowledge of resulting blade deformation. This was difficult, if not impossible, to determine without some form of a trial and error approach. Since consistency in reproducing leading edge blade curl was desired, other methods were explored to test some of the underlying modeling assumptions that were initially made.

4.1.2.3 In-Plane Thickness

As mentioned in the previous chapter, in-plane thickness is the width a two dimensional model can be considered to exist in the third dimension. An ideal value would be the amount of blade width that curls through particle impacts at a single location. The initial value of 0.027 inches was selected based on previous work by John Pitterle [41]. It was expected that increasing the magnitude of the in-plane thickness would result in considerably less blade oscillation, deflection and deformation. A number of tests were run using the parameters listed in Table 4.5 to determine the effect of in-plane thickness on the degree of deformation and curl geometry.

Table 4.5 – In-plane thickness parameters and values

Parameter	Values
Blade Model	2D Baseline
Particle Diameter	40 mil
Particle Velocity	1700 fps
Impact Angle	37°
Boundary Condition	0.375” and full length from LE
Number of Impacts	20
In-plane Thickness	0.03”, 0.05”, 0.08”, 0.1”, 0.5” 0.7”, 0.9”

Figure 4.9 shows the model resulting from twenty 40 mil particle impacts at a velocity of 1700 feet per second, an angle of 37 degrees, and with a boundary condition at 0.375 inches. Increasing the in-plane thickness of the model did result in lesser deformation, as was expected. In fact, with an in-plane thickness of 0.1 inches large deflections ceased to occur as the images in Figure 4.9(d-g) illustrate. The difference in results between the 0.375 inch and full length boundary conditions at 0.1 inches and greater were negligible. However, the overall deformation produced through these values was also negligible. An in-plane thickness value of 0.05 inches with a 0.375 inch boundary condition produced appropriate curl as shown in Figure 4.9b. This was the first time curl was produced using a single velocity angle.

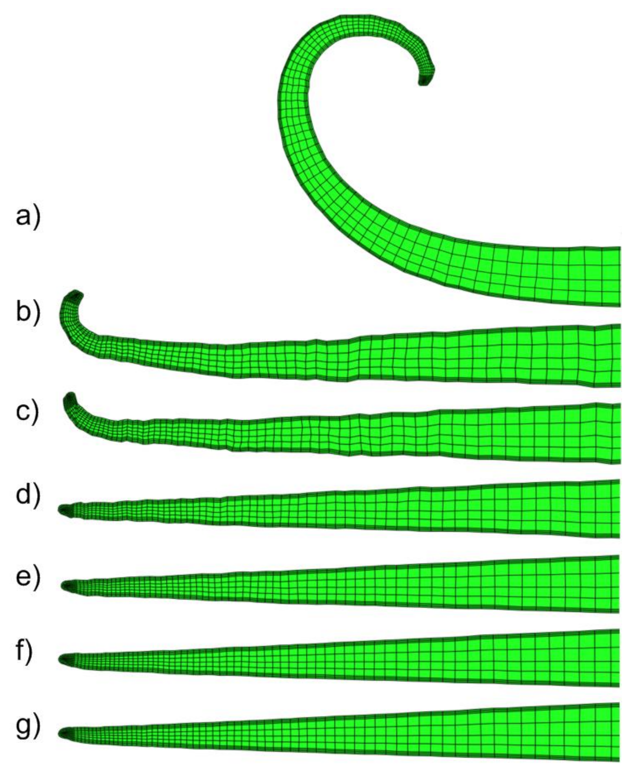

Figure 4.9 – Model results showing the effect of an in-plane thickness value of (a) 0.03", (b) 0.05", (c) 0.08", (d) 0.1", (e) 0.5", (f) 0.7", and (g) 0.9" for the Baseline model under identical impact conditions of twenty 40 mil particle impacts at a velocity of 1700 feet per second, an angle of 37 degrees, and with a boundary condition at 0.375 inches

Increasing the in-plane thickness was observed to control unwanted deflections. In conjunction with a boundary condition, all unwanted deflections were observed to have ceased. Increasing this value also resulted in a form of model instability which produced 'rippling' along the length of the blade model. This rippling effect can be observed in Figures 4.9(b-g). It appears as jaggedness along the outer edges of the Baseline model's mesh. Due to a lack of physical or analytical basis for increasing the in-plane thickness value and to keep consistency with previous modeling efforts, it was decided to keep the in-plane thickness at its original value of 0.027 inches.

4.1.2.4 Thinning the Blade Leading Edge to Simulate Erosion

After mixed success with the previous methods, the possibility that curl does not appear with consistency on the Baseline blade without some preliminary erosion to the leading edge was considered. Two more blade models were created to simulate the occurrence of 50 and 85 percent erosion to the thickness of the leading edge as shown in Figure 4.10. The models were created by having a gradual thinning of the first 0.09 inches of the leading edge of the blade model to 50 or 15 percent thickness values at the tip. These models were referred to as the Baseline 50 and 15 percent tip models.

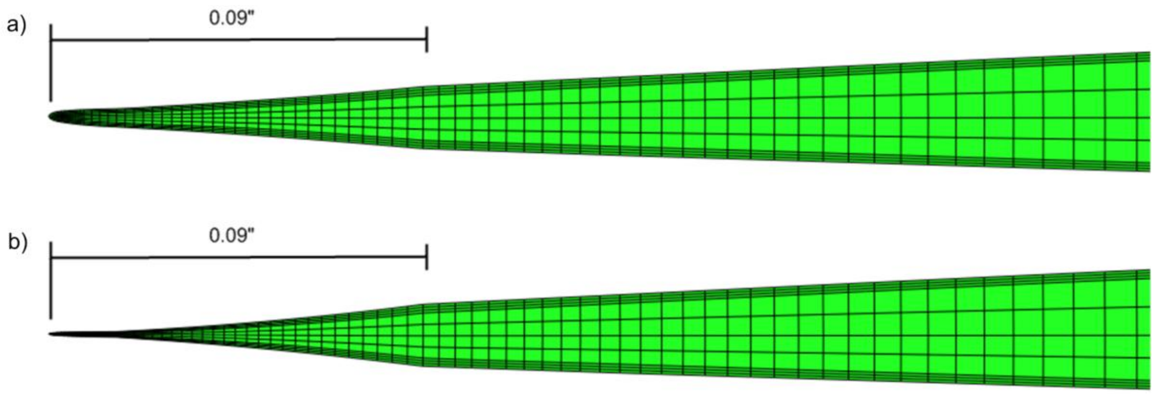

Figure 4.10 - Baseline (a) 50 percent tip and (b) 15 percent tip models.

The primary observations made after running simulations with reduced tip thickness was that thinning of the blade drastically reduced the overall blade deflection. This was believed to have resulted from the energy of the impact being dissipated through deformation of the thinner tip rather than through the elastic deflections seen with the full thickness tip. The complete range of tested values is given in Table 4.6.

Table 4.6 – Blade thinning parameters and values

Parameter	Values
Blade Model	2D Baseline - 15% and 50% tip
Particle Diameter	6, 12, 40 mil
Particle Velocity	900, 1200, 1490, 1700, 1785 fps
Impact Angle	20°, 30°, 37°, 45°, 60°, 90°
Boundary Condition	0%; 0.1”, 0.25” from LE
Number of Impacts	20

The results from the 50 and 15 percent tip simulations were observed to be consistent in the reproduction of realistic curling magnitude and geometry. The most consistent results were produced using particles of 40 mil diameter with a 0.1 or 0.25 inch percent boundary condition. Both 50 and 15 percent tip models tended to result in curling after only one or two particle impacts. The best angle for producing curl was observed to be between 20 and 37 degrees. Curl decreased with higher angles. All tested velocities resulted in some degree of curl on these two models, with higher velocities being more consistent. Figure 4.11 shows curling being observed on both thin tip blade models for various conditions.

Figure 4.11 – Results of various 50 and 15 percent tip simulations after 10 impacts

(e) 50% tip, 40 mil particles, 20 degrees, 1700 fps, 0.25” BC
(f) 50% tip, 40 mil particles, 37 degrees, 1700 fps, 0.25” BC
(g) 15% tip, 40 mil particles, 20 degrees, 1700 fps, 0.25” BC
(h) 15% tip, 40 mil particles, 37 degrees, 1700 fps, 0.25” BC

The primary issue with using these thin tipped models is their reliance on the assumption that significant erosion occurs before curling. This is not always the case, as leading edge curl has been observed in fielded components without significant erosion. Therefore, further testing using these models was ceased, and subsequent attempts to reproduce curl were simulated only on the full-thickness Baseline model.

4.1.2.5 Reducing Blade Deflections Discussion

A number of general conclusions can be made from observations of the initial two dimensional attempts at modeling curl and attempts to control the elastic deflection and resulting oscillations of the Baseline blade. It was apparent that a boundary condition which constrained a majority of the blade model during simulation was necessary in order to control unrealistic blade deflections and allow multiple particle impacts in a single simulation. Altering the initial particle angles in an attempt to follow the leading edge of the blade as it deformed did result in acceptable results, but was unpredictable and inconsistent. The trial and error method necessary for it to work was also decidedly unscientific. A larger in-plane thickness contributed to increased control of the blade deflections and produced curl with a value of 0.05 inches. However, to keep consistency with other modeling efforts, this value was to be kept at 0.027 inches for future simulations. Simulating the erosion of the Baseline blade through the thinner tip models produced leading edge curl after one or two impacts at high velocities (1490 and 1700 feet per second) and angles of 20-37 degrees. Unfortunately, it was also discovered form in-field observations curling appeared on blades that have not undergone an appreciable amount of erosion. Therefore, it was still necessary to develop a consistent methodology for producing curl on the full thickness Baseline model. Since using multiple impacts for a single simulation resulted in uncontrolled elastic blade response, a new approach for simulating curl was necessary.

4.2 Two Dimensional Modeling of Curl on Baseline Blade

Based on the results obtained and observation made through initial modeling work, it was decided that using multiple impacts for a single simulation was unable to consistently produce curl in accurate conditions. Blade oscillations were too large in magnitude and lasted for too long of a time duration for multiple impacts to be feasible with high energy impacts. Therefore, a new method was explored where only a single impact at a time was simulated. This new method was referred to as the multiple iterations method, where a given blade model has single particle impact iteratively simulated.

4.2.1 Multiple Iterations Description

The multiple iterations method for modeling curl on the Baseline blade model was as follows: the Baseline model was impacted with a single particle and then given adequate time for the oscillations to dampen. The resulting deformed model was then imported into a new simulation where it was impacted again. This process was then repeated iteratively until curling or significant deformation was observed. The successive impacts were all simulated under the same velocity and angular conditions. The particles' initial placements for each iteration were automated to 'follow' the leading edge as the blade deformed; a program was created that determined the deformed location of the leading edge and offset the placement of the particles by a calculated amount to keep consistency of future impacts regardless of previous deformation. Keeping a single particle placement position would either result in particles striking the pressure surface of the blade away from the leading edge or not impacting the blade at all. This was dependent on the shape and magnitude of existing deformation and the impacting angle. Although the iterations method was eventually successful in achieving curl, there were a number of initial problems with the method that needed to be overcome.

One of the main reasons that simulating single impacts iteratively was not attempted was due to the large turnaround time between running each iteration of the simulations. With the large number of parameters being studied, there were hundreds of individual models that needed to be simulated. For every iteration run, each blade model needed to be imported into Abaqus, have its parameters set, the particle positioned, possible mesh distortions repaired, as well as have its Abaqus input and portable batch script (PBS) files created, uploaded to the processing cluster, and then submitted for processing. Doing all of this work manually would have consumed many hours of work. Therefore, the ability to create Python scripts within the Abaqus environment was utilized. Programming a script to automate most of these tasks allowed for a new iteration to be simulated almost every day, depending on how long processing took. However, as will be discussed, some tasks were not able to be automated.

After high energy impacts, the model's mesh would sometimes become highly distorted. Depending on the level of distortion, the simulation would continue to run to completion or could also fail and stop processing. This previously allowed multiple impact simulations to run even with a severely deformed mesh. Unfortunately, a simulation will not be allowed to start processing if an initial mesh is distorted. Therefore, it was necessary to repair all mesh distortions that appeared between each iteration. An automatic method for doing so was not attempted due to the perceived complexity required to repair a distorted mesh without altering the existing strains and stresses saved into the deformed model. As a result, every distortion had to be manually repaired. Even though initial mesh configuration and distortions controls were attempted to be optimized for controlling these distortions, they would still regularly appear simply because of the high strains associated with curling deformation. Manual repair of meshes, although time consuming, did not hamper the method of multiple iterations enough to reduce its efficacy for producing accurate curling on the Baseline blade model.

4.2.2 Multiple Iterations Results

Using multiple iterations on the Baseline blade model produced some of the most accurate curling with regard to shape and magnitude as compared to in-field and in-house tested blades. Table 4.7 lists the parameters used for testing with the corresponding results of select models shown in Figure 4.16 for various particle impingement angles and velocities.

Table 4.7 – Multiple iterations parameters and values

Parameter	**Values**
Blade Model	2D Baseline
Particle Diameter	6, 12, 40 mil
Particle Velocity	590, 900, 1200, 1490, 1700 fps
Impact Angle	10°, 20°, 30°, 37°, 45°, 60°
Boundary Condition	0.02”, 0.04”, 0.08”, 0.16” from LE

Figure 4.12 shows model results of 6 iterations for a 40 mil particle at different particle angles and velocities for the Baseline blade model constrained with a 0.04 inch boundary condition. It is observed from Figure 4.12 that curling of the blade occurs for angles of 30, 37 and 45 degrees and particle velocities between 900 and 1700 feet per second. 60 degree impacts did not fully deform the blade vertically, while lower angle impacts of 10 and 20 degrees were more likely to squash the blade horizontally than deform it in the vertical manner necessary for proper curling geometry. Curling magnitude for these conditions was also observed to be relatively independent of velocity. The lower velocity simulations did not significantly deform the blade as shown in Figure 4.12. However, as Figure 4.14 demonstrates, after a greater number of impacts curling was observed.

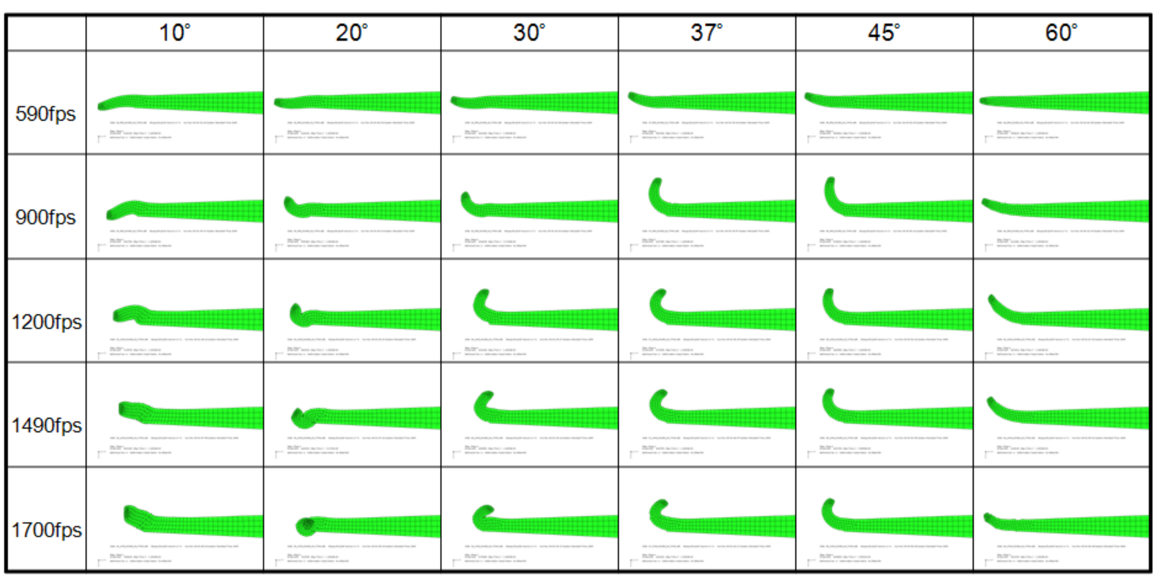

Figure 4.12 – Model reuslts of 6 iterations of 40 mil particles at angles of 10, 20, 30, 37, 45, and 60 degrees, at particles velocities of 590, 900, 1200, 1490, and 1700 feet per second, with a 0.04 inch boundary condition.

To better understand and refine the model, additional simulations were performed in which a 40 mil particle was impacted at 37 degrees at various particle velocities between 590 and 1700 feet per second with boundary conditions of 0.02, 0.04, 0.08, and 0.16 inches as shown in Figure 4.13. Observed in this figure is that a 0.02 inch boundary condition is far too restrictive to the blade and does not allow it to fully curl. A 0.04, 0.08, and 0.16 inch boundary condition all allow the blade to fully curl under these conditions. A primary and counter-intuitive observation is that higher velocity impacts resulted in smaller curl magnitudes. This is believed to be result from high velocity impacts being more capable of deforming the blade, rather than simply causing it to deflect. The lower velocity impacts cause greater deflections of the blade which eventually result in greater magnitudes of curling under these tested conditions.

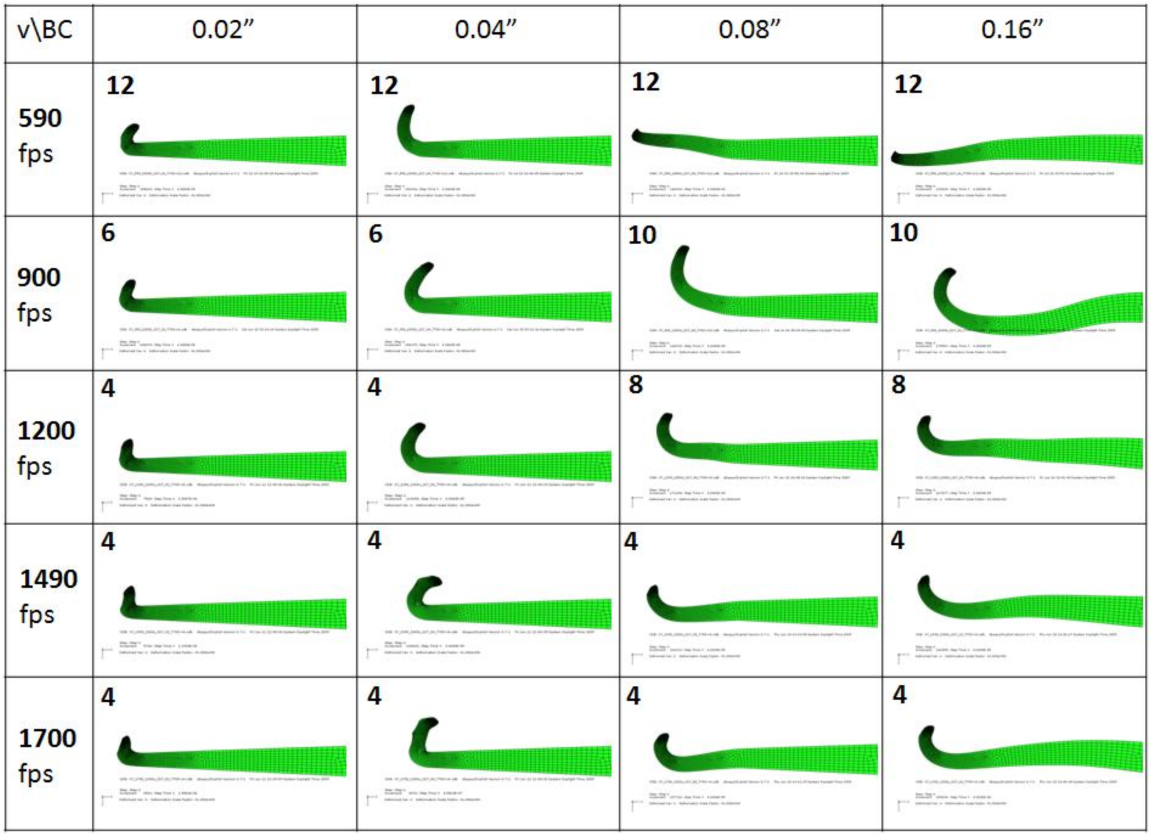

Figure 4.13 – Model results of four to twelve 40 mil particle impacts at an angle of 37 degrees, velocities of 590, 900, 1200, 1490, and 1700 feet per second, with boundary conditions of 0.02, 0.04, 0.08, and 0.16 inches. The number above and to the left of each image shows the number of iterations run on that model.

Figure 4.14 demonstrates the progression through twelve attempted iterations with 40 mil particle impacts at 37 degrees, 590-1700 feet per second, and with a 0.04 inch boundary condition. The higher velocity impacts simulations in Figure 4.18 suffered extensive mesh distortion so future iterations on those models were halted. However, from Figure 4.14, it is observed that curling can be simulated to occur after only two or three impacts at a high velocity. A similar curling geometry can be achieved after numerous more iterations at low velocities. Continuing to simulate impacts beyond the point of curling resulted in distortion of the blade leading edge and eventual mesh failure.

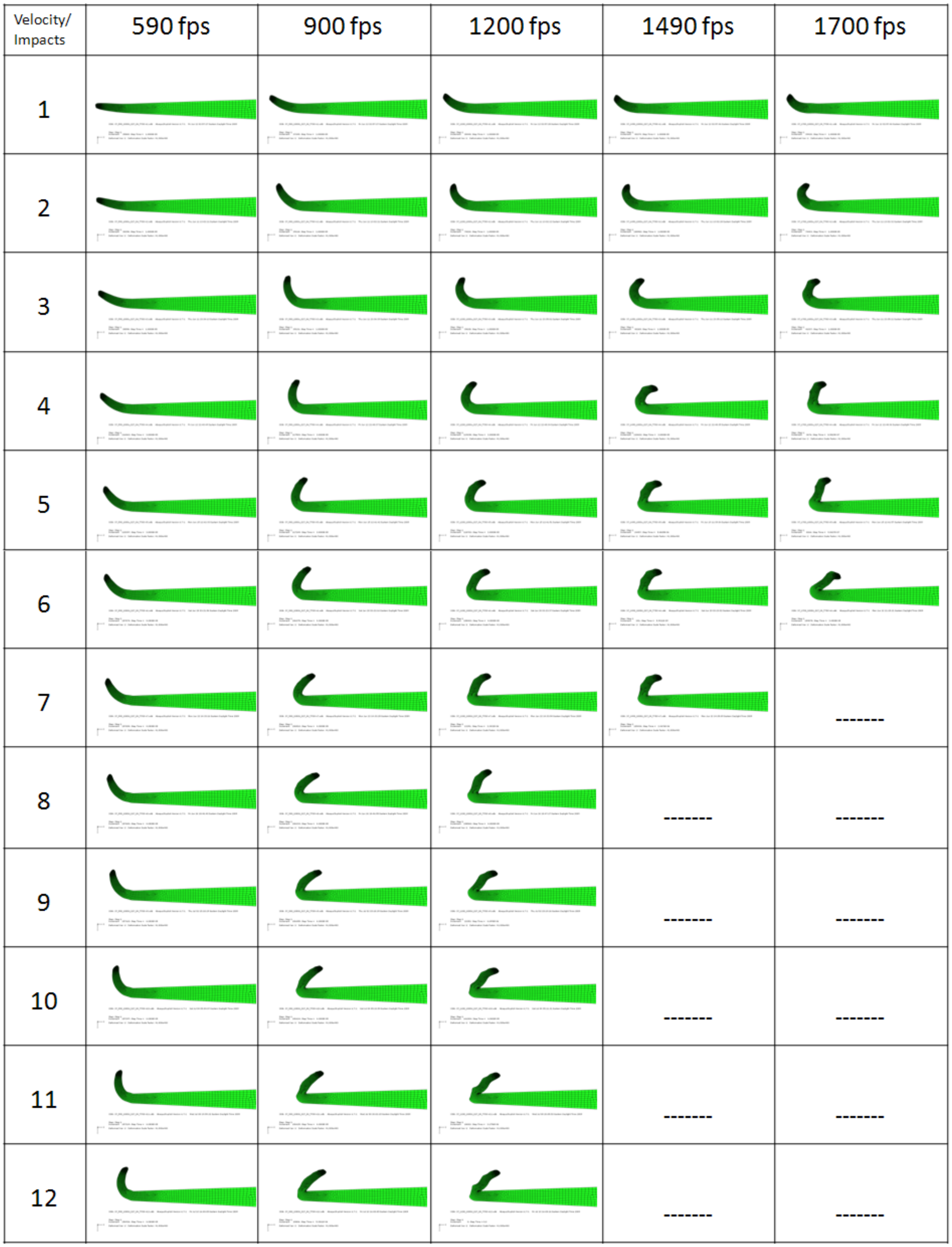

Figure 4.14 – Progression of the model deformation through twelve attempted iterations of 40 mil particles at an angle 37degrees, a velocity of 590, 900, 1200, 1490, and 1700 feet per second, and with a boundary condition of 0.04 inches.

Figure 4.15 shows the results of the 6 and 12 mil particle diameter simulations at an angle of 37 degrees, with a velocity between 590 and 1700 feet per second, and with a boundary condition of 0.02 or 0.04 inches. From Figure 4.15, it is observed that the 6 and 12 mil particle are unable to deform the Baseline blade, even at high velocities. It is possible that given enough iterations, these particle diameters may eventually curl the blade. However, the number of impacts necessary for this to occur may be unfeasible to simulate in a reasonable time frame. This would suggest that for leading edge curl to occur with small particles a component of erosion is required.

Figure 4.15 – Model results from twenty 6 and 12 mil impacts at an angle of 37 degrees, a velocity of 590, 900, 1200, 1490, and 1700 feet per second, with a 0.02 and 0.04 inch boundary condition.

4.3 Three Dimensional Modeling of Curl

Once curl had been successfully demonstrated on two dimensional models, a three dimensional modeling effort was performed. By modeling in three dimensions, the primary two dimensional assumption was eliminated: deformation could only occur equivalently along the entire blade width. The problem of deflections and oscillations was also expected to be minimized for the three dimensional models, as the thicker blade model would be considerably more massive and less likely to deflect upon particle impact.

The three dimensional Baseline blade was initially modeled at a width of 1.7 inches, which was the approximate width of a blisk blade as measured. Eventually, the blade width was shortened to 1.0 inches, then to 0.6 inches, and finally to 0.5 inches. A shorter width required fewer particle impacts along its length to deform and decreased the size of the simulations and required processing time. Observations showed that the deformation response was negligibly different between the blade lengths used as plastic deformation caused by particle impacts tended to only occur locally. Figure 4.16 shows the results of a single 40 mil particle impacting the blade at an angle of 0 degrees and a velocity of 1490 feet per second. This was performed to test the plastic and elastic results from a single impact and observe the blade response along the entire leading edge width.

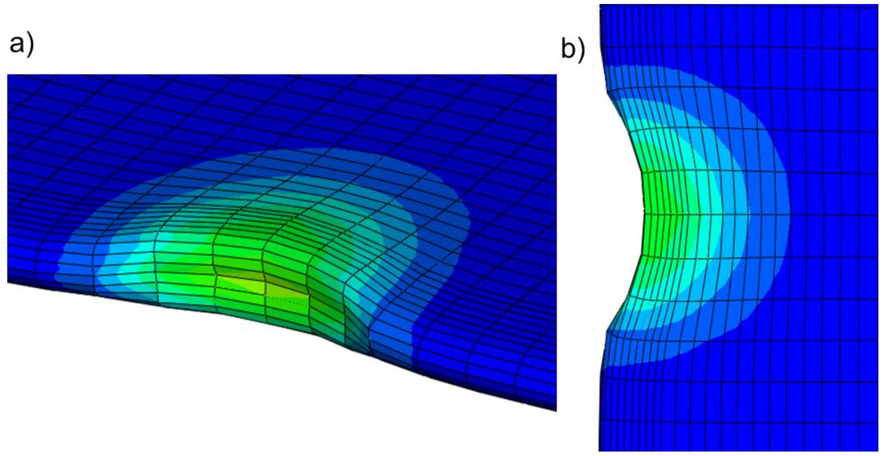

Figure 4.16 – Model result showing the degree of deformation produced from a single 40 mil particle impacted at 0 degrees and 1490 feet per second; (a) gives an isometric view of the deformation while (b) is a view of the suction side of the leading edge.

For three dimensional models, particles were modeled as spheres for simplicity. The particles were impacted along the entire length of the blade in attempt to obtain curling along the entire leading edge of the model. This was achieved through offsetting each particle grouping by a certain amount in order to ensure consistency in impacts along the blade width. A setup of an initial particle configuration is given in Figure 4.17. Initially, five particles per grouping were used, but as the blade width was shortened, the particles per grouping was lowered to four and then eventually to three.

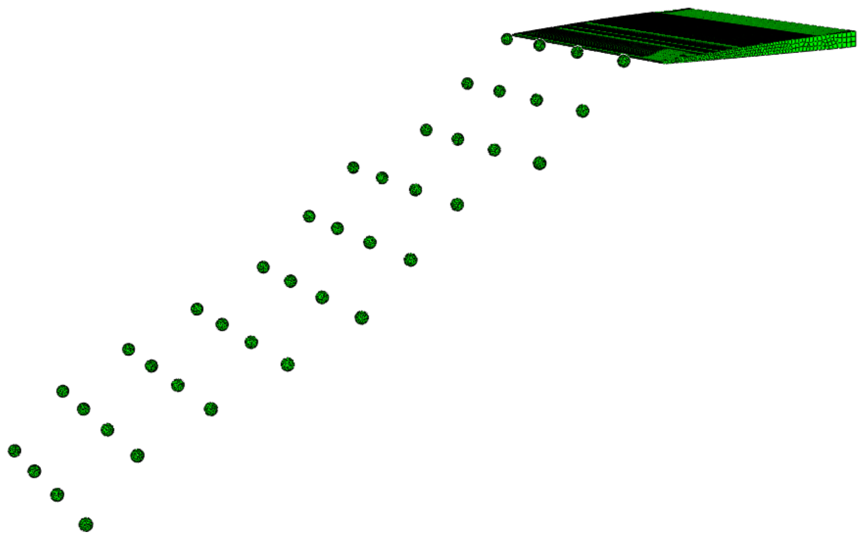

Figure 4.17 - The setup of a three dimensional simulation at 30 degrees with 40 total particles, comprised of four particles each in ten different particle groups.

4.3.1 Three Dimensional Parameters and Model Setup

It was assumed that the three dimensional model, having a greater size and mass, would not deflect with as much magnitude as the two dimensional model, even through direct impacts. However, initial simulations showed uncontrolled oscillations and large magnitude deflections that were similar in appearance to those observed with the two dimensional model as shown in Figure 4.18. This only occurred with 40 mil diameter particles though, as smaller particles resulted in very minimal deflections and deformations. Due to high magnitude deflections from high frequency particle impacts, it was once again necessary to determine a method in which to dampen the blade without affecting the realism of the overall simulation.

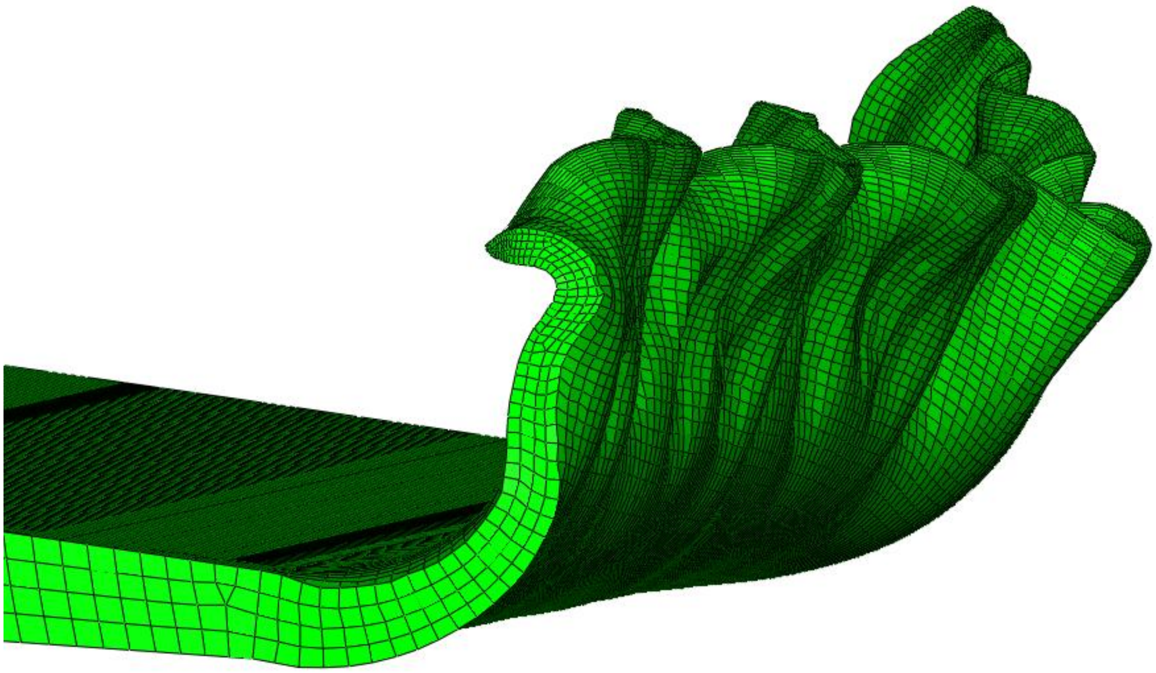

Figure 4.18 - Unrealistic deflections resulting from high frequency particle impacts.

4.3.1.1 Boundary Condition

Due to the reasonable success achieved with boundary conditions on the two dimensional model, it was implemented again on the three dimensional Baseline model. Because particle impacts were occurring along the entire length of the blade, a large number of impacts were necessary for significant deformation to result. Preliminary testing showed large deflections after many particle impacts along the blade length with no boundary condition. A boundary condition was considered to be the primary and most practical way in which to necessarily limit the deflections of the blade.

Based on the results obtained previously with the two dimensional modeling work, two boundary condition locations were tested. These boundary conditions were placed 0.04 inches and 0.16 inches back from the leading edge of the blade. A boundary condition of 0.04 inches is effective in that it is close enough to the leading edge to eliminate all unnecessary deflections of the blade while still leaving enough of the model active as is needed for curling. Using a boundary condition this small, however, can come at the expense of a realistic simulation since it restricts the occurrence of all deformation of a magnitude greater than the boundary condition. Almost all model results with a 0.04 inch boundary condition produced deformation similar to Figure 4.19. Due to this reason, the 0.16 inch boundary condition was used primarily in future three dimensional simulations, since it allowed the response for a greater length of the blade to be observed while still controlling a majority of blade deflections.

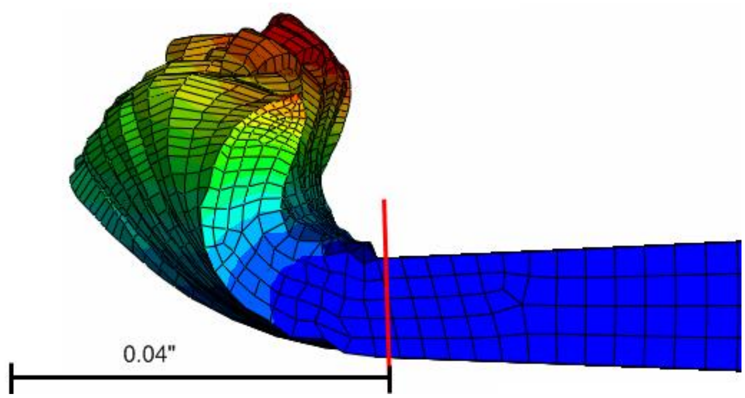

Figure 4.19 – Deformation geometry and magnitude typically observed with a 0.04 inch boundary condition.

4.3.1.2 Iterations

As was done successfully with the two dimensional model, a method utilizing multiple iterations was attempted on the three dimensional model. The methodology for iterations was similar to the two dimensional model, in that the deformed blade model that resulted after a first simulation was then imported into a subsequent simulation that had the same impact parameters. The deformed model resulting from that simulation would then be further imported into a new simulation. Between each simulation, the only adjustment that was made was the impact location. It was adjusted to ensure that the impacting particles would continue to follow the blade's leading edge as the blade deformed. The amount of offset necessary for the particles was determined through an automatic computation based on the degree of leading edge deformation. The major difference between using multiple iterations in three dimensions as compared to in two dimensions was that there were multiple particle impacts per iteration. Having only a single particle impact the leading edge would have been far too impractical, especially considering how curling was not observed to occur on the model until after about one hundred total particle impacts. The large number of required impacts is obviously due to the increased width of the model and the additional particle impacts needed to deform the entire width. Most importantly, using this method allowed for many more particle impacts to be modeled than could be achieved in a single simulation without going beyond computational limits. 21, 42, 84, and 168 particle impacts per iteration were all tested. The model results of these simulations are discussed in the following section.

The biggest difference in setup between these simulations and all previously attempted work was the way in which particles were set to impact the leading edge. In the three dimensional method of multiple iterations the particles were set so that only 'grazing' and indirect impacts could occur. Many particle impacts were modeled, with each impact contributing only slightly to the overall deformation. Grazing impacts were observed in previous two dimensional work to contribute more to deformation, while direct impacts, although still causing a slight amount of deformation, dissipated most of their impact energy into elastically deflecting the blade. Figure 4.20 demonstrated the differences for what is meant between grazing and direct impacts.

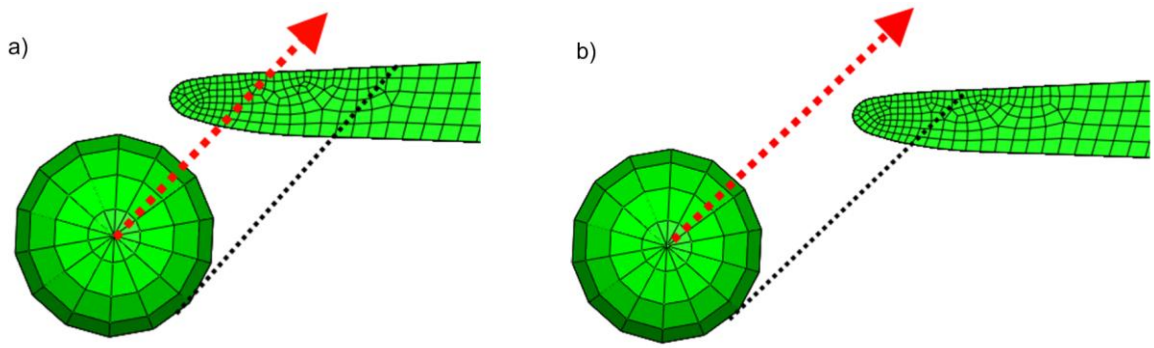

Figure 4.20 – Illustration of the differences in terminology when referring to (a) direct and (b) grazing impacts.

Using the iterations method in three dimensions also had its drawbacks. There were two main obstacles that needed to be overcome for the multiple iterations method to be practical in three dimensions. These obstacles dealt largely with time and computation considerations and restrictions.

The more the three dimensional blade mesh would deform, the higher the likelihood that errors appear in the mesh. Figure 4.21 shows the appearance of a highly distorted mesh. It would be impossible to correct the errors in this mesh manually, preventing any subsequent iterations to be run. The only workarounds would be to re-import the mesh from an increment in the previous simulation where errors had not yet appeared or to rerun the previous simulation under a slightly different impact location and hope the errors do not reappear.

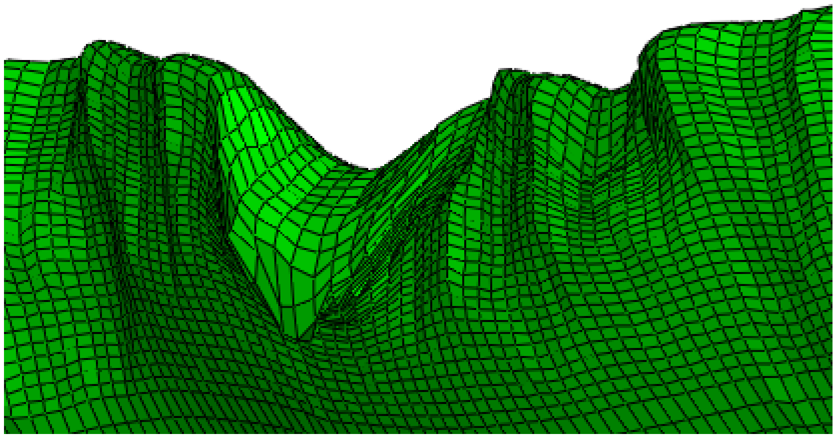

Figure 4.21 - Extremely distorted Baseline three dimensional mesh.

The appearance of mesh errors on the three dimensional Baseline model was similar to what occurred with the two dimensional work. When errors occurred during a simulation, the simulation had a moderate likelihood to continue to run to completion. The larger errors resulted in increased probability of simulation failure. These mesh errors prevented any subsequent simulations from being run using that model until they were corrected. The main problem was that attempting to correct mesh errors for three dimensional meshes was significantly more challenging than correcting two dimensional mesh errors. When errors are small in quantity and have a small displacement magnitude, it was simple but time consuming to correct the errors by individually editing the coordinate values of each node. However, when errors appeared in high quantities (10+) or the mesh was extremely distorted, it became impossible to correct the mesh within a reasonable time period. Unfortunately, there is no tool within Abaqus that could automatically find and correct mesh errors, so all work had to be done manually by correcting the coordinates of each node within the distorted element.

During the initial testing of this method, after only two iterations of 84 impacts, each mesh had become far too distorted to fix. However, this was attempted using one of the initial three dimensional models and mesh configurations. By creating a new model and meshing it a way that would lower the likelihood of resulting errors, it became possible to run some models through over ten iterations, repairing the small quantity of errors as they appeared.

To decrease storage and computation time requirements, the Baseline model was shortened to a final length of 0.16 inches and a width of 0.5 inches. This decreased the overall element count and storage requirements for the input and output files from the simulation. By simply expanding the model from two to three dimensions, these requirements increased by a factor of one hundred or more. Decreasing the model length to 0.16 inches also allowed for more precise configurations to be made on the mesh near the leading edge. The primary reason for shortening the width for simplicity, decreasing impacts necessary for curling and the number of errors that needed to be corrected. The major mesh change was configuring the top of the mesh to have smaller element sizes relative to the lower side, as shown in Figure 4.22. Since the impacting particles directly impacted the pressure side, larger elements that have a larger relative mass were less likely to become largely displaced and result in errors.

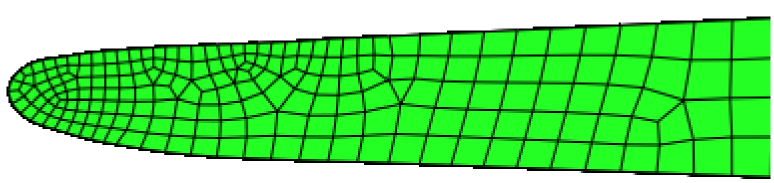

Figure 4.22 – Baseline leading edge mesh configured to prevent distortions and failure.

Another obstacle that needed to be overcome dealt with the way in which simulations were processed. As mentioned previously, simulations were not processed locally since the computational requirements exceeded what was available. Therefore, all simulations were uploaded onto one of Penn State's High Performance Computing Group's supercomputing clusters. The simulations were entered into a queue to be processed after they were uploaded. After the results of the simulation were computed, the output data had to be downloaded from the servers for viewing and analyzing. This entire process to get the output from a single three dimensional simulation iteration would take up to a week, depending on how long the simulation waited in queue, how long computation took, and how long it took to transfer the data. Also, simulations had often waited days in queue only to end up not producing any useable data due to small errors within the model setup or submission files. Many of these errors could be checked for by scanning the input data locally, but some of them did not appear until the simulation actually began to run. However, by carefully constructing the models' meshes, ensuring only small deformations would occur during each iteration, and by gaining expertise in the ability to correct any errors that appeared, the iterations method had produced successful three dimensional results and insight into curling in a reasonable time period.

4.3.2 Three Dimensional Results

Testing began on the three dimensional Baseline models within a limited subset of the parameter space. This allowed for the iterations method to be tweaked as necessary and observations to be made within a limited grouping. The insight gained from this preliminary testing was then used for testing the rest of the desired parameters.

4.3.2.1 Initial Testing With Ideal Curling Parameters

To initially demonstrate and investigate the ability of the iterations method to produce reasonable results, a set of preliminary parameters was chosen based on the results obtained with two dimensional modeling work. Initial simulations were done at an angle of 37 degrees, particle velocities of 1200 and 1490 feet per second, and 21, 42, 84, and 168 impacts per iteration. This created a total of eight different simulation models. It was thought that if curling similar to that observed in field, in house, and with two dimensional modeling could not result under these parameters, than the overall likelihood for three dimensional modeling successes under the current model setup was rather low. Table 4.9 shows the parameters chosen for initial testing.

Table 4.9 – Initial three dimensional iterations testing parameters and values

Parameter	**Values**
Blade Model	3D Baseline
Blade Width	0.5”
Particle Diameter	40 mil
Particle Velocity	1200, 1490
Impact Angle	37°
Boundary Condition	0.16” from LE
Number of Impacts	21, 42, 84, 168 per iteration
Number of Iterations	10 attempted

These initial simulations produced very favorable results. Of the eight models and parameters simulated, six produced curling in realistic shape and magnitude. The other two simulation sets produced curling but either its magnitude was too large or its shape was not ideal. The results from all of these simulations are shown below in Figure 4.23.

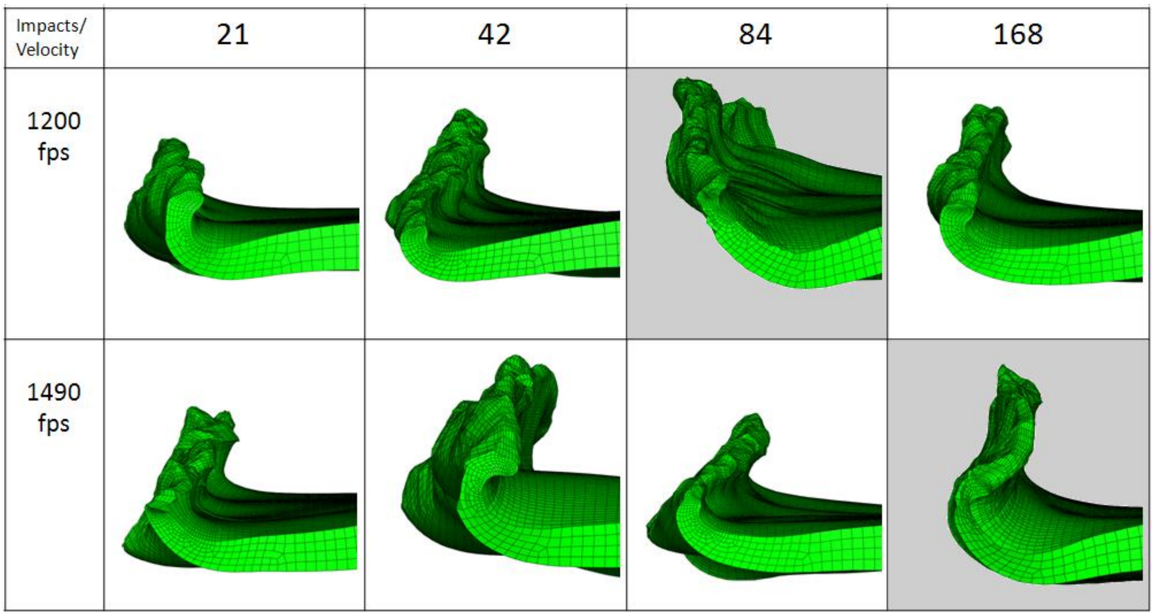

Figure 4.23 – Model results of 40 mil particles impacting at an angle of 37 degrees, with 21, 42, 84, and 168 impacts per iteration, a velocity of 1200 and 1490 feet per second, and a boundary condition of 0.16 inches. Eight iterations were attempted and the two that did not produce appropriate curling are shaded in gray.

Figure 4.23 shows the model results of this initial three dimensional iterations testing with 40 mil particles impacting at 37 degrees, 21-168 impacts per iteration, a velocity of 1200 and 1490 feet per second, and a boundary condition of 0.16 inches. As mentioned, there were only two models that did not show proper magnitude and geometry of curling. These were the 1200 feet per second and 84 impacts per iteration simulation and the 1490 feet per second and 168 impacts per iteration simulation. For both of these simulations, the resulting deformation magnitude was larger than that observed on field tested components and the geometry of the deformation did not closely resemble that of curling. However, both of these simulations still showed results better than what was observed on a greater number of two dimensional work. The other six models all showed curling of both appropriate magnitude and geometry. Due to these observations, it was assumed that the appearance of curling could be affected by the random and non-uniform oscillations of the blade that occurred between particle impacts.

A number of simulation iterations did not run to completion (not all particle groups impacted the blade); the likelihood of failure increased with the number of impacts per iteration. The simulation would either run over its allotted processing time on the server cluster or it would simply fail early due to mesh distortion or another error. Throughout every simulation set there were individual particles that did not impact the blade due to oscillations and non-uniform deformation caused by previous impacts. Therefore, the calculable number of total impacts should be considered nothing more than an estimate.

Regardless of the number of impacts modeled per iteration, a majority of deformation tended to occur within the first 3-5 iterations. Subsequent iterations tended to only have a slight cosmetic effect by adding consistency along the leading edge length or minor changes in curling magnitude and shape. Overall, the number of impacts per iteration did not have any effect on deformation magnitude or curling shape. Of the simulation sets that produced the best curl, all of the tested numbers of impacts per iterations were used. Figures 4.24 and 4.25 show the progression of two different simulations through multiple iterations.

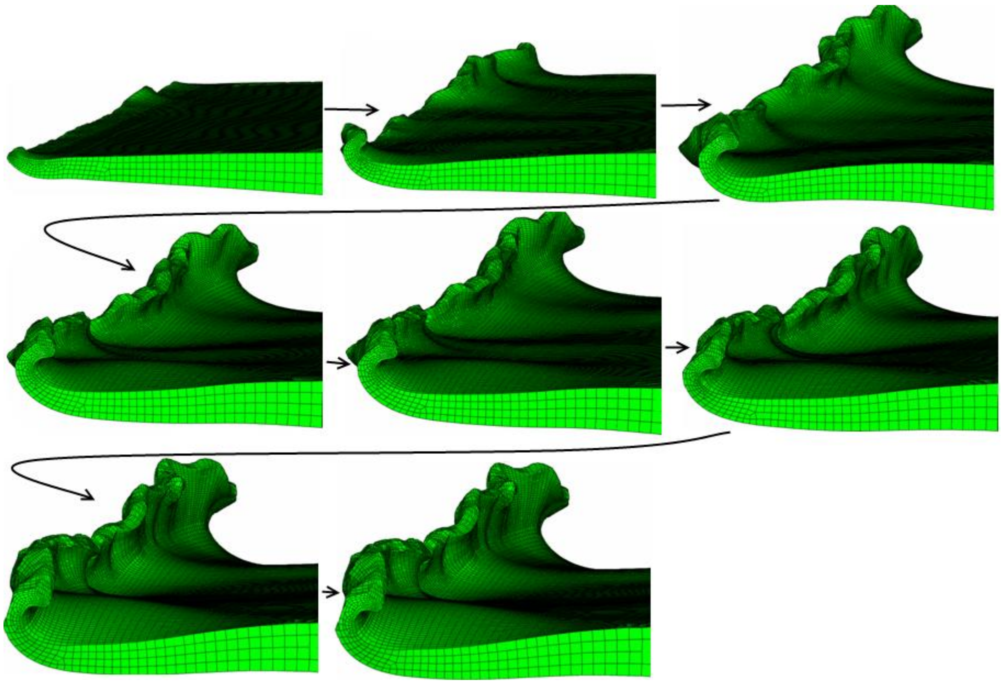

Figure 4.24 - The progression of a 37 degree, 1490 feet per second, 40 mil simulation with 42 impacts per iteration.

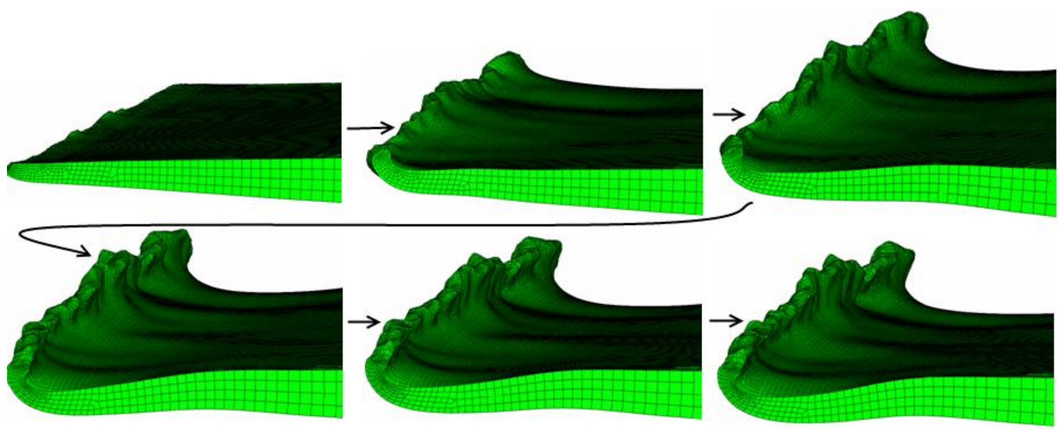

Figure 4.25 - The progression of a 37 degree, 1200 feet per second, 40 mil simulation with 21 impacts per iteration.

Figure 4.24 demonstrated how a majority of the deformation using multiple iterations occurs during the first 3-5 iterations. Figure 4.25 shows this observation as well. As was mentioned, a majority of deformation occurred during the first 3-5 iterations regardless of impacts per iterations and particle velocity.

4.3.2.2 Further Parametric Evaluation – Impact Angle and Velocity

After the success demonstrated with the initial testing parameters of the three dimensional multiple iterations method, the parameters were further expanded for testing on the Baseline model. New models and simulations were run including velocities of 590, 900, and 1700 feet per second and angles of 10, 20, 30, 37, 45, and 60 degrees. The number of impacts per iteration was set at 84. This value was decided upon after positive observations with the previous testing. It was also observed to be the largest number of impacts that can be routinely simulated to completion. A majority of 168 impacts per iterations simulations failed before all particles struck the blade. The complete set of parameters evaluated is given in Table 4.10.

Table 4.10 – Further three dimensional testing parameters and values

Parameter	**Values**
Blade Model	3D Baseline
Blade Width	0.5”
Particle Diameter	40 mil
Particle Velocity	900, 1200, 1490, 1700 fps
Impact Angle	10°, 20°, 30°, 37°, 45°, 60°
Boundary Condition	0.16” from LE
Number of Impacts	84 per iteration
Number of Iterations	5 attempted

In general, the results observed from these simulation groups mirrored, in a relative sense, what had been previously obtained through single runs. Lower impact angles of 10 and 20 degrees did not consistently curl or deform in a way that resembles the curling found on blade cross-sections. Angles of 30, 37, and 45 degrees all produced at least some consistent curling. 60 degree impacts did not result in curling of the leading edge. Figure 4.26 demonstrates these observations, and a more detailed discussion follows.

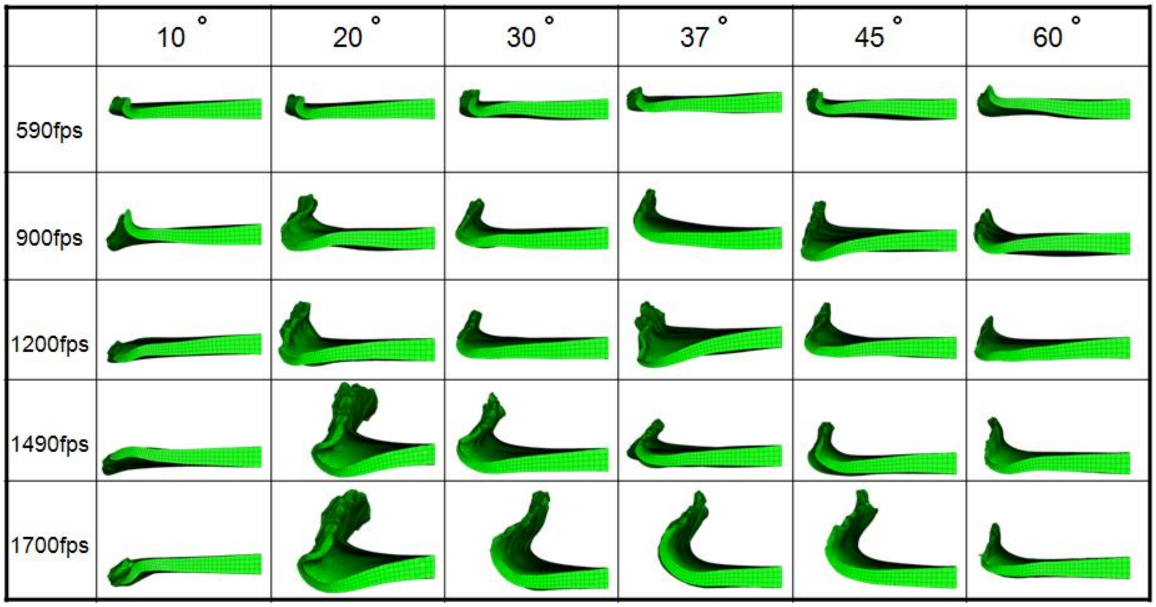

Figure 4.26 – Model results of five iterations of 84 impacts at angle of 10, 20, 30, 37, 45, and 60 degrees, velocities of 590, 900, 1200, 1490, and 1700 feet per second, and with a boundary condition of 0.16 inches.

As Figure 4.26 shows, a 10 degree impingement angle on the Baseline model had an unexpected and previously unseen result. Because impacts were occurring at such a low angle, grazing impacts resulted in the blade deforming downwards for velocities of 1200 feet per second and above. After only a few iterations at 10 degrees, the meshes at these higher velocities would become extensively distorted, far beyond what could be reasonably corrected. This was likely due to the mesh being optimized for higher angle impacts. The lower velocity simulation sets did not immediately result in excessive irreparable deformation, but would rather just slowly deform the opposite direction as to what was anticipated. Due to the observations made in regard to the deformation shape, and the irreparable distortions and errors on the mesh, simulations on the Baseline model at 10 degrees were discontinued earlier than those run at other angles.

Simulation attempts at an angle of 20 degrees resulted in a curled shape, although not quite as appropriate in geometry or magnitude as desired. Similar to the 10 degree simulations, some of the 20 degree simulations also resulted in undesirable geometry due to the modeling setup and methodology. Partial sections of the blade would deform downwards, while other sections would deform upwards in the expected manner. The downwards curling was thought to occur for the same reason that it had occurred at 10 degrees: there was a prevalence of low angle grazing impacts which would contribute more towards deflecting the blade down rather than curling it in the positive vertical direction. The sections of the blade that deformed vertically are thought to have occurred due to deflections altering the location of impacting particles past some necessary threshold.

The 30 degree impact angle simulations produced reasonable curling geometry at a magnitude based on velocity that mirrored previous results. 900, 1200, and 1490 feet per second velocities had all resulted in appropriate curling magnitudes, while 1700 feet per second impacts created larger deformation sizes than what is commonly observed and the 590 feet per second impacts created smaller deformation sizes and did not fully curl the blade.

Due to the initial testing results, the only additional simulations run at 37 degrees were the 590, 900, and 1700 feet per second impact velocities. The results of the 1700 feet per second simulation showed high magnitude curling, while the 900 feet per second simulations produced curling more appropriately sized. The 590 feet per second impacts did not fully curl the blade.

45 degree impact angle simulations also resulted in a positive degree of curling. However, this curling is not quite as defined as those resulting from the 37 and 30 degree simulations. Due to the higher angle, the horizontal deformation that defines curling is not as large in magnitude as what results from lower angles. Although the vertical deformation is of an appropriate magnitude, the horizontal deformation is lower than what is commonly observed.

Finally, 60 degree impacts had the same lack of horizontal deformation that was observed in the 45 degree simulations. The 60 degree simulations showed almost no horizontal deformation or curling geometry.

4.4 Discussion of Overall 2D and 3D Curl Modeling Results

The primary goal of both the two and three dimensional simulations on the Baseline model was to determine under what conditions curl can reasonably and consistently be expected to occur. In these simulations, the conditions were defined by the following parameters: Particle diameter, particle velocity, impacting angle, and number of impacts. In addition, constraints general to simplifying a complex system through finite element modeling were imposed. Through studying the conditions likely to produce curl through modeling, it was possible to model these conditions with protective systems (e.g. coatings) in place to determine their efficacy. The following is a discussion of the general trends observed when modeling under certain conditions.

4.4.1 Effect of Particle Diameter

The diameter of impacting particles appeared to have had the largest effect on the resulting magnitude of the deformation of the leading edge. Particles of diameters 6 and 12 mil produced very little deformation at all velocities on the Baseline 100 percent tip model. However, the thinner 15 and 50 percent tip models did show curl with these particle sizes. Larger diameter particles were able to cause significant deformation and curl, the extent of the curl being largely dependent on the size of the particle. Impacts from 40 mil diameter particles consistently resulted in the most ideal deformation magnitude. This is demonstrated in Figure 4.27.

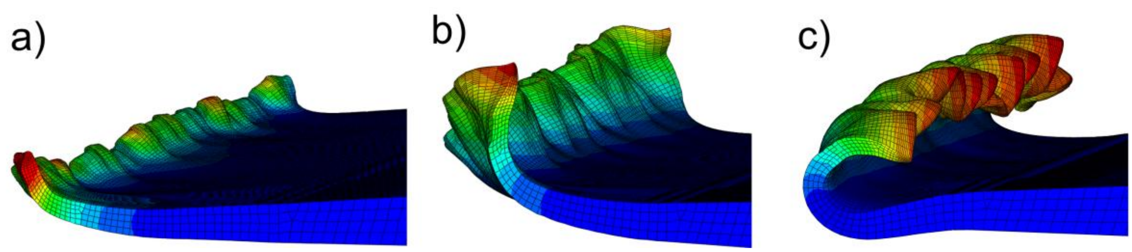

Figure 4.27 – A single iteration of 40 particle impacts from 37 degrees with a velocity of 1490 feet per second and particle diameters of (a) 40 mil, (b) 60 mil, and (c) 120 mil. Smaller particle sizes (6 and 12 mil) are not shown due to their lack of observable deformation.

As shown in Figure 4.27, impacts of 60 and 120 mil diameter particles for the same number of impacts, velocity, and angle resulted in deformation considerably larger than what is commonly observed on micrographs from field tested components. The result from 40 mil particle, shown in Figure 4.27a, demonstrated deformation of a magnitude similar to curling. If more iterations would have been processed, curling of an appropriate magnitude and geometry would have likely been produced. Varying particle diameters alone can produce the desired deformation magnitude, but not the desired curl geometry at the leading edge.

4.4.2 Effect of Particle Velocity

The velocity of the impacting particles was expected to have a considerable effect on the magnitude of the resulting leading edge deformation. This was partially true, but was actually dependent on the modeling methodology. For simulations of multiple impacts where blade oscillations occurred, the deformation size was heavily dependent on the velocity of the impacting particles. For two dimensional multiple iteration simulations, the magnitude of deformation was nearly independent of particle velocity, but strongly affected curl geometry. This is due to the greater 'control' this methodology allowed by removing the compounding effects of high velocity impacts on the deflection and eventual deformation of the blade. For three dimensional modeling, 1700 feet per second velocities resulted in magnitudes far greater than what is commonly observed in the field. The tested velocities of 900 and 590 feet per second both produced curling, but required many more iterations to do so. The two dimensional results from multiple impact simulations, while being generally larger in magnitude than the three dimensional results, followed this basic trend. Figure 4.28 gives an example of the effects of increasing velocities on both the two and three dimensional models.

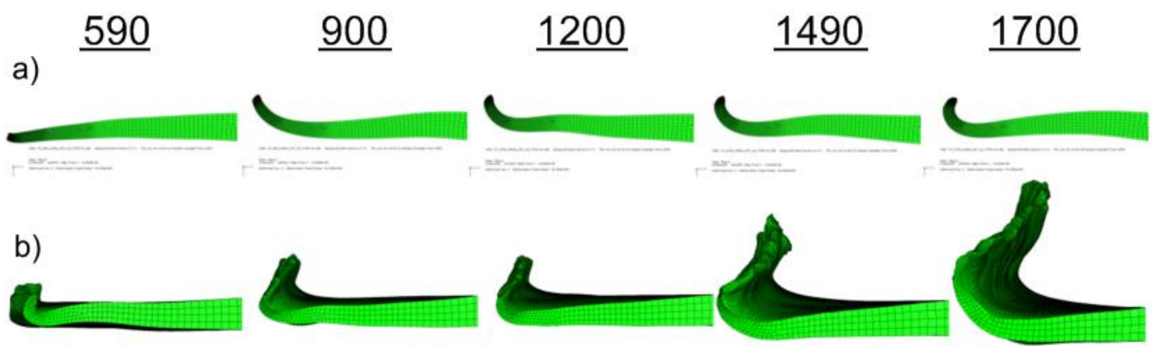

Figure 4.28 – Model results showing the different effects of increasing velocities on (a) two and (b) three dimensional models. The velocities tested were 590, 900, 1200, 1490, and 1700 feet per second.

4.4.3 Effect of Particle Impact Angle and Location

The angle of the impacting particles had the greatest effect on the overall shape of the deformed leading edge. Although the initial modeling work showed promising results from multiple angle impact conditions, it was believed that these conditions were not occurring in situ, so only single angle impacts were considered. For single angle impacts, it was observed that curling occurred most prevalently around the angle of 37 degrees, confirming previous deformation testing results. 30 and 45 degree impacts also produced consistent curling. Lower angles did not tend to deform the blade vertically enough for curling, although some curling was observed at 20 degrees. Angles higher than 45 degrees did not able to deform the blade horizontally enough to provide the proper curled geometry as demonstrated by Figure 4.29.

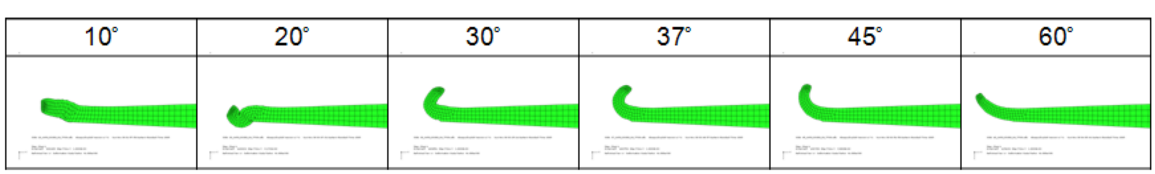

Figure 4.29 – Model results from 6 impact iterations of a 40 mil particle at 1200 feet per second and angle between 10 and 60 degrees.

4.4.4 Model Constraints – Boundary Condition

Although they are not considered to be part of the particle impact conditions, it is import to consider model constraints when discussing the conditions for curling. The major consideration is the boundary condition. A boundary condition too loose will results in large deflections of the blade and unrealistic deformation, while a boundary condition too small will restrict the model to a point where it is unable to curl. An ideal boundary condition size was found to be about 0.16 inches in three dimensional modeling and about 0.04 to 0.08 inches in two dimensional modeling.

4.4.5 Model Verification

One of the most important aspects of finite element analysis is ensuring that the modeling work being done is accurate. This can be accomplished through verifying the results of the simulations against damaged components from the field or from in-house testing. The Applied Research Laboratories' Advanced Coating Department has an in house erosion testing rig as shown in Figure 4.30. This erosion rig allowed for adjustments to be made to the same impact parameters that were studied through finite element modeling simulation for model verification. The rig included a compressed air supply which accelerates particles of multiple possible diameters to a maximum velocity dependent on the allowed air pressure. These particles strike a small blade target which can be set at variable angles.

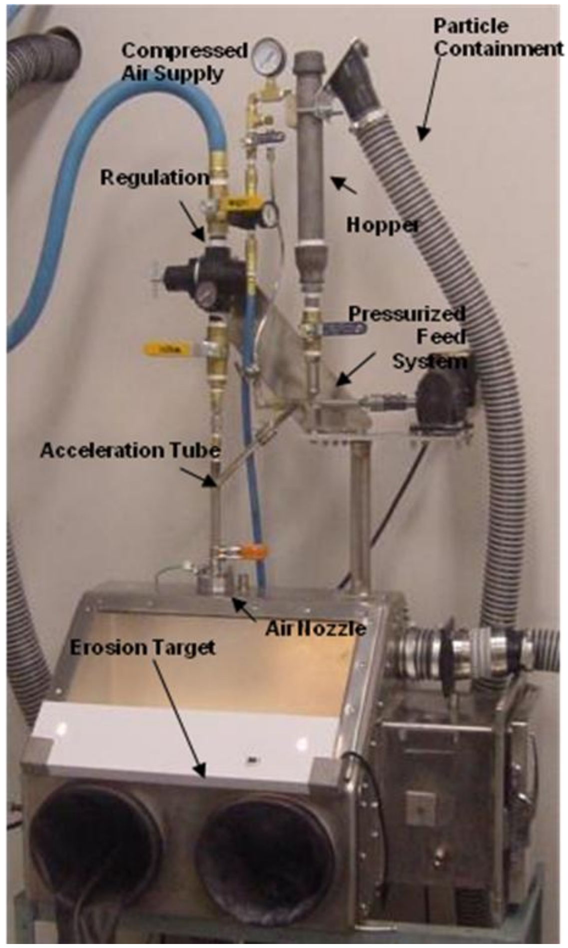

Figure 4.30 – Advanced Coatings Department's erosion rig used for model verification.

By comparing the deformation that results from a variety of different impact parameters with simulation and in house testing to the leading edge curl observed on components taken from the field, a proper verification of the testing and simulating methodology was performed. Figure 4.31 shows various results obtained model simulation, in house testing, and a blisk taken from the field.

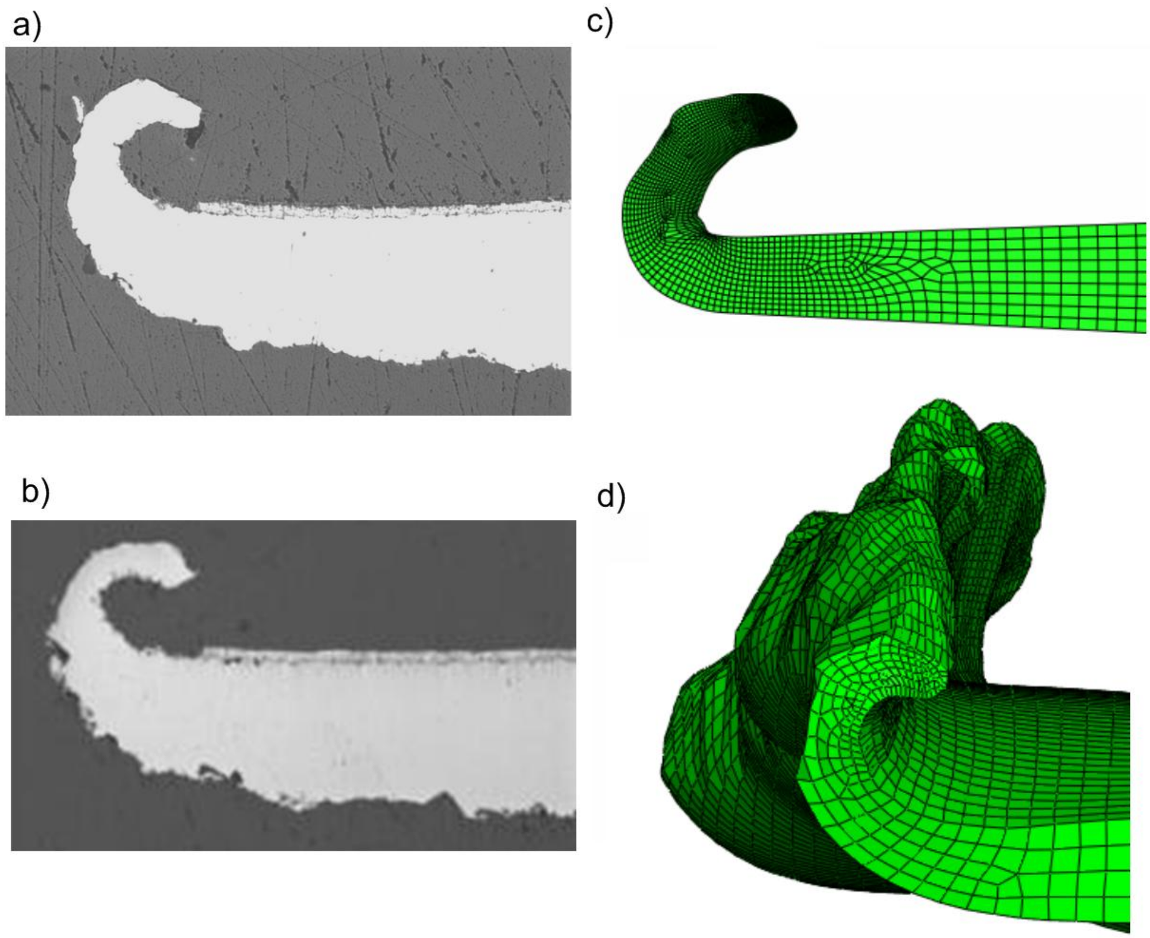

Figure 4.31 – (a) A optical micrograph showing the leading edge cross section of a deformed Baseline blade taken from the field; (b) similar deformation that was obtained through in-house testing; (c) two and (d) three dimensional model simulation results.

The leading edge curl deformation observed on all four images in Figure 4.31 is of a very similar magnitude and geometry. In addition, the curling obtained through simulation on Figures 4.31(c-d) is under the same angular, velocity, and particle conditions (37 degrees, 1490 feet per second, 40 mil). The curling shown from the in-house testing rig was obtained through 37 degrees as well, but due to the physical constraints of the rig itself, particle velocity was restricted to 590 feet per second; however many more particles impacted the blade through testing than through simulation, contributing to a greater resulting deformation at the reduced velocity. The simulated velocities are closer to what is expected for impacts in an actual compressor section. The ability to accurately simulate leading edge curl provides a new technique and computational tool to explore alternative methodologies in suppressing or preventing leading edge curl.

4.5 Methods for Suppression of Leading Edge Curl

There were three methods explored in an effort to determine whether they would be able to prevent, or at least mitigate to some degree, curling of the blade leading edge. These methods included thickening the leading edge geometry of the blade, altering the material properties of the blade, and adding a thin ceramic coating to the blade. Once these methods were successfully integrated into the finite element model, results were compared to the previous modeling of leading edge curl in order to determine the efficacy of these new methods with regard to the prevention of curl.

4.5.1 Thicker Leading Edge Geometry – New Contour Model

The first of the methods attempted to reduce curling of the Baseline leading edge was thickening the blade's leading edge geometry. By thickening the leading edge, it was assumed that increased and higher energy particle impacts would be required to cause blade deformation to the point of required maintenance. A thicker leading edge is expected to be resistant to erosion and blade deformation. Figure 4.32 shows the New Contour leading edge geometry in comparison to the original Baseline model.

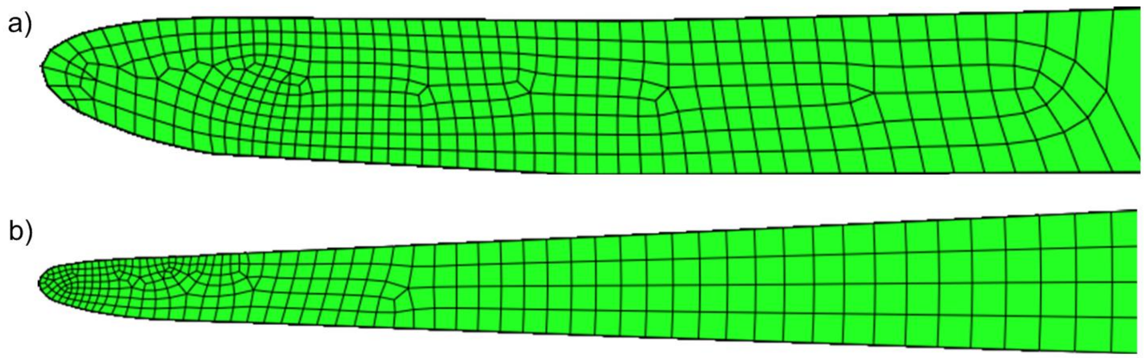

Figure 4.32 - (a) Meshed model of the New Contour blade compared to a (b) meshed model of the original Baseline blade.

4.5.1.1 Model Setup and Parameters

In order to confirm the ability of the New Contour model to resist leading edge curl, the model was simulated under the same conditions that produced curling on the Baseline blade model. These conditions, as concluded before, were 40 mil diameter particles with impacts angles between 30 and 45 degrees (ideally at 37 degrees) and particle velocities between 900 and 1490 feet per second. In addition to these basic parameters, the New Contour blade was also modeled under conditions outside this range in order to give a more comprehensive comparison between the response of this blade geometry and the Baseline. Although these results were not necessarily directly useful for curl modeling, it was believed that they could offer some additional insight with only negligible extra computational and working time requirements.

The New Contour blade geometry was modeled in both two and three dimensions. The testing conditions used for both dimensions were also to be held constant between the Baseline and New Contour simulations including the boundary conditions and number of particle impacts and iterations. This was done to ensure consistency and accuracy in the results and to increase the confidence in the possible ability of the New Contour model to properly prevent or mitigate leading edge curl.

4.5.1.2 Model Results

The two and three dimensional results were obtained under the previously described modeling conditions and parameters. These results, when compared to those obtained with the Baseline model, all showed significantly less deformation and no curling.

4.5.1.2.1 Two Dimensional Results

The two dimensional New Contour blade model was simulated under the conditions described in Table 4.11. These parameters correspond with the Baseline simulation parameters previously listed in Table 4.7.

Table 4.11 - New Contour two dimensional parameters and values

Parameter	**Values**
Blade Model	2D Baseline
Particle Diameter	6, 12, 40 mil
Particle Velocity	590, 900, 1200, 1490, 1700 fps
Impact Angle	10°, 20°, 30°, 37°, 45°, 60°
Boundary Condition	0.02”, 0.04”, 0.08”, 0.16” from LE
Number of Iterations	6

Figure 4.33 presents the results obtained through simulation of four particle impacts at angles between 10 and 60 degrees, under various velocities between 590 and

1700 feet per second, and with a boundary condition of 0.04 inches. Comparing Figure 4.33 with Figure 4.12 (the Baseline model results obtained under the same impact conditions) shows very minimal deformation resulting even from high velocity impacts. Almost no deformation is observed with impact velocities less than 1200 fps. The angle of impingement had minimal effect on the resulting deformation, likely due to the overall minimal deformation magnitude, further confirming this approach in suppressing leading edge deformation.

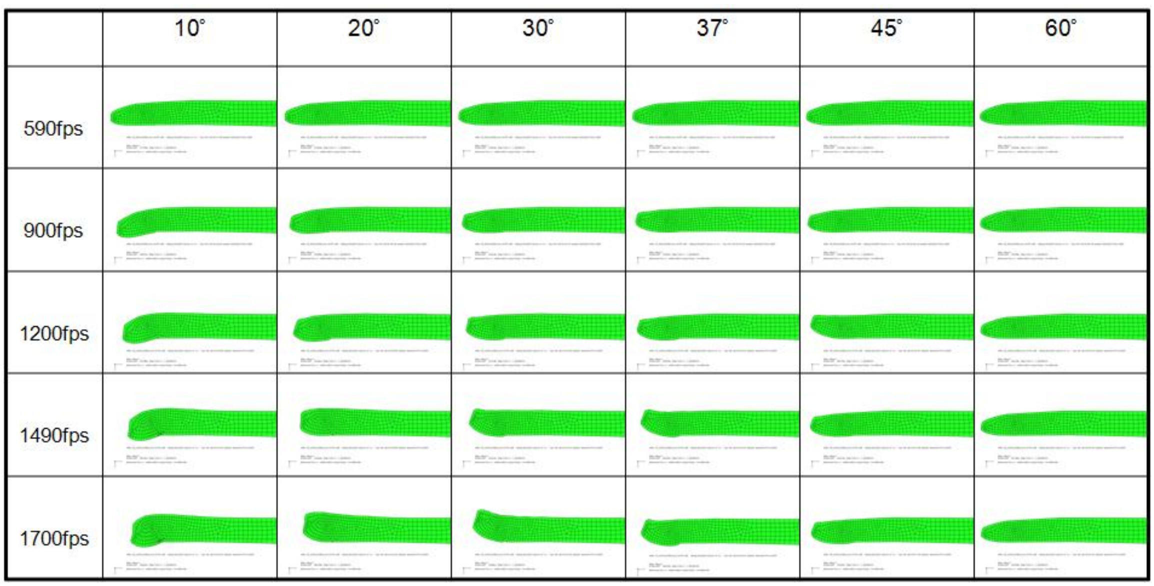

Figure 4.33 – Model results from six iterations of 40 mil particle impacts at 10, 20, 30, 37, 45, and 60 degrees, 590, 900, 1200, 1490, and 1700 feet per second, and with a boundary condition of 0.04 inches.

Figure 4.34 shows the results of the New Contour blade after impacts from 40 mil particles at 37 degrees, with velocities between 590 and 1700 feet per second, and with a boundary condition between 0.02 and 0.16 inches. Comparing Figure 4.34 to Figure 4.13 further demonstrates suppression of leading edge curl. As Figure 4.34 demonstrates, an increase in boundary condition does result in an increase in blade deformation. However, this deformation is still at a much lesser magnitude than that of the Baseline in Figure 4.17. It should also be noted that for velocities less than 1200 feet per second, Figure 4.34 shows minimal deformation on all New Contour models.

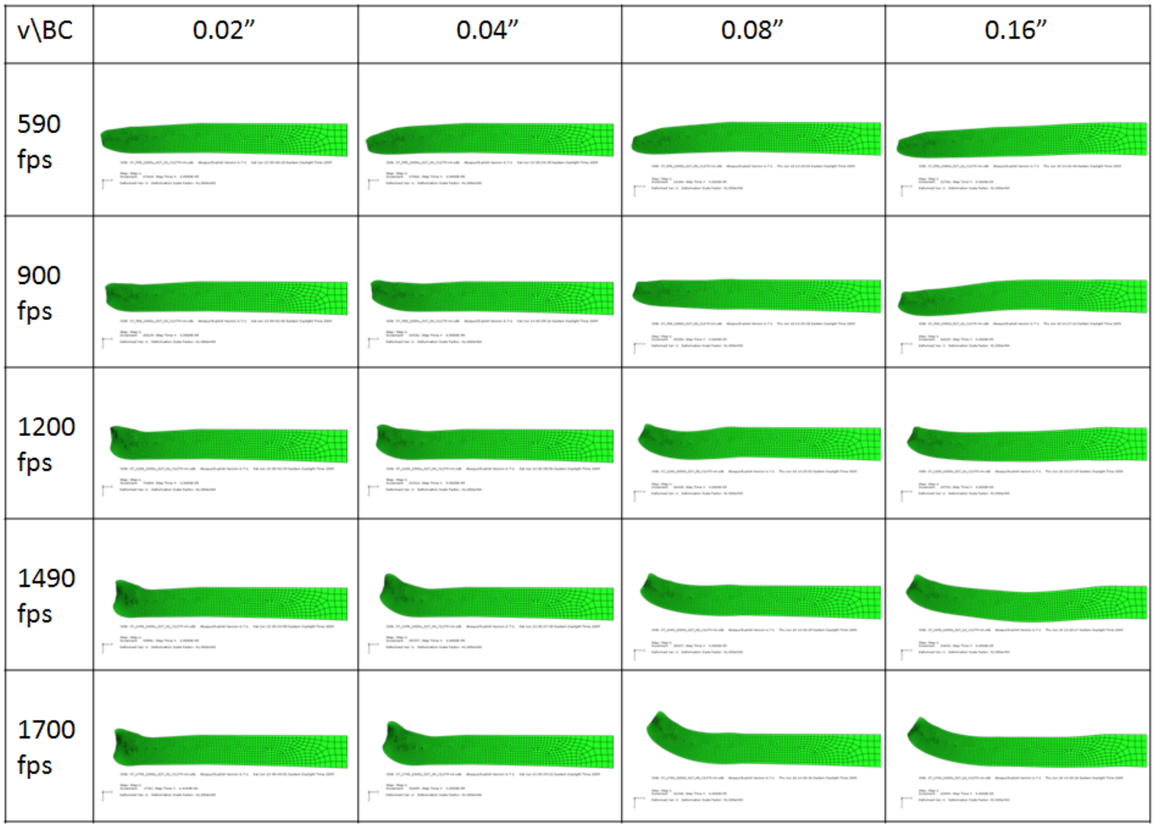

Figure 4.34 – Model results from eight 40 mil particle impacts at 37 degrees, 590, 900, 1200, 1490, and 1700 feet per second, and with boundary conditions at 0.02, 0.04, 0.08, and 0.16 inches.

4.5.1.2.2 Three Dimensional Results

The parameters used for three dimensional modeling on the New Contour blade model are given in Table 4.12. These parameters match those as described in Table 4.10 for Baseline blade modeling.

Table 4.12 – New Contour three dimensional parameters and values

Parameter	Values
Blade Model	3D Baseline
Blade Width	0.5”
Particle Diameter	40 mil
Particle Velocity	900, 1200, 1490, 1700 fps
Impact Angle	10°, 20°, 30°, 37°, 45°, 60°
Boundary Condition	0.16” from LE
Number of Impacts	84 per iterations
Number of Iterations	6 attempted

Figure 4.35 shows the model results from the three dimensional New Contour simulations of five iterations of 84 impacts from 40 mil particles at angles between 10 and 60 degrees, velocities between 590 and 1700 feet per second, and with a 0.16 inch boundary condition. Figure 4.35 can be compared to the Baseline results in Figure 4.26 produced under the conditions. The results obtained through this three dimensional modeling also correlate with those obtained with the two dimensional New COntour model shown in Figure 4.34. For velocities of 590 and 900 fps, very minimal deformation occurs. Deformation magnitude is observed to increase with velocity. Although the New Contour model did not curl due to its increased leading edge thickness, vertical deformation was still observed for impact angles greater than 10 degrees. The angle of impact also affects the vertical deformation in a similar way to the Baseline model in that vertical deformation was at a maximum between 30 and 45 degrees.

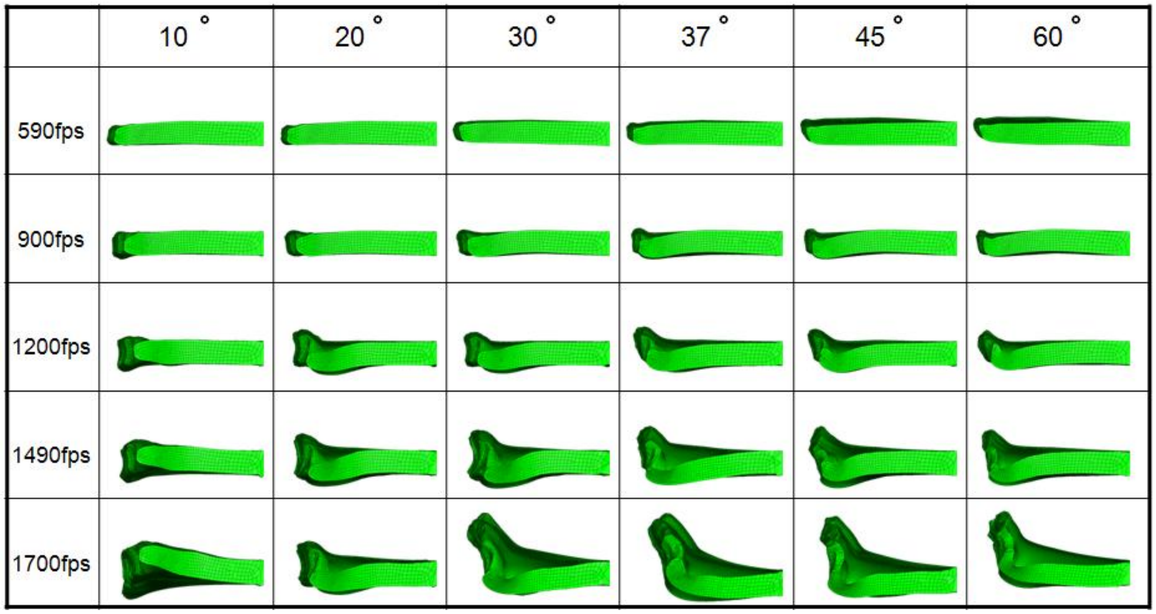

Figure 4.35 – Model results of five iterations of 84 impacts from 40 mil particles at angles of 10, 20, 30, 37, 45, and 60 degrees, velocities of 590, 900, 1200, 1490, and 1700 feet per second, and with a boundary condition of 0.16 inches.

4.5.1.3 Discussion and Comparison to Baseline Model

The primary observation that can be made regarding the New Contour model is that thickening the leading edge suppressed leading edge curl formation. Without erosion and under realistic particle impact conditions, it is apparent that the New Contour blade does not undergo the same curling deformation as the Baseline model. The increased stiffness of the New Contour design does not allow deformation to the extent of what is observed on the Baseline blade under tested conditions.

Figure 4.36 shows a comparison in deformation progression between the two dimensional Baseline and New Contour model through four 40 mil particle impacts at 37 degrees, 1200 and 1490 feet per second, and with a 0.04 inch boundary condition. As mentioned previously, these impact parameters have been demonstrated to be the conditions under which curling is most likely to occur on the Baseline model. It is apparent that while the Baseline model shows significant curling and deformation, the New Contour model does not curl and only shows minimal deformation. This demonstrates success in the New Contour's design to prevent and mitigate curling of the blade leading edge.

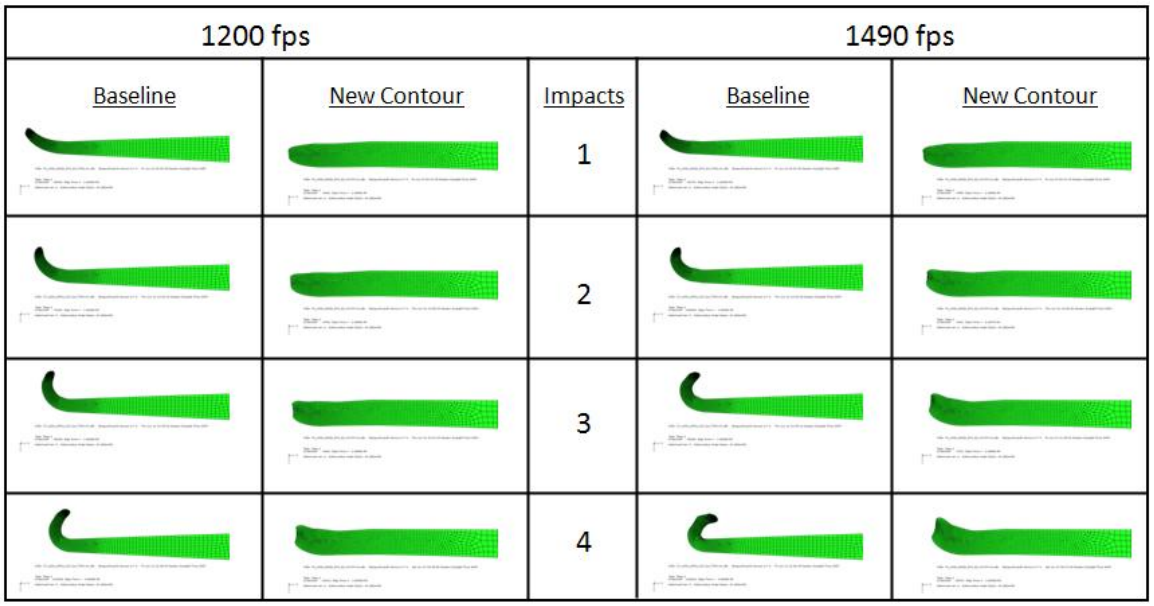

Figure 4.36 – Progression of deformation on the two dimensional Baseline and New Contour models through four impacts of 40 mil particles at 37 degrees, with a velocity of 1200 and 1490 feet per second, and with a boundary condition of 0.04 inches.

Figure 4.37 shows a comparison in deformation between the three dimensional Baseline and New Contour models through five iterations of 84 impacts from 40 mil particle impacts at 30 and 37 degrees, 590, 900, and 1200 feet per second, and with a 0.16 inch boundary condition. Figure 4.37 shows results similar to Figure 4.36 but obtained through three dimensional modeling. Again, it can be observed that the conditions under which curling is evident on the Baseline model do not produce curling on the New Contour model. These results give further evidence of the greater ability of the New

Contour leading edge to resist curl and particle impact deformation in comparison to the Baseline geometry.

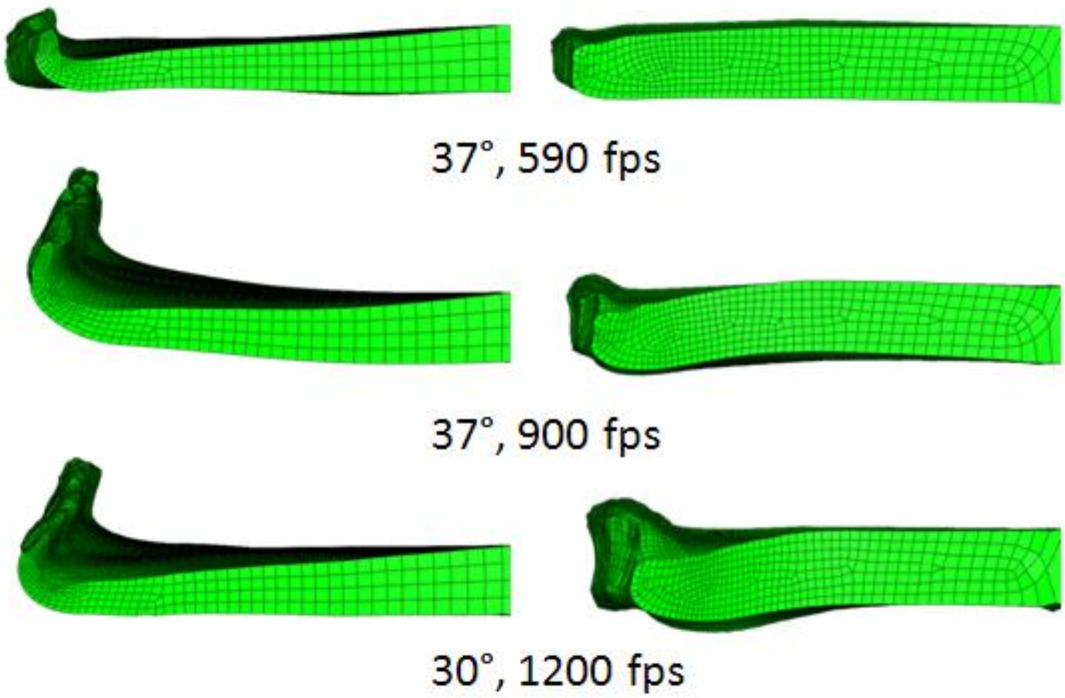

Figure 4.37 - Deformation on the two dimensional Baseline and New Contour models through five iterations from 84 impacts of 40 mil particles at 30 and 37 degrees, with a velocity of 590, 900 and 1200 feet per second, and with a boundary condition of 0.16 inches.

A more comprehensive and numerical listing of model results is given in Table 4.13 detailing the maximum vertical and horizontal displacement deformation obtained through the three dimensional parametric modeling on the Baseline and New Contour models. The standard method for measuring curl was illustrated earlier in Figure 2.3. For blade models where curling did not occur, the horizontal deformation is listed as zero. The measurement listed in Table 4.13 were made after four iterations of 84 impacts for

40 mil particles under angles of 10-60 degrees, velocities of 590-1700 feet per second, and with a boundary condition of 0.16 inches.

Table 4.13 – Measured maximum vertical and horizontal deformation of the three dimensional Baseline and New Contour blade models

Impact angle	**Velocity (fps)**	**Vertical Deformation (mils)**		**Horizontal Deformation (mils)**	
		Baseline	**New Contour**	**Baseline**	**New Contour**
10	900	16.84	3.33	0.00	0.00
-	1200	-6.84	5.44	0.00	0.00
-	1490	-3.51	20.00	0.00	0.00
-	1700	-12.81	28.42	0.00	0.00
20	900	13.90	4.39	9.82	0.00
-	1200	27.02	8.25	13.33	0.00
-	1490	41.05	23.86	22.98	0.00
-	1700	48.77	17.37	33.33	0.00
30	900	16.32	4.56	11.58	0.00
-	1200	16.67	8.57	8.42	0.00
-	1490	25.61	20.35	15.44	0.00
-	1700	52.63	16.49	26.49	0.00
37	900	16.49	4.74	6.14	0.00
-	1200	20.88	6.67	0.00	0.00
-	1490	16.32	17.89	7.37	0.00
-	1700	55.61	11.22	18.60	0.00
45	900	12.46	2.98	6.14	0.00
-	1200	15.79	8.07	6.49	0.00
-	1490	23.68	18.25	11.75	0.00
-	1700	56.14	11.75	24.74	0.00
60	900	10.88	3.33	0.00	0.00
-	1200	10.53	6.49	0.00	0.00
-	1490	26.14	7.72	0.00	0.00
-	1700	21.40	14.56	0.00	0.00

From the values listed in Table 4.13, it is evident that the measured deformations are significantly greater on the Baseline blade for almost all examined conditions. The exception is at 10 degrees, but this was likely a result of modeling methodology and how the Baseline blade deformed negatively in the vertical direction which is unrealistic. This deformation, as mentioned, was due to the how the particles were modeled to only graze the leading edge and deflected the blade negatively rather than deform it positively. Except for 10 degrees however, Table 4.13 shows a reduced deformation of almost half for the New Contour blade compared to the Baseline under all other conditions. This further demonstrates the ability of the New Contour model to resist deformation under particle impact conditions which result in curling on the Baseline blade model.

4.5.2 New Blade Material – Ti-6Al-4V and Inconel 718

The next method attempted for mitigating leading edge blade curl on the Baseline blade model was exploring different material properties for the blade component. This was achieved through altering the material properties (based on material composition) of the Baseline blade model within the simulation. The new materials used for testing were a titanium alloy (Ti-6Al-4V) and a nickel-chromium based superalloy (Inconel 718). The titanium alloy was selected as it has a much greater ductility than the Baseline's AM355, while the Inconel alloy has a higher Young's modulus. The different responses and behaviors of the blade under curl-producing particle impact conditions and different material make-ups were to be examined and discussed below.

It was not believed that either of the new blade materials would be able to fully mitigate curling of the Baseline blade. Fully mitigating leading edge curl deformation was considered difficult under realistic material parameters and with the Baseline blade's geometry. However, it was still considered possible for the new materials to mitigate curling or deformation to at least some degree. Any deformation of a smaller magnitude when compared the Baseline blade with AM355 would be considered a success. Table 4.14 lists the parameters tested for this modeling effort. These parameters and values have all resulted in curling of the Baseline blade in previous simulations.

Table 4.14 – New blade materials testing parameters and values

Parameter	Values
Blade Model	2D Baseline
Blade Material	AM355, Ti-6Al-4V, Inconel 718
Particle Diameter	40 mil
Particle Velocity	590, 900, 1200, 1490, 1700 fps
Impact Angle	37°
Boundary Condition	0.2", 0.3", 0.5", 0.16" from LE
Number of Iterations	6 attempted

Using the three different blade material properties (AM355, Ti-6Al-4V, Inconel 718) a model was created with the same particle impact condition and the results were observed. As mentioned, particle impact conditions chosen for testing were based on previous results. Only an impact angle of 37 degrees was considered, along with particle velocities between 590 and 1700 feet per second. Because curling was only observed with the large 40 mil particles, they were the only particle size considered.

4.5.2.1 Model Results

Figure 4.38 shows a comparison between the Baseline blade modeled under the original and new materials after six impacts from 40 mil particles at a angle of 37 degrees, a velocity of 590, 900, 1200, 1490, and 1700 feet per second, and with a boundary condition of 0.02 and 0.03 inches. Curling is visible on almost every model shown, with the exception of the models run at 590 feet per second. More iterations would have likely resulted in curling on those models as well.

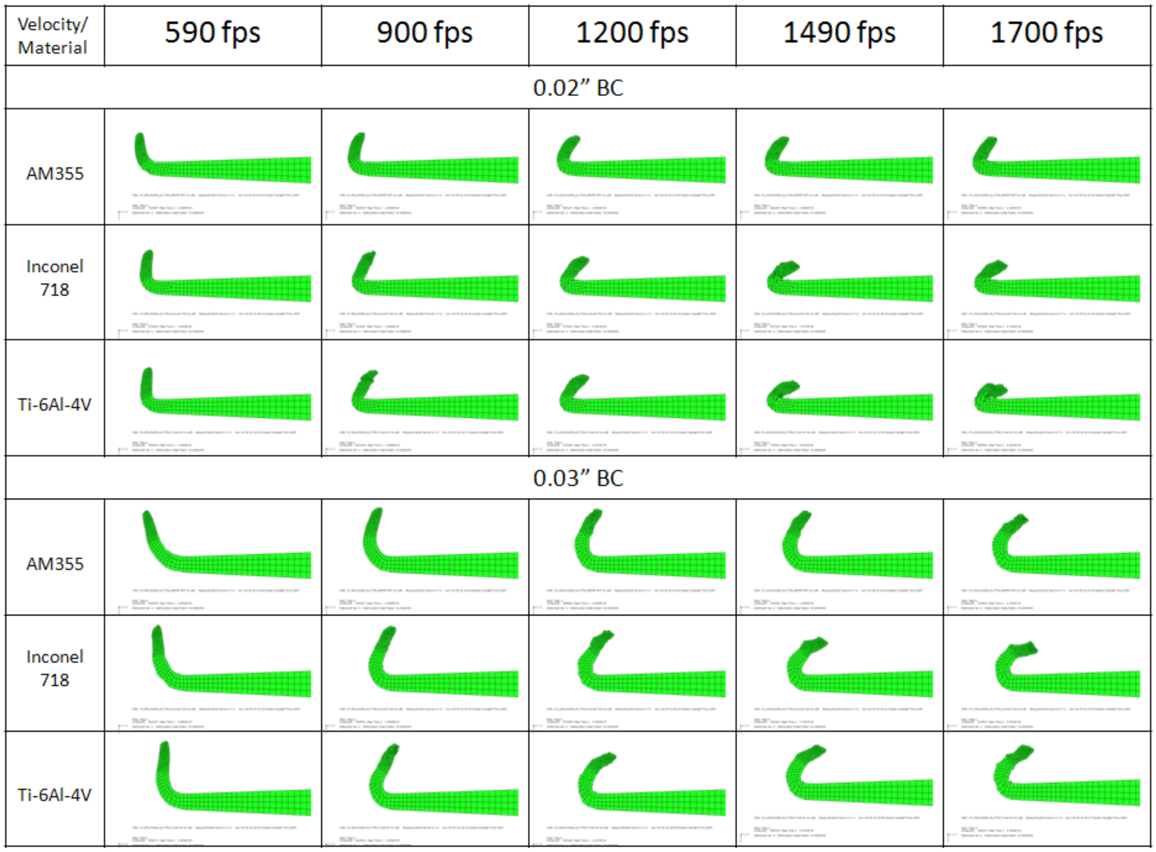

Figure 4.38 – Comparison between AM355, Ti-6Al-4V, and Inconel 718 on the Baseline blade after six impacts from 40 mil particles at 37 degrees, 590, 900, 1200, 1490, and 1700 feet per second, and with a 0.02 and 0.03 inch boundary condition.

4.5.2.2 Comparison to Baseline Model

From Figure 4.38 it is apparent that neither of the new materials performed better than AM355 under the same impact conditions. Both of the new materials showed higher magnitudes of curling and deformation after the same number of particle impact iterations. From this, a number of conclusions can be reached. It appears that curling is primarily dependent on the plastic response of the material. The yield stresses for both the Inconel and titanium alloys are less than that of AM355, while the Inconel alloy has a higher Young's modulus and the titanium alloy has a low Young's modulus. Additional models incorporating higher yield stresses are suggested for future work to suppress leading edge curl.

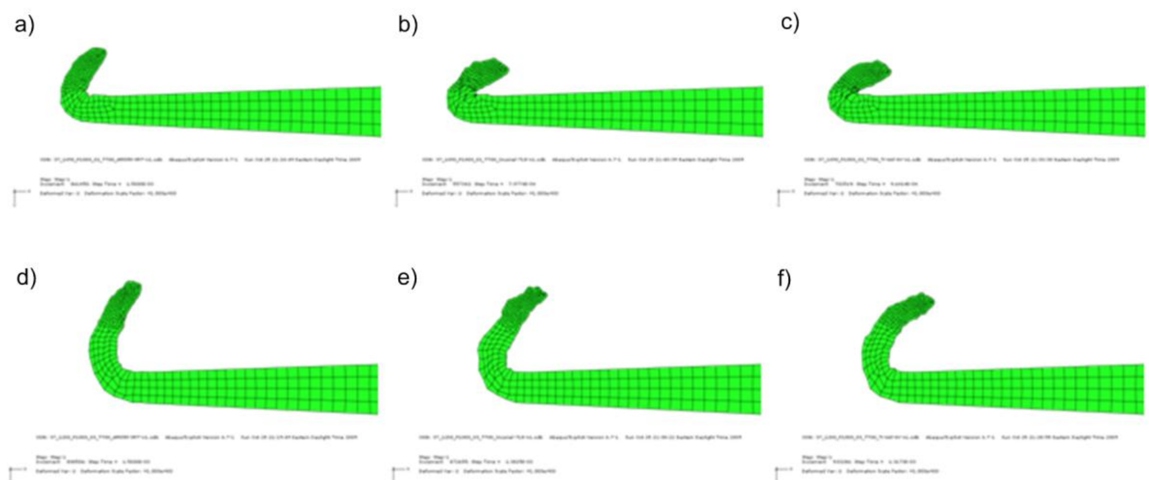

Figure 4.39 - Differences in response of the Baseline blade using (a, d) AM355, (b, e) Ti-6Al-4V and (d, f) Inconel-718. (a-c) have a 0.02 inch boundary condition while (d-f) have a 0.03 inch boundary condition.

Figure 4.39 provides a closer look at the differences in blade deformation for all of the results shown for the particle velocity of 1490 feet per second in Figure 5.38. These images further show that AM355 performed better than either of the new alloys under the same tested conditions. While curling occurred on all models, the magnitude of the curling was less on the AM355 Baseline blade after the same number of impacts.

4.5.3 Using a Thin Titanium Nitride Coating to Suppress Leading Edge Curl

The final method tested for the mitigation of leading edge curl and deformation was the addition of a thin ceramic coating. This modeling effort attempted to examine any additional benefits for leading edge protection offered by the application of a thin erosion resistant coating. Coating models of thicknesses 20 and 50 microns were created and applied to the two dimensional New Contour blade model. The coating was modeled as a titanium nitride coating using available material data from Latella at al. [18]. In addition to the obtained material parameters, the Young's modulus of the coating was both increased and decreased by a factor of 50 percent in order to determine any effect this might have on leading edge curl suppression and erosion protection.

The coated and uncoated models were all simulated under the same particle impact conditions in an effort to determine the effectiveness of the coating for mitigating leading edge deformation. Only two dimensional modeling was attempted due to computational constraints. The mesh required for accurately modeling erosion of the coating needed to be extremely fine, which added a significant count of elements to the simulation and increased computation time is accordance. Modeling the coating to the accuracy necessary to model erosion in three dimensions would have been challenging with the available computational capabilities. Figure 4.40 shows the 20 and 50 micron coatings applied to the New Contour blade model. As can be observed, the mesh for the coating is considerably finer than that of the blade and was required to simulate erosion accurately.

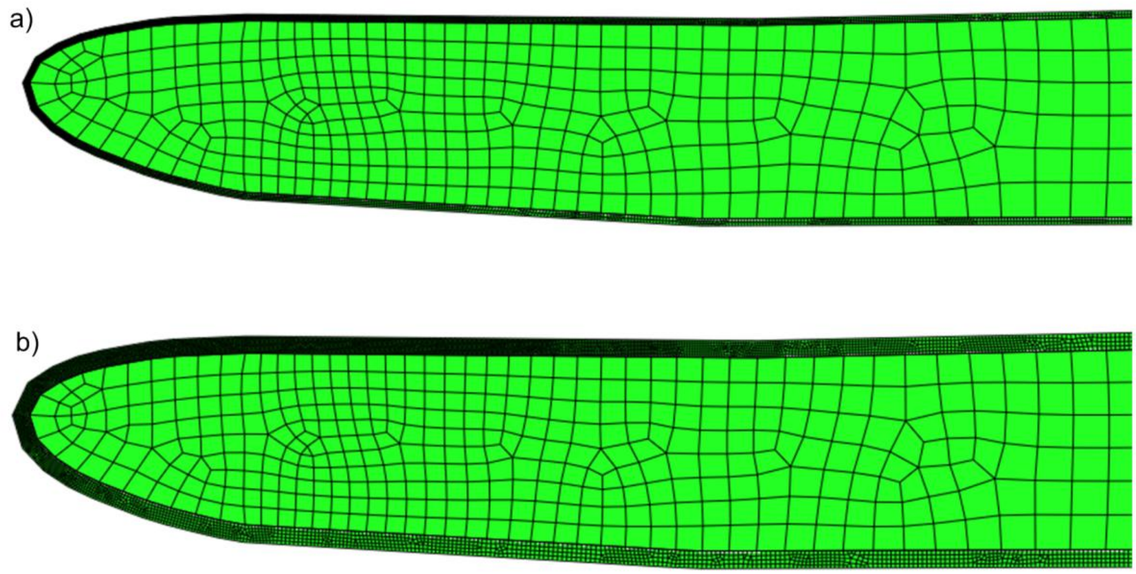

Figure 4.40 - The New Contour blade model with a (a) 20 and (b) 50 micron coating applied.

4.5.3.1 TiN Coating Model and Parameters

The coated and uncoated New Contour models were tested similarly to previous efforts. Impact parameters that were shown to produce curling and large deformation of the Baseline and New Contour models were chosen in order to gauge the ability of the coatings for leading edge protection efficacy. In addition to the standard parameter set, the 6 and 12 mil particles were reintroduced for simulation. Preliminary testing showed minimal coating damage under impact from small and low velocity particles. Therefore, the 6 and 12 mil particles were also tested under the same velocity and angle conditions as the 40 mil particles in an attempt to determine the necessary particle sizes and velocities for coating damage to initiate.

As is listed in Table 4.15, along with all other tested parameters, the New Contour model was constrained under 0.02, 0.04, 0.08, and 0.16 inch boundary conditions. The coating itself did not have a boundary condition but was modeled to be infinitely bonded to the blade. This assumption was necessary due to how, as mentioned in the previous chapter, attempts to model cohesive behavior, including normal and tangential bond strengths, were unsuccessful. Based on previous testing, the cohesive element model in Abaqus is not particularly suited for modeling the interface between a ductile material and a ceramic being modeled to erode. This seemed to be especially true for highly dynamic and short-duration simulations where large strains were expected to occur.

Table 4.15 – Thin ceramic coating testing parameters and values

Parameter	**Values**
Blade Model	2D New Contour
Coating Thickness	20, 50 microns
TiN Young's Modulus	30, 60, 90 (x10^6) psi
Particle Diameter	6, 12, 40 mil
Particle Velocity	590, 900, 1200, 1490, 1700 fps
Impact Angle	37°
Boundary Condition	0.3", 0.5", 0.8", 0.16" from LE
Number of Iterations	20 attempted

4.5.3.2 Model Results

Simulations were run on the New Contour blade to 20 iterations on particle impacts. Most of the simulations ran to completion without considerable failure. Figures 4.41 to 4.46 give the model results obtained from testing the coated and uncoated New Contour models at an angle of 37 degrees, a velocity of 590, 900, 1200, 1490, and 1700 feet per second, and with a boundary condition of 0.03 and 0.05 inches. Twenty impacts from 6, 12, and 40 mil particles were attempted on each model, although mesh failure prevented this number of impacts from being simulated on a number of models.

Figure 4.41 gives the model results after 20 impacts from 6 mil particles at an angle of 37 degrees, with velocities between 590 and 1700 feet per second, with a boundary condition of 0.03 inches, uncoated and with the six coating configurations. From this figure, it is observed that higher velocity impacted resulted in considerably more coating erosion. The 20 micron coating showed moderately more erosion resistance, except at 590 feet per second where the 50 micron coating with the original and increased Young's modulus showed almost no erosion. None of the models showed much deformation, so the ability for each coating configuration to suppress deformation cannot be compared.

Figure 4.41 – Model results from twenty impacts from 6 mil particles at an angle of 37 degrees, a velocity of 590, 900, 1200, 1490, and 1700 feet per second, a boundary condition of 0.03 inches, and with the 20 and 50 micron coatings with the baseline and adjusted Young's modulus values. The grayed model did not run to completion.

Figure 4.42 gives the model results after 20 impacts from 12 mil particles at an angle of 37 degrees, with velocities between 590 and 1700 feet per second, with a boundary condition of 0.03 inches, uncoated and with the six coating configurations. Compared to the 6 mil impacts, these model results show moderately more erosion and leading edge deformation. Compared to the uncoated model, each coating configuration showed a similar degree of deformation prevention. Erosion resistance is slightly greater for the 20 micron coating. The different Young's moduli for both the 20 and 50 micron coatings have no noticeable effect on erosion resistance or deformation prevention.

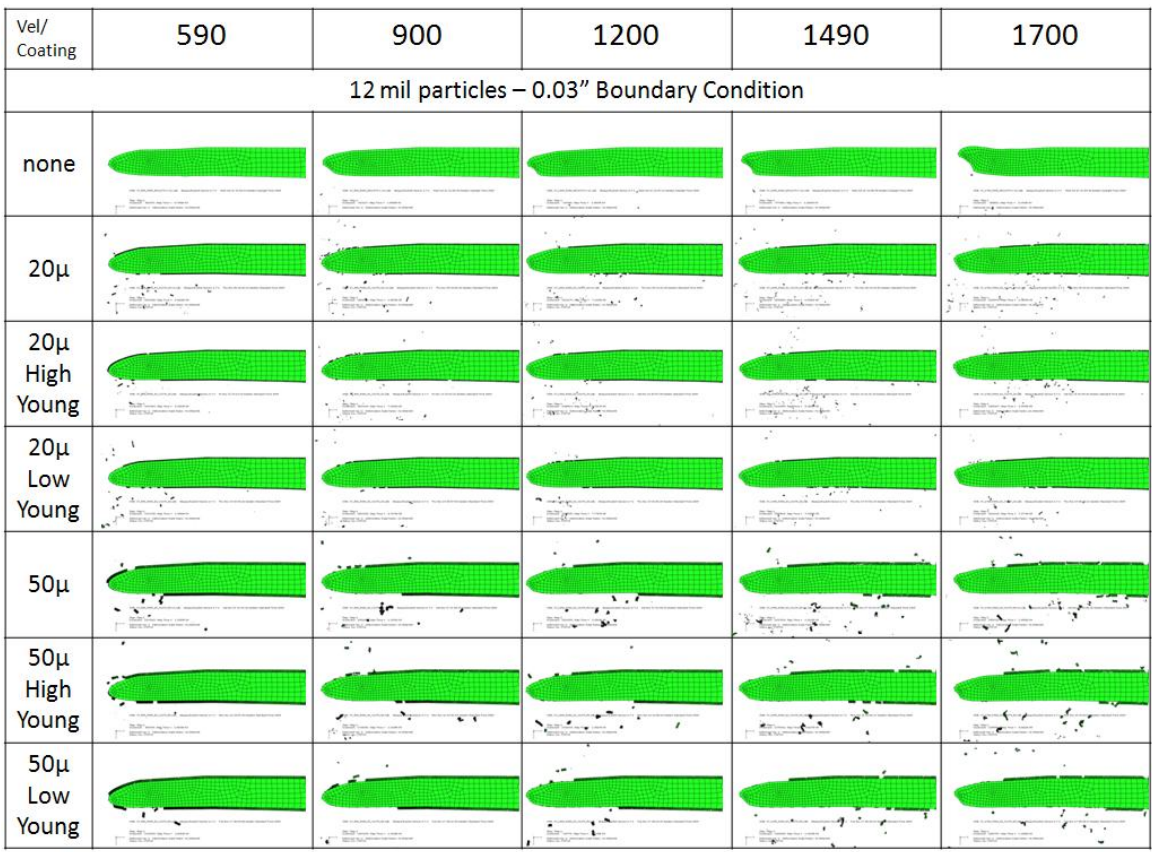

Figure 4.42 – Model results from twenty impacts from 12 mil particles at an angle of 37 degrees, a velocity of 590, 900, 1200, 1490, and 1700 feet per second, a boundary condition of 0.03 inches, and with the 20 and 50 micron coatings with the baseline and adjusted Young's modulus values.

Figure 4.43 gives the model results after 20 impacts from 40 mil particles at an angle of 37 degrees, with velocities between 590 and 1700 feet per second, with a boundary condition of 0.03 inches, uncoated and with the six coating configurations. Similar to Figure 4.42, every coated model shows a decreased level of leading edge deformation compared to the uncoated model. The least deformation is apparent on the 20 micron coating with the high Young's modulus. For the 50 micron coatings, the low Young's modulus coating resulted in the least deformation.

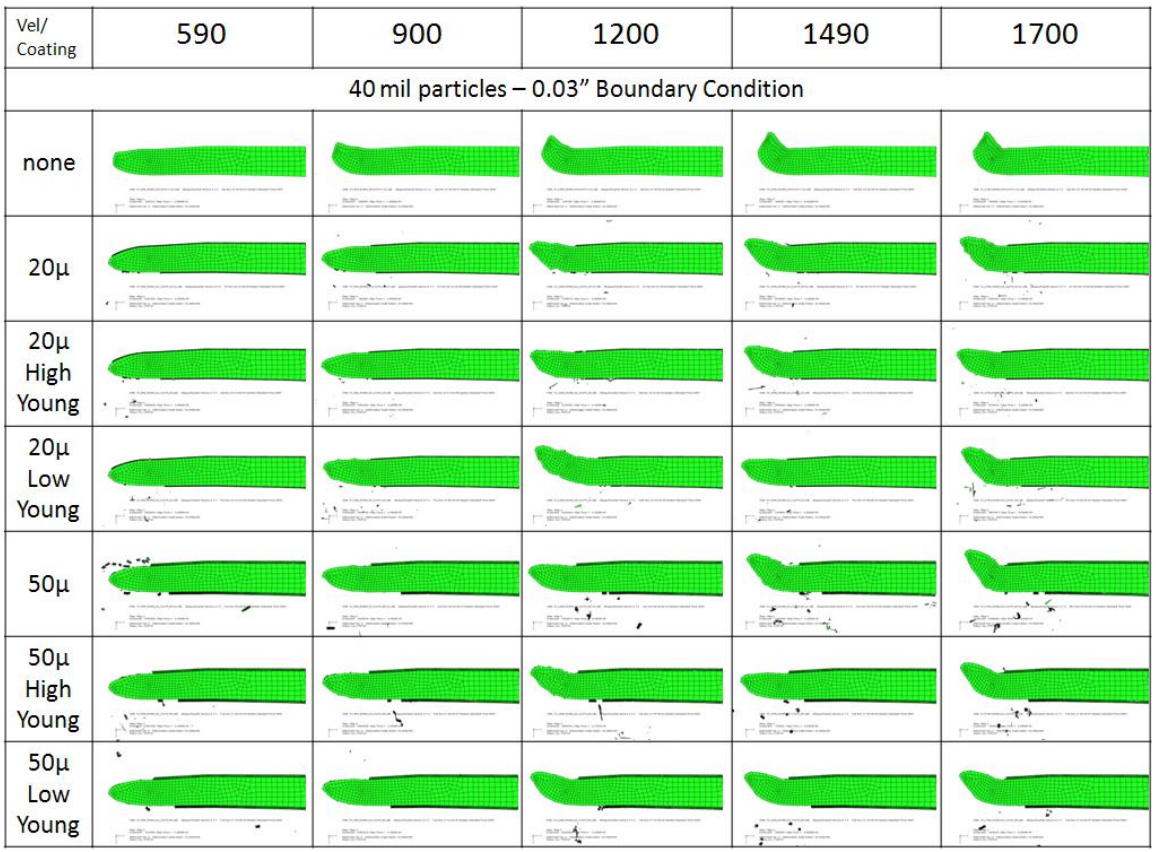

Figure 4.43 – Model results from twenty impacts from 40 mil particles at an angle of 37 degrees, a velocity of 590, 900, 1200, 1490, and 1700 feet per second, a boundary condition of 0.03 inches, and with the 20 and 50 micron coatings with the baseline and adjusted Young's modulus values.

Figure 4.44 gives the model results after 20 impacts from 6 mil particles at an angle of 37 degrees, with velocities between 590 and 1700 feet per second, with a boundary condition of 0.05 inches, uncoated and with the six coating configurations. Similar to Figure 4.41, the 20 micron coating showed overall better erosion resistance while the 50 micron coating models no erosion at 590 feet per second. In general, the results shown in Figure 4.44 mirror those previously shown in Figure 4.41. This is expected since the increased boundary condition should only have a noticeable effect when large deformations are present.

Figure 4.44 – Model results from twenty impacts from 6 mil particles at an angle of 37 degrees, a velocity of 590, 900, 1200, 1490, and 1700 feet per second, a boundary condition of 0.05 inches, and with the 20 and 50 micron coatings with the baseline and adjusted Young's modulus values.

Figure 4.45 gives the model results after 20 impacts from 12 mil particles at an angle of 37 degrees, with velocities between 590 and 1700 feet per second, with a boundary condition of 0.05 inches, uncoated and with the six coating configurations. These results mirror those shown in Figure 4.42. The 20 micron coating is observed to have the best erosion resistance under the tested conditions, with the higher Young's modulus configuration demonstrating the least erosion.

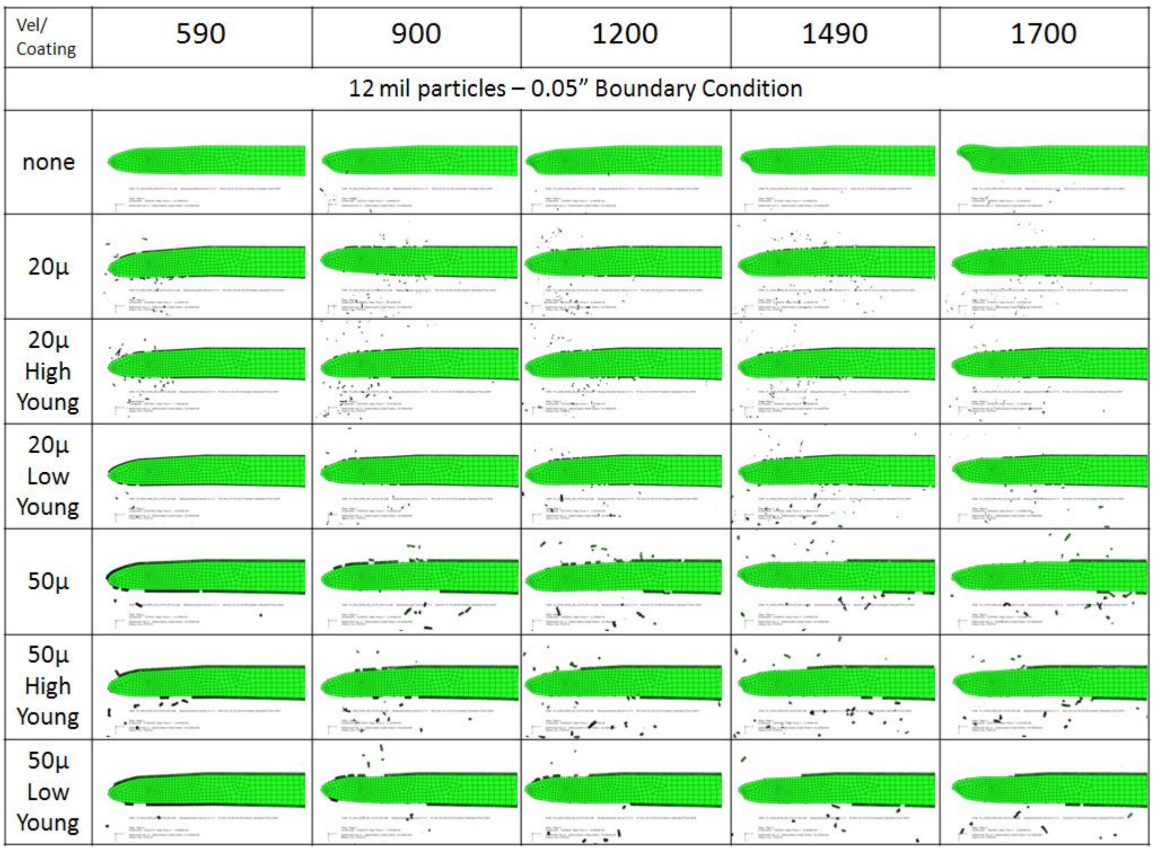

Figure 4.45 – Model results from twenty impacts from 12 mil particles at an angle of 37 degrees, a velocity of 590, 900, 1200, 1490, and 1700 feet per second, a boundary condition of 0.05 inches, and with the 20 and 50 micron coatings with the baseline and adjusted Young's modulus values.

Figure 4.46 gives the model results after 20 impacts from 40 mil particles at an angle of 37 degrees, with velocities between 590 and 1700 feet per second, with a boundary condition of 0.05 inches, uncoated and with the six coating configurations. As with the previous two figures, Figure 4.46 mirrors the results observed with the 0.03 inch boundary condition shown in Figure 4.43. The least deformation is observed on the 20 micron coating with the increased Young's modulus. All of the coatings are observed to have completely eroded around the leading edge after impacts from large diameter particles.

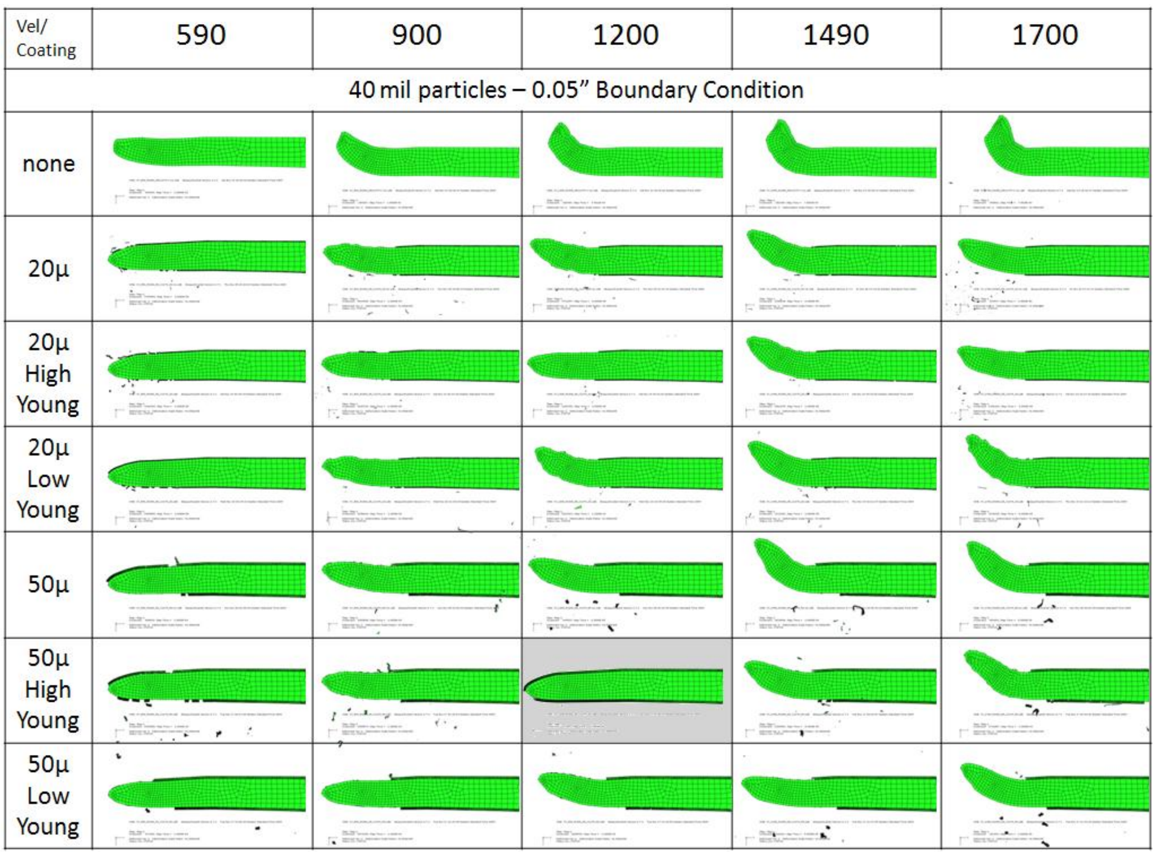

Figure 4.46 – Model results from twenty impacts from 40 mil particles at an angle of 37 degrees, a velocity of 590, 900, 1200, 1490, and 1700 feet per second, a boundary condition of 0.05 inches, and with the 20 and 50 micron coatings with the baseline and adjusted Young's modulus values. The grayed model did not run to completion.

Figure 4.47 demonstrated the progression of erosion for a 50 micron coating through nine impacts from a 6 mil particle at an angle of 37 degrees and a velocity of 900 feet per second. The manner in which the modeled coating erodes closely matches that observed in field tested components. It should be noted that larger particles and higher velocities are likely to cause complete erosion of the coating to the underlying substrate after a single impact.

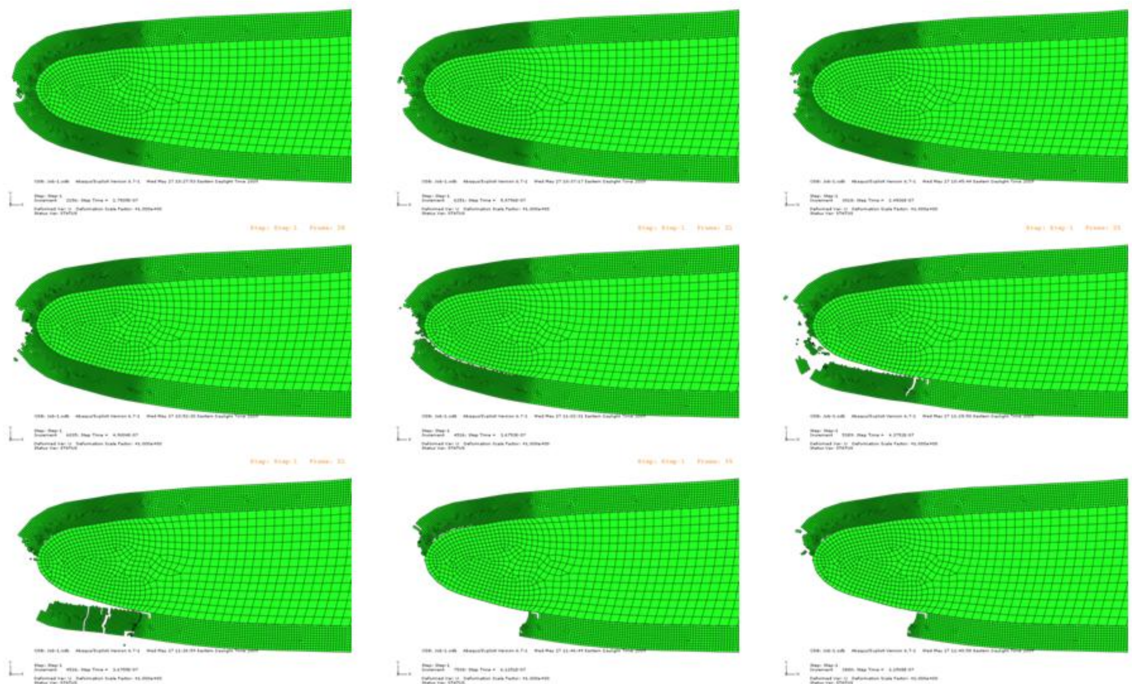

Figure 4.47 – Demonstration of erosion of 50 micron coating through nine impact iterations from a 6 mil particle at an angle of 37 degrees and with a velocity of 900 feet per second.

4.5.3.3 Discussion and Comparison to Baseline Model

Under all conditions, the addition of a thin coating to the leading edge of the New Contour blade model decreased the amount of deformation after 20 impact iterations. Surprisingly, the 20 micron thickness coating performed significantly better than the 50 micron coating under most conditions with regard to erosion resistance and deformation prevention. This likely resulted from the thinner coating's ability to deflect with the blade upon particle impact. The thicker coating acts much more brittle and fractures instead of elastically deflecting with the blade. There was an appreciable difference in deformation magnitude with different Young's moduli. The 20 micron coating showed increased deformation resistance with the higher Young's modulus, while the 50 micron coating showed increased erosion resistance with a lesser Young's modulus. This likely corresponds with the previous observation, in that the lower modulus on the 50 micron coatings allows the coating to deflect with the blade initially, preventing some degree of erosion of the coating due to tensile stresses resulting in brittle cracking. The higher modulus on the 20 micron coating offers greater stiffness which absorbs energy from the particle impacts and mitigates or prevents a degree of deformation.

4.6 Discussion and Evaluation of Curl Suppression Results

Three different approached were tested in an attempt to determine their ability to mitigate or suppress leading edge curl deformation on the Baseline blade. These methods were investigating the blade's leading edge geometry, altering the blade's material composition, and the application of a thin ceramic coating. The efficacy of an approach to suppress curling was determined by comparing the model results obtained with and without the approach for a given set of particle impact conditions. This allowed a direct examination to be made in regard to the approach's ability to suppress or mitigate curling and deformation of the leading edge.

Altering the geometry of the blade leading edge proved to be the most effective method of curl prevention. The thicker New Contour geometry was able to prevent any deformation from 6 and 12 mil particles, and showed significantly less deformation from 40 mil particles. Based on measurements taken from simulation results, the reduction of deformation magnitude was over 50 percent in the conditions curling was seen on the Baseline model. No curling was observed on the New Contour model. The New Contour model is unlikely to curl under realistic impact conditions without considerable erosion or thinning of the blade leading edge.

Changing the material properties of the blade did not have any perceived benefit. The blade material was changed from the Baseline's initial precipitate hardened steel, AM355, to a material more ductile and elastic, Ti-6Al-4V, and to a material that was stronger and less elastic, Inconel 718. Neither of these materials performed better than AM355, in that they both showed a greater magnitude of curling after being impacted under the same conditions. Based on these observations, it is likely that curling magnitude is primarily dependent on the yield stress and overall plastic response of the material. This is concluded from AM355 showing the least deformation while having the highest yield strength.

The addition of a thin titanium nitride coating was shown to have a positive benefit on the resulting blade deformation. Small particles and low velocities did not result in any damage to the coating and the underlying substrate, while large particles and high velocity impacts resulted in immediate failure and complete removal of the coating from the leading edge. Overall deformation was observed to be lesser in magnitude with the addition of the ceramic coating. The 20 micron coating was slightly more erosion resistant than the 50 micron coating, likely due to its ability to withstand deflection of the blade upon particle impact. The changes made to the coating material's Young's modulus had some appreciable effect on erosion resistance of the coating. Increasing the modulus on the 20 micron coating showed a decrease in blade deformation, while decreasing it on the 50 micron coating showed a decrease in deformation. Developing a material model for TiN that incorporates fracture toughness may have provided additional insight. It should also be noted that although coatings did offer significant protection compared to the uncoated model, under the impact conditions that produce the most significant damage coating erosion is highly probable.

Chapter 5

Conclusions

There were two primary goals for this thesis. These goals included exploring the phenomenon of leading edge curl as well as possible methods for preventing its occurrence. Leading edge curl was examined under different particle impact conditions, including particle size, particle velocity, angle of impact, and simulation parameters. Once the ability to model curling on the Baseline blade was achieved, simulations were run with measures implemented that intended to prevent or mitigate curling. These included modifying the leading edge geometry, changing the blade’s material composition, and adding a thin nitride coating.

5.1 Leading Edge Curling Conclusions

Based on the observations made during modeling and simulation on the two and three dimensional Baseline models, a number of conclusions can be reached regarding the occurrence of leading edge curl on engine compressor blades.

It was observed that small particles on the order of 6 to 12 mil do not have enough energy to cause significant plastic deformation to the Baseline leading edge. Even at high velocities, only minor deformation more similar to indentation than curling was observed. This was noted on both the two and three dimensional simulations. Large diameter particles were able to cause substantial deformation, and at velocities of 1490 feet per second and higher, showed deformation magnitudes far greater than is commonly observed. Testing particle diameters above 40 mil, including 60, 80, and 120 mil all showed curling but at a very high magnitude. Based on these observations, it can be concluded that particle diameters approximately 40 mil or greater are necessary to deform and curl the blade, while smaller particles may likely contribute more towards erosion or small local deformations.

Particle velocities between 590 and 1785 feet per second were simulated. Using 40 mil diameter particles, deformation resembling curl was observed with all velocities. The magnitude of this deformation appeared to correspondingly increase with increases in velocity. Velocities of 1200 and 1490 feet per second were observed to result in the most appropriately sized curl magnitudes. Higher velocities tended to overly deform the blade while lower velocities did not always fully curl the blade.

A range of impact angles between 0 and 90 degrees was examined during simulation. Based on the known geometry and dynamics of a compressor blisk and particle stream combined with previous knowledge of the leading edge curl phenomenon, curling was expected at 37 degrees. This assumption held true. Distinct curling geometry was most noticeable at 30 and 37 degrees. Curling was also observed at 20 and 45 degrees, but this curling geometry was less than ideally shaped. Lower angles did not deform the blade vertically enough to curl, while higher angles did not deform the blade horizontally enough to fully curl.

There were a number of simulation parameters examined during these modeling efforts. A boundary condition was found to be necessary to limit elastic deflections and oscillations during simulations with multiple particle impacts. It was also determined that impacting particles at the very leading edge resulted in the best method to simulate curling since it allowed greater control and flexibility with multiple impact simulations. The primary observations was that grazing impacts were most likely to plastically deform the blade and immediately rebound off, while direct impacts were not as transient and imparted a great deal of energy into elastically deflecting a larger portion of the blade leading edge.

Conditions for Curling:

- Particle Diameter: between 12 and 40 mil, but likely closer to 40 mil or larger
- Particle Velocity: between 1200 and 1490 feet per second
- Impact Angle: between 30 and 37 degrees
- Boundary Condition: simulate at most first 0.16 inches of leading edge

5.2 Leading Edge Curling Suppression Conclusions

Once the conditions under which curling occurs were determined, efforts to mitigate curl were examined. These efforts included modifying the geometry and material properties of the blade, as well as applying a coating to the new blade geometry to determine it efficacy at preventing deformation. The material properties of the coating were also examined. The conditions used for testing the ability of each deformation suppression approach was based on the information obtained through previous model evaluation determined to cause curl on the Baseline blade.

5.2.1 New Contour Model

The thicker leading edge geometry model of the Baseline blade, known as the New Contour model, was expected to reduce deformation and curling of the Baseline blade. This was due to its thicker leading edge being more capable of absorbing impacts from high velocity particles without deforming. Based on observations made on two and three dimensional modeling, the New Contour model performed exceptionally well when compared to the Baseline under the same particle impact conditions. A reduction in deformation magnitude between 2-3x was observed under all conditions that had produced curling on the Baseline blade.

5.2.2 New Materials – Inconel 718 and Ti-6Al-4V

New materials were tested and compared to the Baseline's AM355 material. These materials included a stronger material with a higher Young's modulus and hardness, Inconel 718, and a more elastic material with a lower Young's modulus and hardness, Ti-6Al-4V. Neither of these materials performed as well as AM355 with regard to the ability to prevent deformation and curling. It was also noted that neither of these new materials had a yield stress as high as AM355's. The resulting magnitude and ability of a blade to curl is primarily determined on the blade material's yield stress, as curling and deformation are primarily plastic behavioral responses.

5.2.3 Titanium Nitride Coating

A 20 micron and 50 micron titanium nitride coating were applied to the New Contour blade model in order to test whether there would be any additional benefit with regard to deformation mitigation. In addition, the dependence of the coating's ability to withstand erosion on the coating's Young's modulus was also examined. It was determined that under all conditions the coated blades performed better than the uncoated blades with regard to deformation magnitude. The 20 micron coating was observed to perform slightly better than the 50 micron coating. This is attributed to the thicker coating's inability to elastically deflect causing an increased erosion rate. The Young's modulus of the coating material had little effect on the erosion resistance of the coating under the conditions tested.

Prevention and Mitigation of Curl

In summary, prevention and suppression of leading edge curl for compressor components can be achieved with knowledge of the following observations and conclusions:

- Thicker leading edge geometry prevents curling and shows 2-3x reduction in deformation magnitude
- Inconel 718 and Ti-6Al-4V did not result in a significant reduction of curling or deformation. Higher yield stresses are likely the means to prevent curling of the leading edge.

- Both a 20 and 50 micron coating helped mitigate deformation to the leading edge.
    - Large particles were observed to damage the entire thickness of the coating in a single impact. Smaller particles and lower velocities required multiple impacts to progressively erode the coating
    - Thicker coatings show decreased blade deformation with lesser Young's modulus while thinner coatings show decreased blade deformation with a higher Young's modulus

The best method to prevent curling, based on these modeling efforts, would be the incorporation of the New Contour leading edge geometry with a 20 micron coating designed to have a high Young's modulus.

Chapter 6

Future Work

Based on the conclusions reached through the work of this thesis, a number of recommendations for future work can be made.

Further studies investigating different blade geometries to suppress leading curling are suggested. The compressor blade geometries for different turbo jet engines are highly variable. This is coupled with the fact that the operating condition for separate aircraft can also be highly variable. Studying and modeling the different blade geometries and impact conditions for a variety of turbojet aircraft engines could be attempted. A parametric study of multiple engines could allow for generalized conclusions about curling and compressor deformation.

The new blade materials studied in this thesis did not perform as well as the Baseline's AM355 with regard to curl prevention. However, this does not imply that other materials would not have benefits. Modeling a material with a yield stress higher than that of AM355-SCCRT would potentially show greater ability to mitigate curling.

The addition of a thin nitride coating to the New Contour blade model showed a very significant benefit. Exploring different coating thicknesses and materials would help examine and gain greater insight into this benefit. Different coating materials including ternary nitrides could also be modeled. In addition, multilayer coating systems can be attempted. Modeling the interaction between the coating layers in addition to other model parameters will be difficult. Modeling of coatings can also be extended into the third dimension. Three dimensional models will give greater insight into the performance of coatings along the entire width of the leading edge rather than give the simplified two dimensional results. However, methods to decrease the computational requirements for this three dimensional work will be necessary. Modeling erosion accurately requires a very fine mesh with multiple layers of elements. Expanding this mesh to three dimensions will quickly consume computational resources.

The efforts suggested here are just some of the ways that the conditions for leading edge curl suppression of compressor blade components can be explored in the future.

References

1 – A. Hamed and W. Tabakoff, “Experiment and Numerical Simulations of the Effects of Ingested Particles in Gas Turbine Engines,” Propulsion and Energetics Panel (PEP) Symposium, Rotterdam, The Netherlands, April 1994.

2 – D. R. Nagy, V. R. Parameswaran, J. D. MacLeod, and J. P. Immarigeon; “Protective Coatings for Compressor Gas Path Components,” Propulsion and Energetics Panel (PEP) Symposium, Rotterdam, The Netherlands, April 1994.

3 – T. J. Carter, “Common failures in gas turbine blades,” *Engineering Failure Analysis*, 12 (2005) pp. 237-247.

4 – X. Chen, “Foreign object damage on the leading edge of a thin blade,” *Mechanics of Materials*, 37 (2005) pp. 447-457.

5 –Squadron Leader R C Sirs RAF; “The Operation of Gas Turbine Engines in Hot and Sandy Conditions; Royal Air Force Experiences in the Gulf Conflict.” Propulsion And Energetics Panel (PEP) Symposium, Rotterdam, The Netherlands, April 1994.

6 - G.a D'Alessio,.D.N., "Performance of Erosion Resistant Coatings for Compressor Airfoils," *Journal of the Candian Ceramic Society*, 63(1) (1994) pp. 59-63.

7 - A.V. Levy, Solid particle erosion and erosion-corrosion of materials, ASM International, Materials Park, OH (1995) pp. 220.

8 - I. Finnie, "Erosion of surfaces by solid particles: Oberflachenerosion durch feste teilchen," *Wear,* 3 (1960) pp. 87-103.

9 – K. Haugen, 0. Kvernvold, A. Ronold, and R. Sandberg, "Sand erosion of wear-resistant materials: Erosion in choke valves," *Wear*, 186-187 (1995) pp. 179-188.

10 – W. Tabakoff, "Protection of coated superalloys from erosion in turbomachinery and Other systems exposed to particulate flows," *Wear*, 233-235 (1990) pp. 200-208.

11 – K. Bose, R. J. K. Wood, and D. W. Wheeler, "High energy solid particle erosion mechanisms of superhard CVD coatings," *Wear*, 259 (2005) pp. 135-144.

12 – H. Wensink and M. C. Elwenspoek, "A closer look at the ductile-brittle transition in solid particle erosion," *Wear*, 253 (2002) pp. 1035-1043.

13 – W. Tabakoff and V. Shanov, "Erosion rate testing at high temperature for turbomachinery use," *Surface and Coatings Technology*, 76-77 (1995) pp. 75-80.

14 – V. R. Parameswaran, J.P. Immarigeon, and D. Nagy "Titanium nitride coating for aero engine compressor gas path components," *Surface and Coatings Technology*, 52 (1992) 251-260.

15 – Atlas of Stress-Strain Curves 2nd Edition, ASM International, Materials Park, OH, 2002.

16 – ASM International Handbook Committee, ASM Handbook Volume 19: Fatigue and Fracture, ASM International, Materials Park, OH, 1996.

17 – W. Tabakoff, "Study of Single-State Axial Flow Compressor Performance Deterioration," *Wear*, 119 (1987) pp. 51-61.

18 - B. A. Latella, B.K. Gan, K.E. Davies, D.R. McKenzie, and D.G. McCulloch, Titanium nitride/vanadium nitride alloy coating: mechanical properties and adhesion characteristics," *Surface & Coatings Technology*, 200 (2006) pp. 3605-3611.

19 – H. O. Pierson, Handbook of Refractory Carbides & Nitrides: Properties, Characteristics, Processing and Applications, Noyes Publications (2006) pp. 193.

20 – R.O.E. Vijgen and J.H. Dautzenberg, "Mechanical measurement of the residual stress in thin PVD films," *Thin Solid Films*, 270 (1995) pp. 264-269.

21 – P. Jedrzejowski, J. E. Klemberg-Saphieha, and L. Martinu, "Relationship between The mechanical properties and the microstructure of nanocomposite $TiN/SiN_{1.3}$ coatings prepared by low temperature plasma enhanced chemical vapor deposition," *Thin Solid Films*, 426 (2003) pp. 150-159.

22 – H. C. Barshilia, M. S. Prakash, A. Jain, and K.S. Rajam, "Structure, hardness, and thermal stability of TiAlN and nonlayer TiAlN/CrN multilayer films," *Vaccum*, 77 (2005) pp. 169-179.

23 – M.H. Zhu, B. Lei, Y. X. Leng, and N. Huang, "Comparison of tribological behavior of AlCrN and TiAlN coatings – Depositied by physical vapor deposition," *Wear*, 263 (2007) pp. 1423-1429.

24 – W. Grzesik, Z. Zalisz, S. Krol, and P. Nieslony, "Investigations on friction and wear mechanisms of the PVD-TiAlN coated carbine in dry sliding against steels and cast iron," *Wear*, 261 (2006) pp. 1191-1200.

25 – D. E. Wolfe and J. Singh, "Cutting Tool Life Enhancement Hard Carbide and Boride Multilayer Coatings," Technical Memorandum No. 00-179, Applied Research Laboratory, The Penn State University, November 2000.

26 – D. B. Lee, "TEM study on oxidized TiCrN coatings ion-plated on a steel substrate," *Surface and Coatings Technology*, 173 (2003) pp. 81-86.

27 – D. B. Lee, M. H. Kim, Y. C. Lee, and S. C. Kwon, "High temperature oxidiation of TiCrN coatings depositied on a steel substrate by ion plating," *Surface and Coatings Technology*, 141 (2001) pp. 232-239.

28 – P. Panjan, B. Navinsek, A. Cvelbar, A. Zalar, and I. Milosev, "Oxidiation of TiN, ZrN, TiZrN, CrN, TiCrN and TiN/CrN multilayer hard coatings reactively sputtered at low temperature," *Thin Solid Films*, 281-282 (1996) pp. 298-301.

29 – Y. Y. Chang, S. J. Yang, D. Y. Wang, "Characterization of TiCr(C,N)/amorphous carbon coatings synthesized by a cathodic arc deposition process," *Thin Solid Films*, 515 (2007) pp. 4722-4726.

30 – X. Chen and J. W. Hutchinson, "Particle impact on metal substrates with an application to foreign object damage to aircraft engines," *Journal of the Mechanics and Physics of Solids*, 50 (2002) pp. 2669-2690.

31 – M.S. ElTobgy, E. Ng, M. A. Elbestawi, "Finite element modeling of erosive wear," *Internation Journal of Machine Tools & Manufacture*, 45 (2005) pp. 1337-1346.

32 – G. L. Sheldon and A. Kanhere, "An investigation of impingement erosion using single particles," *Wear*, 21 (1978) 195-209.

33 – I. Finnie, "The mechanism of erosion of ductile metals," Proceedings of the Third National Congress on Applied Mechanics, New York, 1958, pp. 527-532.

34 – M. Hashish, “Modified Model for erosion, Seventh International Conference on Erosion by Liquid and Solid Impact, Cambridge, England, 1987, pp. 461-480.

35 – S. A. Meguid, G. Shagal, and J. C. Stranart, “Finite element modeling of shot-peening residual stresses,” *Journal of Materials Processing Technology*, 92-93 (1999) pp. 401-404.

36 – Y. Sun, A. Boyce, and T. Bell, “Finite element analysis of plastic deformation of various TiN coating/substrate systems under normal contact with a rigid sphere,” *Thin Solid Films*, 271 (1995) pp. 122-131.

37 – M. Bielawski and W. Beres, “FE modeling of surface stresse in erosion-resistant coatings under a single particle impact,” *Wear*, 262 (2007) pp. 167-175.

38 – S. Hassani, J. E. Klemberg-Sapeiha, M. Bielawski, W. Beres, L. Martinu, and M. Balazinksi, “Design of hard coating architecture for the optimization of erosion resistance,” *Wear*, 265 (2008) pp. 879-887.

39 – ABAQUS Inc, “Abaqus Analysis User’s Manual,” Dassault Systèmes, 2007.

40 – Mark’s Standard Handbook for Mechanical Engineers, McGraw-Hill, 1996.

41 – J. T. Pitterle and D. E. Wolfe, “Finite Element Blade Impact Analyses for [Baseline] Stage I Compressor Blisk,” Personal Correspondence, 2006.

42 – M. Meo, R. Vignevic, “Finite element analysis of residual stress induced by shot peening process,” *Advances in Engineering Software*, 34 (2003) pp. 569-575.

Academic Vita of George M. Slota

Name: George M. Slota
Address: 2402 Traci Dr
Pittsburgh, PA 15237
E-mail Address: gms5016@psu.edu

Education
School: The Pennsylvania State University
Date: September 2005 – December 2009
Major: Computer Engineering
Minors: Physics and Mathematics
Honors: Materials Science and Engineering
Thesis Title: Finite Element Modeling of Leading Edge Curl Phenomenon
Thesis Supervisor: Dr. Douglas E. Wolfe

Work Experience
Date: June 2007-December 2009
Title: Research Assistant
Description: Used Abaqus finite element analysis software to model the deformation of compressor blades. Analyzed various conditions for deformation including particle impact and simulation parameters. Also examined methods for prevention to compressor blade damage. Modeled various material parameters, blade geometries, and coatings. Independently developed methodology for modeling blade deformation and coating erosion.
Company: Applied Research Laboratory, Advanced Coatings Department
Supervisor: Dr. Douglas E. Wolfe

Miscellaneous
Dean's List, 3.61 overall GPA
Schreyer Honors College
College of Engineering Leonhard Scholar
Applied Research Laboratory Undergraduate Honors Program

Activities: Penn State Jazz Ensemble
Penn State Ultimate Frisbee Team
Korean Karate Club
Golden Key International Honour Society – Officer
Honor Society of Phi Kappa Phi